

REPAIR OF IMPACT-DAMAGED PRESTRESSED BRIDGE GIRDERS USING  
STRAND SPLICES AND FIBER-REINFORCED POLYMER

Justin A. Liesen

Thesis submitted to the faculty of the Virginia Polytechnic Institute and State  
University in partial fulfillment of the requirements for the degree of

MASTER OF SCIENCE

In

CIVIL ENGINEERING

Thomas E. Cousins, Chair  
Carin L. Roberts-Wollmann  
Ioannis Koutromanos

May 11, 2015

Blacksburg, Virginia

Keywords: Prestressed concrete repair, flexural tests, FRP, Strand Splices

# REPAIR OF IMPACT-DAMAGED PRESTRESSED BRIDGE GIRDERS USING STRAND SPLICES AND FIBER-REINFORCED POLYMER

Justin A. Liesen

## ABSTRACT

This study is part of a VDOT sponsored project focusing on repair techniques for impact damaged prestressed bridge girders. The investigation included evaluation of the repair installation and flexural strength of four AASHTO Type III girders that were intentionally damaged and repaired. In addition, nonlinear finite element modeling was used to aid in the development of design protocols for each repair method. This report discusses two of the three repair techniques. Three Master of Science students report on the project results: Justin Liesen, Mark Jones, and Michael Gangi. Liesen and Jones (2015) had responsibility for the installation and testing of the repaired girders and Gangi (2015) performed the finite element modeling of the girders.

Three repair methods were identified for experimental investigation: strand splice, bonded FRP, and FRCM. During this investigation the repair methods were evaluated by conducting six flexural tests on four AASHTO Type III girders. Flexural tests were conducted instead of shear tests because typical impact damage from overheight vehicles occurs around the mid-span and flexural strength dominated region of bridge girders. The cracking and failure moments for each test were evaluated and compared to predictions of the girder's behavior using AASHTO calculations, a moment-curvature diagram, and non-linear finite element modeling. All photographs by author unless otherwise noted, 2015.

## Table of Contents

ABSTRACT.....	ii
Table of Contents.....	iii
List of Figures.....	vi
List of Tables.....	xiii
Abbreviations.....	xvi
CHAPTER I: Introduction.....	1
1.1: Background.....	1
1.2: Purpose and Scope.....	4
1.3: Thesis Organization.....	5
CHAPTER II: Review of Literature.....	6
2.1: Use of Prestressed Concrete for Bridges.....	6
2.2: Damage Classification.....	7
2.3: Repair Techniques.....	10
2.3.1: Strand Splice.....	13
2.3.2: Fiber Reinforced Polymer (FRP) .....	18
2.3.3: Additional Techniques.....	24
2.4: Summary.....	25
CHAPTER III: Experimental Testing Methods.....	27
3.1: Materials Testing.....	34
3.2: Instrumentation Types.....	41
3.3: Test Procedures.....	42
3.3.1: Test 1 – Control Test.....	42

3.3.2: Test 2 – Girder with Eight Severed/Re-tensioned Strands.....	49
3.3.3: Test 3 – FRP Repaired Girder with Four Severed Strands.....	58
3.3.4: Test 4 – Girder with Four Severed/Re-tensioned Strands.....	72
CHAPTER IV: Results and Discussion.....	82
4.1: Introduction.....	82
4.2: Material Properties.....	82
4.2.1: Girder Concrete.....	82
4.2.2: Tstrata IRC Repair Concrete.....	83
4.2.3: Girder Reinforcement.....	84
4.2.4: Prestressing Strand.....	85
4.2.5: V-Wrap C400 FRP Repair System Materials.....	87
4.2.6: Grabb-It Splice Chuck.....	88
4.3: Analytical Modeling.....	91
4.3.1: Calculations Based on AASHTO Guidelines.....	91
4.3.2: Moment-Curvature Based on Strain Compatibility.....	93
4.3.3: Non-Linear Finite Element.....	97
4.4: Laboratory Tests.....	98
4.4.1: Test Results Overview.....	98
4.4.2: Test 1 – Control Test.....	100
4.4.3: Test 2 – Girder with Eight Severed/Re-tensioned Strands.....	104
4.4.4: Test 3 – FRP Repaired Girder with Four Severed Strands.....	108
4.4.5: Test 4 – Girder with Four Severed/Re-tensioned Strands.....	112
4.6: Data Analysis.....	118

4.6.1: Strand Splice Repair.....	120
4.6.2: FRP Repair.....	122
4.6.3: Analysis Methods.....	124
CHAPTER V: Conclusions and Recommendations.....	128
5.1: Conclusions.....	128
5.2: Recommendations.....	130
References.....	132
APPENDIX A: Arcadia Bridge Blueprints.....	137
APPENDIX B: AASHTO Calculations.....	148
APPENDIX C: Strain-Compatibility Moment-Curvature Calculations.....	154
APPENDIX D: FRP Repair Calculations.....	166
APPENDIX E: Applied Moment Calculations.....	183
APPENDIX F: Shear Calculations.....	184
APPENDIX G: Curvature-Ductility Calculations.....	186
APPENDIX H: Specimen Preparation for Strand Splice and FRP Repairs.....	187
APPENDIX I: Installation of Strand Splices.....	189
APPENDIX J: Fiber Reinforced Polymer Repair Procedures.....	190

## List of Figures

Figure 1. Overheight Impacts as Reported by State Adapted From Agrawal, A. K., Xu, X., & Chen, Z. (2013, January 15). <i>Strikes on Low Clearance Bridges by Over-Height Trucks in New York State</i> . Retrieved December 05, 2014, from United States Department of Transportation: <a href="http://www.rita.dot.gov/utc/publications/spotlight/2013_01/html/spotlight_0113.html">http://www.rita.dot.gov/utc/publications/spotlight/2013_01/html/spotlight_0113.html</a> , Used under fair use, 2015.....	2
Figure 2. Typical AASHTO Type III Girder Cross Section Tested.....	4
Figure 3. Percent of Bridges Built Annually Aktan, A. E., Culmo, M. P., Frangopol, D. M., French, C. W., Rabbat, B. G., Sanders, D. H., . . . Woods, S. W. (1994). <i>Concrete Bridges</i> . Washington D.C.: Transportation Research Board: Committee on Concrete Bridges. Retrieved December 8, 2014, Used under fair use, 2015.....	7
Figure 4. Splice Chuck Installation.....	16
Figure 5. Four Splice Chucks.....	17
Figure 6. Eight Splice Chucks.....	17
Figure 7. Carbon Fiber Stress Strain Curve Wipf, T. J., Klaiber, F. W., Rhodes, J. D., & Kempers, B. J. (2004b). <i>Effective Structural Concrete Repair: Repair of Impact Damaged Prestressed Concrete Beams with Carbon Fiber Reinforced Polymer (CFRP)</i> . Iowa State University, Department of Civil, Construction, and Environmental Engineering. Ames: Iowa Department of Transportation. Retrieved December 12, 2014, Used under fair use, 2015.....	19
Figure 8. Fiber Reinforced Polymer Saturation Process.....	23
Figure 9. Fiber Reinforced Polymer Installation Process.....	23
Figure 10. Fiber Reinforced Polymer Installed Over Damaged Section.....	24
Figure 11. Girder Cross Section from Bridge Plans.....	28

Figure 12. Typical AASHTO Type III Girder Cross Section Tested.....	29
Figure 13. Shear Reinforcement Spacing for No 5 Reinforcing Bars.....	30
Figure 14. Test 1 Set-up.....	31
Figure 15. Test 2 Set-up.....	32
Figure 16. Test 3, Iteration 1 Set-up.....	32
Figure 17. Test 3, Iteration 2 Set-up.....	32
Figure 18. Test 4, Iteration 1 Set-up.....	33
Figure 19. Test 4, Iteration 2 Set-up.....	33
Figure 20. Test 5 Set-up.....	33
Figure 21. Test 6 Set-up.....	34
Figure 22. Concrete Core Removal (Photo used with permission of Mark Jones, 2015).....	36
Figure 23. Prestress Strand Tensile Test.....	38
Figure 24. Extensometer Attached to Strand (Photo taken by Mark Jones, used under fair use 2015).....	39
Figure 25. Cutting of Strands (Photo taken by Mark Jones, used under fair use 2015).....	40
Figure 26. Extensometer Location on Strand (Photo taken by Mark Jones, used under fair use 2015).....	40
Figure 27. Nominal Moment Capacity versus Calculated Failure Moment for Test 1.....	44
Figure 28. Nominal Shear Capacity versus Calculated Shear for Test 1.....	44
Figure 29. Pin Bearing (Photo taken by Mark Jones, used under fair use 2015).....	45
Figure 30. Roller Bearing (Photo taken by Mark Jones, used under fair use 2015).....	46
Figure 31. Frame to Prevent Tipping.....	46

Figure 32. Control Test Loading System (Photo taken by Mark Jones, used under fair use 2015).....	47
Figure 33. Test 1 Set-up and Instrumentation Plan.....	48
Figure 34. Wire Pots below Load Point to Measure Deflection (Photo taken by Mark Jones, used under fair use 2015).....	48
Figure 35. Girder B Damage Location.....	50
Figure 36. Girder B Cross Section through Damaged Area with Severed Strand Locations Shown.....	50
Figure 37. Nominal Moment Capacity versus Calculated Failure Moment for Test 2.....	52
Figure 38. Nominal Shear Capacity versus Applied Shear for Test 2.....	52
Figure 39. Roller Bearing (Photo taken by Mark Jones, used under fair use 2015).....	53
Figure 40. Pin Bearing (Photo taken by Mark Jones, used under fair use 2015).....	54
Figure 41. Test 2 Loading System (Photo taken by Mark Jones, used under fair use 2015).....	54
Figure 42. Test 2 Set-up.....	55
Figure 43. Test 2 Set-up and Instrumentation Plan.....	56
Figure 44. Wire Pot 1 at 14.5 Ft from Roller (Photo taken by Mark Jones, used under fair use 2015).....	56
Figure 45. Strain Profile Instrumentation Set-up (Photo taken by Mark Jones, used under fair use 2015).....	57
Figure 46. LVDT at Repair Interface.....	57
Figure 47. Girder C Damage Locations.....	59
Figure 48. Girder C Cross Section through Damaged Area with Severed Strand Locations Shown.....	59

Figure 49. Nominal Moment Capacity versus Calculated Failure Moment for Test 3, Iteration 1 .....	61
Figure 50. Nominal Shear Capacity versus Calculated Shear for Test 3, Iteration 1.....	61
Figure 51. Nominal Moment Capacity versus Calculated Failure Moment for Test 3, Iteration 2 .....	62
Figure 52. Nominal Shear Capacity versus Calculated Shear for Test 3, Iteration 2.....	62
Figure 53. Test 3 Set-up.....	64
Figure 54. Test 3, Iteration 1 Pin Location (Photo taken by Mark Jones, used under fair use 2015).....	64
Figure 55. Test 3, Iteration 2 Pin Location (Photo taken by Mark Jones, used under fair use 2015).....	65
Figure 56. Test 3 Roller Location (Photo taken by Mark Jones, used under fair use 2015).....	65
Figure 57. Test 3 Load Point.....	66
Figure 58. Test 3, Iteration 1 Test and Instrumentation Set-up.....	67
Figure 59. Test 3, Iteration 2 Test and Instrumentation Set-up.....	67
Figure 60. Strain Transducers on Damaged/Repaired Side of Girder (Photo taken by Ioannis Koutromanos, used under fair use 2015).....	68
Figure 61. Strain Transducers on Undamaged Side of Girder.....	68
Figure 62. LVDT at FRP and Concrete Interface.....	69
Figure 63. Shear Cracking in Midspan Region during Iteration 1 (Photo taken by Ioannis Koutromanos, used under fair use 2015).....	70
Figure 64. Cracking Near Peak Load for Iteration 1 (Photo taken by Ioannis Koutromanos, used under fair use 2015).....	71

Figure 65. Brace for Actuator (Photo taken by Mark Jones, used under fair use 2015).....	72
Figure 66. Nominal Moment Capacity versus Calculated Failure Moment for Test 4, Iteration 1 .....	74
Figure 67. Nominal Shear Capacity versus Calculated Shear for Test 4, Iteration 1.....	74
Figure 68. Nominal Moment Capacity versus Calculated Failure Moment for Test 4, Iteration 2 .....	75
Figure 69. Nominal Shear Capacity versus Calculated Shear for Test 4, Iteration 2.....	75
Figure 70. Test 4, Iteration 1 Roller Location (Photo taken by Mark Jones, used under fair use 2015).....	77
Figure 71. Test 4, Iteration 2 Roller Location (Photo taken by Mark Jones, used under fair use 2015).....	77
Figure 72. Test 4 Pin Location (Photo taken by Mark Jones, used under fair use 2015).....	78
Figure 73. Test 4, Iteration 1 Set-up and Instrumentation Plan.....	79
Figure 74. Test 4, Iteration 2 Set-up and Instrumentation Plan.....	79
Figure 75. Damage on Girder near Strain Transducer Location (Photo taken by Ioannis Koutromanos, used under fair use 2015).....	80
Figure 76. Strain Transducer Set-up Below Load Point.....	80
Figure 77. Girder Concrete Tensile Test.....	83
Figure 78. Reinforcing Bar Stress Strain Relationship.....	85
Figure 79. Prestress Tensile Test Strand Rupture (Photo taken by Mark Jones, used under fair use 2015).....	86
Figure 80. Strand Splice Torque-Tension Relationship.....	90

Figure 81. Prestress Steel Stress - Strain Relationship Gangi, M. (2015). <i>Nonlinear Beam Modeling of the Repair of Impact-Damaged Prestressed Bridge Girders</i> . Virginia Polytechnic and State University, Department of Civil and Environmental Engineering. Blacksburg: Virginia Center for Transportation Innovation and Research, Used under fair use, 2015.....	95
Figure 82. Calculated Moment-Curvature Behavior.....	96
Figure 83. Test 1 Moment Deflection Behavior.....	102
Figure 84. Test 1 Moment-Curvature Relationship.....	104
Figure 85. Test 2 Moment Deflection Behavior.....	105
Figure 86. Flexural Cracks in Patch Concrete near Failed Strand Splice (Photo taken by Ioannis Koutromanos, used under fair use 2015).....	106
Figure 87. Test 2 Moment-Curvature Relationship.....	108
Figure 88. Test 2 Failed Splice and Ruptured Strand (Photo taken by Mark Jones, used under fair use 2015).....	107
Figure 89. Test 3 Moment Deflection Behavior.....	109
Figure 90. Test 3 Moment-Curvature Relationship.....	111
Figure 91. Crack Propagation from FRP into Web (Photo taken by Ioannis Koutromanos, used under fair use 2015).....	112
Figure 92. Test 4, Iteration 1 Moment Deflection Behavior.....	113
Figure 93. Test 4, Iteration 2 Moment Deflection Behavior.....	114
Figure 94. Test 4 Moment-Curvature Relationship.....	115
Figure 95. Cracking Pattern at Load Point at Final Load for Iteration 1 (Photo taken by Ioannis Koutromanos, used under fair use 2015).....	116

Figure 96. Cracking Patterns near Maximum Applied Load (Photo taken by Ioannis Koutromanos, used under fair use 2015).....	117
Figure 97. Flexural Compression Failure in the Deck (Photo taken by Ioannis Koutromanos, used under fair use 2015).....	118
Figure 98. Strand Splice Strength Regenerated Trend Lines.....	122
Figure 99. Nominal to Tested Ratio.....	126
Figure 100. Arcadia Bridge Blueprint Page 1.....	137
Figure 101. Arcadia Bridge Blueprint Page 2.....	138
Figure 102. Arcadia Bridge Blueprint Page 3.....	139
Figure 103. Arcadia Bridge Blueprint Page 4.....	140
Figure 104. Arcadia Bridge Blueprint Page 5.....	141
Figure 105. Arcadia Bridge Blueprint Page 6.....	142
Figure 106. Arcadia Bridge Blueprint Page 7.....	143
Figure 107. Arcadia Bridge Blueprint Page 8.....	144
Figure 108. Arcadia Bridge Blueprint Page 9.....	145
Figure 109. Arcadia Bridge Blueprint Page 10.....	146
Figure 110. Arcadia Bridge Blueprint Page 11.....	147

## List of Tables

Table 1. Damage Classifications Harries, K. A., Kasan, J., Miller, R., & Brinkman, R. (2012). <i>Updated Research for Collision Damage and Repair of Prestressed Concrete Beams</i> . NCHRP Project 20-07, Task 307, University of Pittsburgh, Department of Civil Engineering, Pittsburgh. Retrieved December 10, 2014, Used under fair use, 2015.....	9
Table 2. Summary of Repair Techniques Harries, K. A., Kasan, J., & Aktas, C. (2009). <i>Repair Methods for Prestressed Girder Bridges</i> . University of Pittsburgh, Department of Civil and Environmental Engineering. Harrisburg: Commonwealth of Pennsylvania Department of Transportation, Used under fair use 2015.....	13
Table 3. Suggested Installation Torque Prestress Supply Incorporated. (2010). <i>Grabb-It Cable Splice</i> . Retrieved December 12, 2014, from Prestress Supply: <a href="http://www.prestresssupply.com/Products/StrandRepair/GRABBITCableSplice.aspx">http://www.prestresssupply.com/Products/StrandRepair/GRABBITCableSplice.aspx</a> , Used under fair use 2015.....	14
Table 4. Recommended FRP Repair Based on Maximum Number of Damaged Strands Harries, K. A., Kasan, J., Miller, R., & Brinkman, R. (2012). <i>Updated Research for Collision Damage and Repair of Prestressed Concrete Beams</i> . NCHRP Project 20-07, Task 307, University of Pittsburgh, Department of Civil Engineering, Pittsburgh. Retrieved December 10, 2014, Used under fair use 2015.....	20
Table 5. Project Scope Responsibilities and Summary.....	26
Table 6. Testing Schedule and Summary.....	31
Table 7. Girder and Deck Concrete Compressive Strength.....	82
Table 8. Girder Concrete Tensile Strength.....	83
Table 9. Repair Concrete Compressive Strength.....	84

Table 10. Reinforcing Bar Failure Tensile Strength.....	84
Table 11. Prestress Strand Strength.....	86
Table 12. Effective Prestress Force.....	87
Table 13. FRP Tensile Test Results.....	88
Table 14. Strand Splice Chuck Torque Test Results.....	89
Table 15. Spliced Strand Tension Test.....	90
Table 16. AASHTO Mn Calculation Summary.....	93
Table 17. Moment-Curvature Calculation Summary.....	96
Table 18. Finite Element Analysis Results.....	99
Table 19. Girder Self-Weight Moments.....	99
Table 20. Nominal and Failure Moment Summary.....	100
Table 21. Cracking Moment Test Results Summary.....	100
Table 22. Experimental and Calculated Cracking and Nominal Moment Capacities for Test 1 .....	103
Table 23. Experimental and Calculated Cracking and Nominal Moment Capacities for Test 2 .....	105
Table 24. Experimental and Calculated Cracking and Nominal Moment Capacities for Test 3 .....	110
Table 25. Experimental and Calculated Cracking and Nominal Moment Capacities for Test 4 .....	114
Table 26. Nominal versus Tested Strength Regained.....	119
Table 27. Cracking versus Tested Strength Regained.....	119
Table 28. Curvature-Ductility Comparison.....	120

Table 29. Ratio of Predicted to Measured Moment Capacity.....	125
Table 30. AASHTO Design Nominal Moment Calculations With and Without Deck.....	127
Table 31. Material Test Averages.....	128
Table 32. Test 1 AASHTO Calculations.....	150
Table 33. Test 2 AASHTO Calculations.....	151
Table 34. Test 3 AASHTO Calculations.....	152
Table 35. Test 4 AASHTO Calculations.....	153
Table 36. Test 1 Moment-Curvature Calculations.....	154
Table 37. Test 2 Moment-Curvature Calculations.....	157
Table 38. Test 3 Moment-Curvature Calculations.....	160
Table 39. Test 4 Moment-Curvature Calculations.....	163

## **Abbreviations**

CFRP – Carbon Fiber Reinforced Polymer

FRCM – Fabric Reinforced Cementitious Matrix

FRP – Fiber Reinforced Polymer

NCHRP – National Cooperative Highway Research Program

ksi – Kips per Square Inch

in – inch

ft – foot

lb – pound

k-ft – kip-feet

NSM CFRP – Near Surface Mounted Carbon Fiber Reinforced Polymer

PT-CFRP – Post-Tensioned Carbon Fiber Reinforced Polymer

EB-CFRP – Externally Bonded Carbon Fiber Reinforced Polymer

bPT-CFRP – Bonded Post-Tensioned Carbon Fiber Reinforced Polymer

uPT-CFRP – Unbonded Post-Tensioned Carbon Fiber Reinforced Polymer

LVDT – Linear Variable Differential Transformers

MLVDT – Mini Linear Variable Differential Transformers

BDI – Bridge Diagnostics Incorporated

VDOT – Virginia Department of Transportation

ASTM – American Society for Testing and Materials

Tstrata IRC – Tstrata Infuseable Rapid Cure Restoration Material

## **CHAPTER I: Introduction**

### **1.1: Background**

Prestressed concrete bridge girders are a common type of structure for short to medium span highway bridges (Taly, 2015). According to a report published by Transportation for America, 11% of bridges in the United States are classified as deficient; for example, they require “significant maintenance, rehabilitation, or replacement” (Davis & Goldberg, 2013). Each year in the United States, an average of 25 to 35 bridges are damaged by overheight vehicle collisions in each state (ElSaftey, Graeff, & Fallaha, 2014). In a poll conducted by Agrawal and Chen (2013), the state of Virginia reported 41 bridges damaged from overheight vehicle impacts from 2005 to 2008. Figure 1 shows the number of reported impacts by state based on a response to the same poll. The majority of the states that responded, highlighted in dark grey, admitted that the damage of bridges from impact is a major problem (Agrawal, Xu, & Chen, 2013).

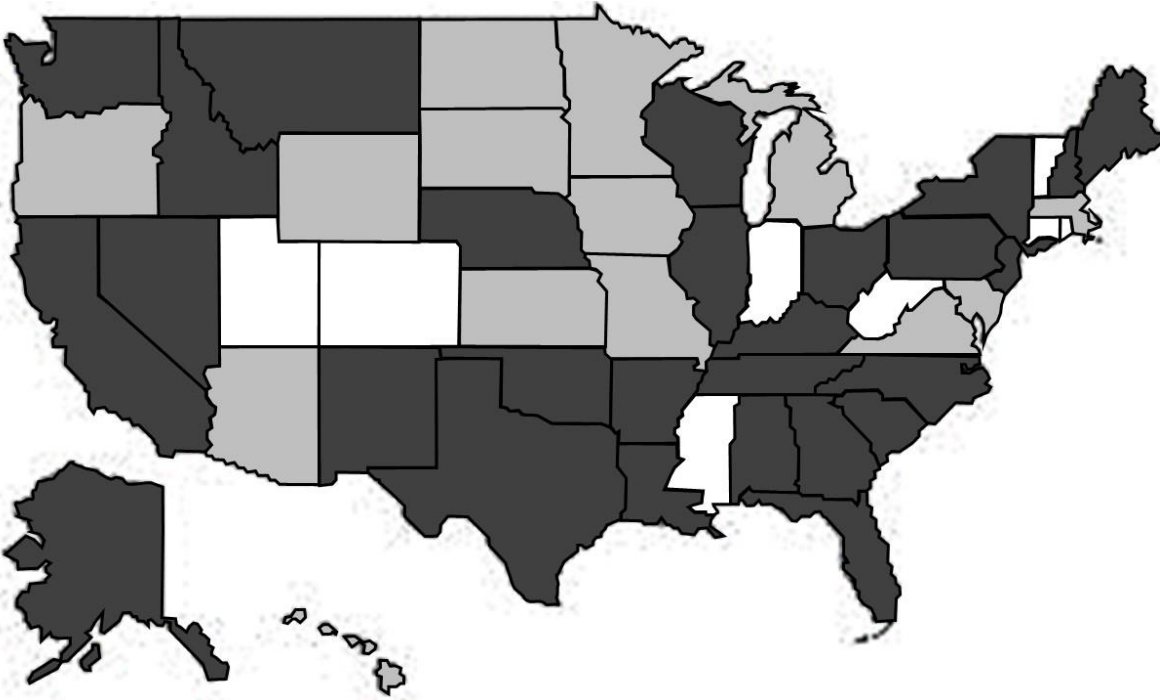


**Figure 1. Overheight Impacts as Reported by State Adapted From Agrawal, A. K., Xu, X., & Chen, Z. (2013, January 15). *Strikes on Low Clearance Bridges by Over-Height Trucks in New York State*. Retrieved December 05, 2014, from United States Department of Transportation:**

**[http://www.rita.dot.gov/utc/publications/spotlight/2013\\_01/html/spotlight\\_0113.html](http://www.rita.dot.gov/utc/publications/spotlight/2013_01/html/spotlight_0113.html), Used under fair use,**

**2015**

The damage caused by impacts can range from minor to severe and can result in significant costs for the surrounding community and bridge owner. Initially, there is potential for damaged property and even loss of life depending on the type of impact and volume of use. In the long run, costs result from repairing or replacing the damaged sections, diversion of traffic, and damages to commerce and industry in the vicinity of the damaged bridge. Four states; Iowa, Kentucky, Louisiana, and Mississippi, reported an average cost of repair and/or cost of property damage of approximately \$500,000 per damaged bridge in 1999 (Fu, Burhouse, & Chang, 2003). Because of these potential losses, it is important for bridge owners to have and develop cost effective and easily implementable repair schemes.

According to a report from The Transportation Research Board Committee on Concrete Bridges published in 1994, prestressed bridges made up more than 50% of all bridges in the United States. In addition, they predicted that the “application of prestressing to bridges has grown rapidly and steadily” (Aktan, et al., 1994). As research is conducted in making concrete lighter and stronger, the application of prestress to bridges extends the span capability of bridges of up to 800 ft for segmental concrete bridges (Aktan, et al., 1994). With the increasing number of prestress bridges in the United States, the probability of these bridges being impacted by overheight vehicles increases.

The application of prestress that allows bridges to span greater lengths poses a more complex problem when the girders are damaged than when a steel girder or non-prestressed girder bridge is damaged. Damage that causes strands to become exposed makes them susceptible to corrosion similar to mild steel reinforcement. Furthermore, strand exposure or damage can change the capacity of the girder by reducing the effective prestress force in the girder. Severed strands continue to provide flexural resistance in areas that are undamaged, however, the capacity of the damaged section is reduced. Therefore, it is important to accurately assess and sufficiently repair damaged members to restore the original strength. If that strength cannot be restored, the bridge may be posted or replaced. Some of the current techniques used to repair prestressed bridge girders include strand splices and Fiber Reinforced Polymer (FRP). Other techniques include Steel Jacketing, External Post Tensioning, Fabric Reinforced Cementitious Matrix (FRCM) and Replacement (Kasan, 2009).

This research project is intended to evaluate the efficiency of each of three repair methods for impact damaged bridges. Through a review of previous applications and research of these repair techniques, the most promising three will be included in a testing program. Test

girders for evaluation of the repair methods have been provided by the Virginia Department of Transportation (VDOT). The girders are from an Interstate-81 overpass near Arcadia, Virginia damaged by an overheight vehicle. The bridge plans are provided in APPENDIX A: Arcadia Bridge Blueprints. Due to the damage from this and previous impacts, VDOT determined the bridge needed to be replaced. The four AASHTO Type III prestressed girders, pictured in Figure 2, were provided to Virginia Tech to test repair techniques.

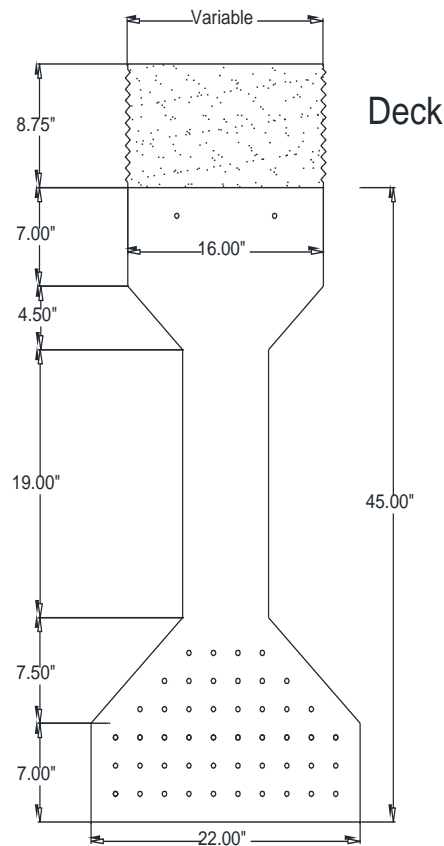


**Figure 2. Typical AASHTO Type III Girder Cross Section Tested**

### **1.2: Purpose and Scope**

This study is part of a VDOT sponsored project focusing on repair techniques for impact damaged prestressed bridge girders. The investigation included evaluation of the repair installation and flexural strength of four AASHTO Type III girders that were intentionally

damaged and repaired. In addition, nonlinear finite element modeling was used to aid in the development of design protocols for each repair method. This report discusses two of the three repair techniques. Three Master of Science students report on the project results: Justin Liesen, Mark Jones, and Michael Gangi. Liesen and Jones (2015) had responsibility for the installation and testing of the repaired girders and Gangi (2015) performed the finite element modeling of the girders. The investigation will include testing and analysis and will result in the development of installation and design strength calculation protocols.

### **1.3: Thesis Organization**

CHAPTER II: Review of Literature of this thesis reviews the literature associated with constructing prestressed bridges, damages to prestressed bridges, and repair techniques for damaged prestressed bridges. CHAPTER III: Methods discusses the methods, set-up and procedures followed for each test. CHAPTER IV: Results and Discussion discusses the results of each test. CHAPTER V: Conclusions and Recommendations reviews and compares the results of the tests and proposes recommendations for use and further research.

## CHAPTER II: Review of Literature

### 2.1: Use of Prestressed Concrete for Bridges

“Prestressing can be defined in general terms as the preloading of a structure, before application of the service loads, so as to improve its performance in specific ways” (Nilson, 1987). It is used to control the stress in the structural member; allowing the designer to limit cracking and offset deflections under service loads. In prestressed bridge construction, a girder is designed with a prestress force that offsets the stress and deflections caused by the self-weight and superimposed dead, prestress, and live loads (Nilson, 1987).

Eugene Freyssinet, a French engineer, “introduced a system for prestressing using wedge-anchored high strength steel cables” (Nilson, 1987), in 1940 that allowed long span bridges to be built with relatively small depths. “The application of prestressing to bridges has grown rapidly and steadily, beginning in 1949 with high-strength steel wires in the Walnut Lane Bridge in Philadelphia, Pennsylvania” (Aktan, et al., 1994). The application of a preload allowed designers to offset the deflection, reduce materials required, increase the span lengths, and accelerate the construction timeline through the use of precast and segmental construction techniques. Because of these advantages, the popularity of using prestressing in the construction of bridges has increased. Since the construction of the Walnut Lane Bridge, the percent of prestressed concrete bridges built each year has risen from 0% to 50% of all bridges built in the United States. Figure 3 shows the steady increase of use of prestressed members in bridge construction between 1950 and 1994 as compared to steel and non-prestressed concrete as the primary material. With improvements in ultra-high and very-high performance concrete with higher compressive strengths and lighter-weight materials, the life-cycle costs of prestressed

concrete bridges continues to decrease, increasing its popularity as a construction technique (Aktan, et al., 1994).

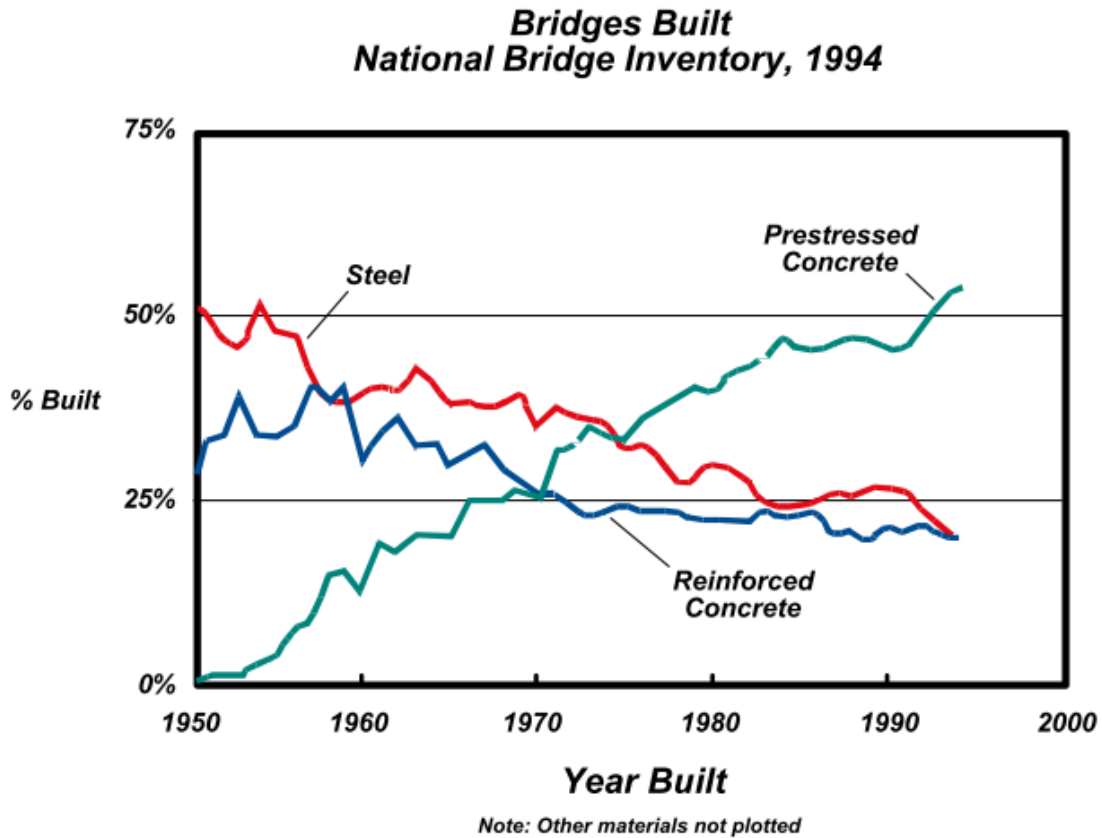


Figure 3. Percent of Bridges Built Annually Aktan, A. E., Culmo, M. P., Frangopol, D. M., French, C. W., Rabbat, B. G., Sanders, D. H., . . . Woods, S. W. (1994). *Concrete Bridges*. Washington D.C.: Transportation Research Board: Committee on Concrete Bridges. Retrieved December 8, 2014, Used under fair use, 2015

## 2.2: Damage Classification

As the percent of prestressed bridges continues to rise, the likelihood of damage due to impact from overweight vehicles increases. Upon impact, a bridge can sustain damages that can be classified as minor, moderate, or severe (Harries, Kasan, Miller, & Brinkman, 2012).

“Shallow spalls, nicks and cracks, scrapes and some efflorescence, rust or water stains” (Kasan, 2009) are typical with minor damage. Repairs to girders with minor damage are for aesthetic or

preventative purposes. “Larger cracks and sufficient spalling or loss of concrete to expose strands” (Kasan, 2009) is typical of moderate damage. Repairs to girders with moderate damage are for prevention of further deterioration. Kasan (2009) separated the classification of severe damage into two categories, Severe I and Severe II. “Severe I damage requires structural repair that can be affected using a non-prestressed/post-tensioned method” (Kasan, 2009). Repair to a member with severe I damage is done to restore design strength. “Severe II damage requires structural repairs involving replacement of prestressing force through new prestress or post-tensioning” (Kasan, 2009). Repair to a member with severe II damage is done to restore a service limit state. If an element must be replaced because damage is too extensive and repair is not practical, it is classified as severe III (Kasan, 2009). Table 1 is a summary of the severe damage classifications and repair philosophies based on the determined damages.

**Table 1. Damage Classifications Harries, K. A., Kasan, J., Miller, R., & Brinkman, R. (2012). *Updated Research for Collision Damage and Repair of Prestressed Concrete Beams*. NCHRP Project 20-07, Task 307, University of Pittsburgh, Department of Civil Engineering, Pittsburgh. Retrieved December 10, 2014, Used under fair use, 2015**

Damage Classification	SEVERE I	SEVERE II	SEVERE III
Repair philosophy	ULS only	ULS and SLS	-
Action	non PT repair	PT repair	replace
Live load capacity replacement	up to 5%	up to 30%	100%
Ultimate load capacity replacement	up to 8%	up to 15%	100%
Replace lost strands	2-3 strands	up to 8 strands	>8 strands
Vertical Deflection	loss of camber	up to 0.5%	>0.5%
Lateral Deflection (Sweep) (Shanafelt and Horn 1985)	within construction tolerance		permanent lateral deflection exceeding construction tolerance

		strand loss	camber
<b>MINOR</b>	Concrete with shallow spalls, nicks and cracks, scrapes and some efflorescence, rust or water stains. Damage does not affect member capacity. Repairs are for aesthetic and preventative purposes only ( <i>NCHRP 280</i> ).	no exposed strands	no effect of girder camber
<b>MODERATE</b>	Larger cracks and sufficient spalling or loss of concrete to expose strands. Damage does not affect member capacity. Repairs are intended to prevent further deterioration ( <i>NCHRP 280</i> ).	exposed strands no severed strands	no effect of girder camber
<b>SEVERE I</b>	Damage affects member capacity but may not be critical – being sufficiently minor or not located at a critical section along the span [2.5]. Repairs to prevent further deterioration are warranted although structural repair is typically not required.	less than 5% strand loss	partial loss of camber
<b>SEVERE II</b>	Damage requires structural repair that can be affected using a non-prestressed/post-tensioned method. This may be considered as repair to affect the STRENGTH (or ultimate) limit state.	strand loss greater than 5%	complete loss of camber
<b>SEVERE III</b>	Decompression of the tensile soffit has resulted [2.6.1.2]. Damage requires structural repair involving replacement of prestressing force through new prestress or post-tensioning. This may be considered as repair to affect the SERVICE limit state in addition to the STRENGTH limit state.	strand loss exceeding 20%. In longer and heavily loaded sections, decompression may not occur until close to 30% strand loss.	vertical deflection less than 0.5%
<b>SEVERE IV</b>	Damage is too extensive. Repair is not practical and the element must be replaced.	strand loss greater than 35%	vertical deflection greater than 0.5%

### **2.3: Repair Techniques**

In 1980, Shanafelt and Horn conducted research for The National Cooperative Highway Research Program (NCHRP) in which they investigated 11 different repair techniques to include external post-tensioning, steel jacketing, strand splicing, combinations of these methods, and replacement. Their results were published in NCHRP Report 226 along with an initial damage classification system. The report suggested standards for inspection and repair of damaged prestressed bridge girders to include proper techniques, tools, and forms (Harries, et. al., 2012). Subsequent research into repair techniques have built on and expanded the research reported in NCHRP Report 226.

Strand splices are one of the cheapest and easiest methods to design and install for repairing damaged prestressed girders. They can restore most of the strength and some of the prestress force lost due to the damage. The size and stiffness of the splice must be considered to ensure that proper positioning and cover are given and to account for any unintended eccentricities. In addition, the advertised minimum strength of a strand splice is 85% of the nominal strength of the strands it is joining. This must be considered as it will create a potential critical failure point (Kasan, 2009).

Fiber reinforced polymers (FRP) provide a wide array of options for repair, but the designer must consider the unique material properties of the different types of fabrics along with the specific repair method they choose. In addition, the installation process requires skilled laborers and the adhesive used to bond the system to the girder must be protected from the environment to prevent deterioration from ultraviolet rays and fire (Kasan, 2009).

External post-tensioning is designed similar to an unbonded post-tensioned girder and can restore prestress as well as strength and serviceability. The process is simple, but the design

must consider the force transfer to the girder and any eccentricity created by the addition of loads. Also, after the system is installed, it needs to be protected from the environment to prevent corrosion (Harries, et. al., 2012).

Steel Jacketing not only increases the strength through its own material properties, but it also provides confinement for the concrete that it encases. The jacket can be designed to fit around the outside of the girder, but the designer must consider how to anchor the jacket and transfer shear forces between the jacket and the girder. Installation of the jacket may require field welding to close the encasement and grouting is often required along the entire girder for environmental protection and for aesthetics to offset size differences (Harries, et. al., 2012).

Fabric-Reinforced Cementitious Matrix (FRCM) is a “cement based matrix reinforced with dry fibers in the form of open single or multiple meshes” (ACI Committee 549, 2013). The matrix bonds to the member and provides reinforcement. The dry fabric mesh has a primary and secondary orientation which allows it to provide bi-axial tensile strength and gives it some shear resistance. However, the installation procedure requires a specified temperature range and a specialized professional. Since it is relatively new in comparison to some of the other techniques, finding someone with installation experience may prove difficult. In addition, there is a longer cure process for the cementitious matrix than epoxy. If the matrix is not given the proper cure time or temperatures are not within range, a good bond between the fabric and the substrate may not form. Without a proper bond, the repair will not function properly (ACI Committee 549, 2013).

Replacement is typically seen as the safest and surest way to handle a damaged girder. By replacing a girder, any realized or unrealized damage that may affecting performance later is fixed, however it is the most expensive and time consuming. According to a study conducted for

the Washington Department of Transportation, most girder replacements cost between \$500,000 and \$1,000,000 depending on the size and scope (average of around \$8,000 per foot of girder replaced) and took approximately one to two months to complete the replacement (Brice, 2013).

Ultimately, any repair method, or combination of repair methods is going to be more cost and time effective than replacing a damaged girder. In addition, if designed appropriately, the repaired section may outperform the original design capacity of the girder. Each type of repair has its advantages and disadvantages as indicated in Table 2. These advantages and disadvantages should be considered carefully based on the specific situation of the damaged girder. The specifics of each type of repair is discussed in further detail in subsequent sections. The repairs presented in Table 2 include replacement, steel jacketing, strand splicing, post tensioned steel, post tensioned CFRP, prestressed CFRP, near surface mounted (NSM) CFRP, CFRP fabrics, and preformed CFRP strips. If any aspect of a repair is under question, it is always best to exercise caution and replace the damaged girder.

**Table 2. Summary of Repair Techniques Harries, K. A., Kasan, J., & Aktas, C. (2009). *Repair Methods for Prestressed Girder Bridges*. University of Pittsburgh, Department of Civil and Environmental Engineering.**

**Harrisburg: Commonwealth of Pennsylvania Department of Transportation, Used under fair use 2015**

Damage Assessment Factor	Repair Method								
	preform CFRP strips	CFRP fabric	NSM CFRP	prestressed CFRP	PT CFRP	PT steel	Strand Splicing	Steel Jacket <sup>1</sup>	Replace Girder
Damage that may be repaired	Severe I	low Severe I	Severe I	Severe II	Severe II	Severe II	low Severe I	Severe II	Severe III
Active or Passive repair	passive	passive	passive	marginally active	active	active	active or passive	passive or marginally active	n/a
Applicable beam shapes	all	all	IB, limited otherwise	all	all	all	IB, limited otherwise	IB	all
Behavior at ultimate load	excellent	excellent	excellent	excellent	excellent	excellent	excellent	uncertain	excellent
Resistance to overload	limited by bond	limited by bond	good	limited by bond	good	excellent	excellent	uncertain	excellent
Fatigue	limited by bond <sup>2</sup>	limited by bond <sup>2</sup>	good	limited by bond <sup>2</sup>	excellent (unbonded)	excellent	poor	uncertain	excellent
Adding strength to non-damaged girders	excellent	good	excellent	excellent	excellent	excellent	n/a	excellent	n/a
Combining splice methods	possible	possible	unlikely	possible	good (unbonded)	good	excellent	excellent	n/a
Number of strands spliced	up to 25%	limited	limited by slot geometry	up to 25%	up to 25%	up to 25%	few strands	up to 25%	unlimited
Preload for repair <sup>3</sup>	no	no	no	no	no	no	possibly	possibly	n/a
Preload for patch <sup>3</sup>	possibly	no	yes	possibly	possibly	possibly	yes	no	n/a
Restore loss of concrete	patch prior to repair	patch prior to repair	patch prior to repair	patch prior to repair	patch prior to repair	patch prior to repair	excellent	patch prior to repair	n/a
Speed of Mobilization	fast	fast	moderate	moderate	moderate	moderate	fast	slow	very slow
Constructability	easy	easy	difficult	difficult	moderate	moderate	difficult	very difficult	difficult
Speed of repair	fast	fast	moderate	moderate	moderate	moderate	fast	slow	very slow
Environmental impact of repair process	VOCs from adhesive	VOCs from adhesive	VOCs from adhesive & concrete sawing dust	VOCs from adhesive	minimal	minimal	minimal	welding	typical erection issues
Durability	requires environmental protection	requires environmental protection	excellent	requires environmental protection	requires environmental protection	requires corrosion protection	excellent	requires corrosion protection	excellent
Cost	low	low	moderate	moderate	moderate	low	very low	moderate	high
Aesthetics	excellent	excellent	excellent	excellent	fair	fair	excellent	excellent	excellent

n/a: not applicable  
<sup>1</sup> Due to their complexity and the fact that they are untested, steel jacket repairs are not recommended; it is believed that CFRP repairs address all advantages of steel jackets while overcoming some of their drawbacks.  
<sup>2</sup> see Harries et al. (2006) for a discussion of fatigue of bonded CFRP repair systems.  
<sup>3</sup> Preload may be required for the repair or simply to pre-compress associated concrete patches. Jackets render the need to pre-compress the patch unnecessary.

In the next three sections, this report presents in depth information about strand splices and fiber reinforced polymer (FRP) repair methods and summarizes some of the additional techniques presented in NCHRP Report 226 and the research inspired by Report 226.

### **2.3.1: Strand Splice**

In the event that one or more strands are severed on a damaged prestressed girder, the severed ends can be reconnected using a strand splice or splice chuck. The re-connected strand

can then be stressed to reintroduce some or all of the force that was initially in the strand using one of three methods. The bridge can be preloaded introducing a negative moment, or upward camber, and after the strands are connected and the load removed, tension is induced. Another option is to heat the strand to cause strand elongation before the splice is connected. Once the strand cools, it shrinks and tension is introduced. The final technique is to use a wrench to torque the strand splice chuck and induce tension. As introducing a negative moment is not an option in most cases and strand heating may change the material properties of the strands, torquing the turnbuckle on the splice chuck is the most common way to induce tension into the severed strands (Harries, et. al., 2012). Commercial manufactures of splice chucks provide tables that associate a tensile force to a specified torque measured on a torque wrench (Prestress Supply Incorporated, 2010). Table 3 shows an example of a suggested installation torque chart to achieve 80% of ultimate strength in a strand based on strand size and ultimate strength.

**Table 3. Suggested Installation Torque Prestress Supply Incorporated. (2010). Grabb-It Cable Splice.**

**Retrieved December 12, 2014, from Prestress Supply:**

**<http://www.prestressupply.com/Products/StrandRepair/GRABBITCableSplice.aspx>, Used under fair use**

**2015**

GRABB-IT* CABLE SPLICE					
SUGGESTED INSTALLATION TORQUE VALUES					
STEM SIZE 3/4"-16 (UNF) NOM. DIA. 3/4" (.7500")					
STRESS AREA: .3750 IN <sup>2</sup> (EQUIV. GRADE 7)					
GRADE	CABLE			GRABB-IT*	
	CABLE DIA.	80% ULTIMATE (LBS)	ULTIMATE STRENGTH (LBS)	TORQUE VALUES	
				LUBRICATED	
				IN-LBS	FT-LBS
250 K	3/8"	16000	20000	1800	150
	7/16"	21600	27000	2430	203
	1/2"	28800	36000	3240	270
270 K	3/8"	18400	23000	2070	173
	7/16"	24800	31000	2790	233
	1/2"	33000	41300	3713	309

Installing strand splices is relatively quick and simple in comparison to other techniques. The concrete is removed around the damaged section and severed strands to provide room for the splice chuck. The area is then sand blasted and pressure washed to provide good patch concrete bond and to prevent the substrate from drawing moisture from the patch concrete during curing. If a preload negative moment is to be used, it is applied to shorten the strand length. The chucks are positioned in order to ensure that their weak points do not overlap, using additional strand extensions with wedges if necessary, then the turnbuckle is tightened to a specific torque, or a turn-of-the-nut method is used to apply the desired stress in the strands. The negative moment is then removed and a positive moment preload is applied and the patch material placed. After the concrete has had time to cure, the positive moment is removed. The result of the repair with the preloading is a spliced strand in tension with a concrete patch that is compressed (Zobel, Jirsa, Fowler, & Carrasquillo, 1997).

Depending on the size of the damage, the entire process takes a well-trained crew about one to three days from set-up until the patch has cured. Each splice chuck takes about 15 minutes to position and tightened to the desired tension. In addition, the cost of each splice chuck is roughly \$50-\$100 (Prestress Supply Incorporated, 2010). When using more than one strand splice, it is important to stagger the placement of the splice chucks so that a weakened point in the girder is not created. The large size of the splice chuck may require the removal of additional strands causing further reduction in the initial prestress force. The larger size and stiffness of the splice chuck can also cause unintended eccentricities and reduce the clear cover on exterior strands (Wipf, Klaiber, Rhodes, & Kempers, 2004b). Even with these issues, because of low cost and quick installation time, strand splices are often used in conjunction with other repair techniques (Harries, et. al., 2012). Figure 4 shows a splice chuck being tightened with a

torque wrench during the installation process. Figure 5 and Figure 6 show the layout for a repair using four and eight splice chucks respectively.



**Figure 4. Splice Chuck Installation**



**Figure 5. Four Splice Chucks**



**Figure 6. Eight Splice Chucks**

### **2.3.2: Fiber Reinforced Polymer (FRP)**

Fiber reinforced polymer (FRP) is a polymer matrix high performance fibers inside of it. The fibers can be made from aramid, carbon, glass, high performance steel, or a hybrid of these materials (Harries, et. al., 2012). Carbon fiber reinforced polymer (CFRP) laid as a unidirectional fabric is one of the most common forms of FRP and is supplied in large rolls of fabric. The CFRP system is composed of primer, putty, saturant, carbon fiber sheets, and a protective topcoat (Wipf, et. al., 2004b). Carbon fiber reinforced polymer has a tensile stress capacity about 1.5 times prestressing strands and a Young's modulus of 75% of that of steel (Harries, et. al., 2012). This is evident in the stress-strain relationship for carbon fiber shown in Figure 7 (Wipf, et. al., 2004b). These properties allow carbon fiber to reach a much higher strain than steel, but it does not have the plastic behavior or strain hardening characteristics associated with steel (Harries, et. al., 2012).

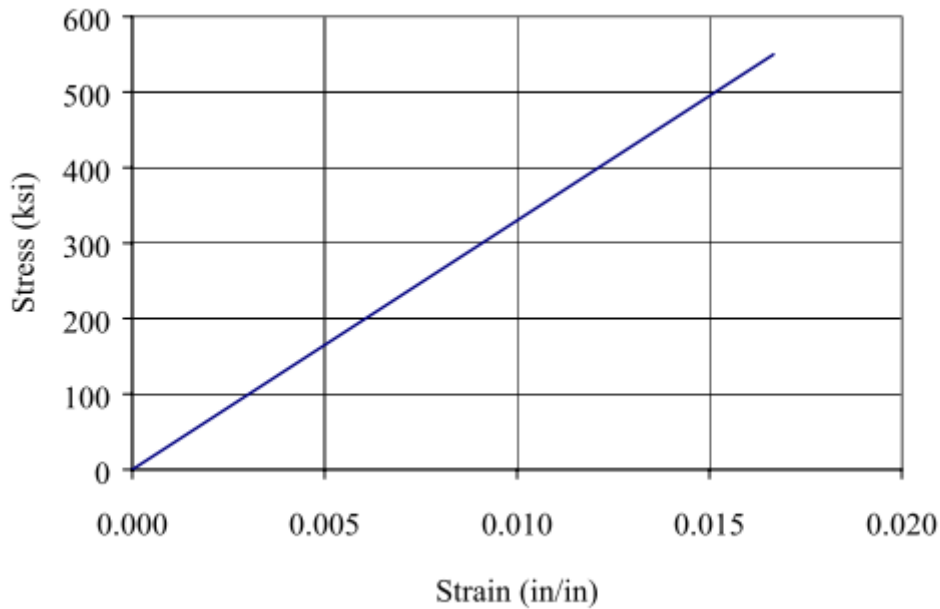


**Figure 7. Carbon Fiber Stress Strain Curve Wipf, T. J., Klaiber, F. W., Rhodes, J. D., & Kempers, B. J. (2004b). *Effective Structural Concrete Repair: Repair of Impact Damaged Prestressed Concrete Beams with Carbon Fiber Reinforced Polymer (CFRP)*. Iowa State University, Department of Civil, Construction, and Environmental Engineering. Ames: Iowa Department of Transportation. Retrieved December 12, 2014, Used under fair use, 2015**

FRP can be installed using various techniques. It can be installed as sheets or rolled fabric using a wet-lay process. External non-post tensioned FRP can be installed as preformed strips, or using rolls in a wet lay or a spray lay process. Preformed strips generally have a high fiber volume and are stronger and stiffer than wet lay fabrics. The strips are formed in a factory where their quality is under better control resulting in a more consistent and durable product. The wet lay fabric, however, is better for wrapping applications. When using CFRP, Table 4 can serve as a basis for determining the recommended maximum number of damaged 3/8 in, 250 ksi strands before a girder must be replaced (Harries, et. al., 2012). The table presents recommendations for externally bonded CFRP (EB-CFRP), bonded post-tensioned CFRP (bPT-

CFRP), unbonded post-tensioned CFRP (uPT-CFRP), and near surface mounted CFRP (NSM-CFRP). For example, in this project, an AASHTO Type III girder with 3/8 in, 250 ksi strands, using externally bonded CFRP, can have a maximum of eight damaged strands as indicated before a different repair technique should be selected or the girder replaced.

**Table 4. Recommended FRP Repair Based on Maximum Number of Damaged Strands Harries, K. A., Kasan, J., Miller, R., & Brinkman, R. (2012). *Updated Research for Collision Damage and Repair of Prestressed Concrete Beams*. NCHRP Project 20-07, Task 307, University of Pittsburgh, Department of Civil Engineering, Pittsburgh. Retrieved December 10, 2014, Used under fair use 2015**

Shape (PCI 2003)	H (in.)	b (in.)	typical strands <sup>3</sup> (PCI 2003)	equivalent 3/8" 250 ksi strand <sup>4</sup>						
				EB- CFRP	bPT-CFRP		uPT-CFRP		NSM- CFRP	
				n <sub>max</sub>	n <sub>max</sub>	n <sub>max-PT</sub>	n <sub>max</sub>	n <sub>max-PT</sub>	n <sub>max</sub>	
AASHTO I-girders	I	28	16	20	6	13	10	10	6	7
	II	36	18	30	7	15	11	12	7	8
	III	45	22	50	8	19	14	14	8	9
	IV	54	26	66	10	22	16	17	10	11
	V	63	28	80	11	24	18	18	10	12
	VI	72	28	80	11	24	18	18	10	12
	C <sup>1</sup>	40	22	50	8	19	14	14	8	9
Boxes	B-36	27, 33, 39	36	34	13	28	26	21	15	13
	B-48 <sup>2</sup>	& 42	48	46	17	37	34	29	20	18
Bulb Tees	BT	54, 63 & 72	26	40	10	22	16	17	10	11
Deck Tees	-	35, 53 & 65	25	32	9	20	17	16	10	10
Slabs	S-36	12, 15, 18	36	17	13	27	26	21	15	13
	S-48	& 21	48	23	17	37	34	29	20	18

<sup>1</sup> IB Prototype

<sup>2</sup> AB and SB prototype

<sup>3</sup> Typical number of strands in a section; taken as:

maximum number of strands that may be located in confines of the bottom flange or bulb;

maximum number of strands in one layer for slabs; or

<sup>4</sup> to convert tabulated values to...

equivalent 3/8" 270 ksi strand, multiply tabulated value by  $(0.080/0.085)(250/270) = 0.87$

equivalent 1/2" 250 ksi strand, multiply tabulated value by  $(0.080/0.144) = 0.56$

equivalent 1/2" 270 ksi strand, multiply tabulated value by  $(0.080/0.153)(250/270) = 0.48$

equivalent 0.6" 250 ksi strand, multiply tabulated value by  $(0.080/0.216) = 0.37$

equivalent 0.6" 270 ksi strand, multiply tabulated value by  $(0.080/0.215)(250/270) = 0.34$

FRP strips can be used to return some of the lost prestress through either pre-tensioning or post-tensioning the FRP strips. In order to install prestressed FRP, the material is stressed,

bonded to the concrete, and the stress is released once the epoxy has cured. Unbonded post-tensioned FRP transfers force through mechanical anchors that stress the material and lock it in place once the desired load is achieved. Bonded post-tensioned FRP is installed and stressed in the same way as unbonded post-tensioned FRP, but it is then bonded to the girder. This method reduces some of the adhesive creep since the adhesive system is not under stress (Harries, et. al., 2012).

Installing wet lay FRP takes longer than splice chucks because the concrete used to patch the damaged section must have time to cure before the primer and epoxy can be applied to it. Also, it is quite common to use strand splices in addition to the FRP. FRP repair is still relatively fast in comparison to replacing the entire girder. In order to install the FRP, first, the concrete is removed in the damaged section. The area is then sand blasted and pressure washed to provide a good surface for the patch concrete to bond with and to prevent the substrate from drawing moisture from the patch concrete during curing. If there are severed strands and splice chucks are to be used, they are installed as previously described. If a preload positive moment is to be used, it is applied and the patch material placed. After the concrete has had time to cure, the positive moment is removed. Next, the surface of the patch and the surface of the solid concrete of the original girder along the length required for the FRP is sanded to provide a rough surface for the epoxy to bond with. The epoxy is mixed creating a liquid saturant and a putty. A primer coat of saturant is applied to the girder, then a coat of putty is applied. The sheets of FRP are cut to length, soaked in the saturant and run through a roller to ensure that the liquid has penetrated all of the fibers. It is then spread over the first layer of putty and any air pockets or inconsistencies are worked out.

If more layers are required, the putty is spread across the outside of the FRP sheet and the process is repeated. The final layer of FRP is laid perpendicular to the direction of the sheets to provide confinement and strength in the transverse direction. The direction of the sheets can be alternated by layer if additional strength is needed in either direction. After the last layer of sheets is applied, a final layer of putty is spread across the fabric sheets in order to provide some protection and ensure a good bond (Zobel, et. al., 1997). Depending on the size of the damage, the entire process takes a well-trained crew about one week from set-up until the epoxy has cured.

While using FRP has many advantages, there are some things that the designer must consider. The epoxy is susceptible to ultraviolet and fire damage and must be protected in some fashion. The material properties of the various types of FRP are different than steel and need to be considered as they will change the behavior of the girder from its original design. While the strength of the FRP is greater than with steel, it is stiffer and lacks the plastic behavior which can result in a more sudden failure mode. If too much material is used, the result may be a compressive failure rather than a tension failure. Also, it takes a specially trained crew to install the system. If it is not installed correctly, there is potential for the epoxy to set incorrectly resulting in an insufficient bond which may cause the material to “un-zip” from the girder (Wipf, et. al., 2004b). Figure 8 shows the saturation process for a wet lay-up FRP strip, Figure 9 shows an externally bonded wet-lay FRP being installed, and Figure 10 shows the final product.



**Figure 8. Fiber Reinforced Polymer Saturation Process**



**Figure 9. Fiber Reinforced Polymer Installation Process**



**Figure 10. Fiber Reinforced Polymer Installed Over Damaged Section**

### **2.3.3: Additional Techniques**

Most of the techniques for repair presented in NCHRP Report 226 by Shanafelt and Horn (1980) made use of a vertical preload to restore precompression to patch materials and reduce tensile stresses during live loads. Preloads are introduced as either a positive or a negative moment and are most effective in systems that have a smaller dead-to-live load ratio. External post-tensioning used steel rods, strands, or bars anchored to the exterior of the girder, which can be tensioned to induce a stress to the cross section. The design of these systems is fairly simple and similar to the design of an unbonded post tensioned system; however, the designer needs to consider the eccentricity of the externally applied forces. Steel jacketing is a method that involves encasing the girder with steel plates that act as a jacket for the girder to restore it to its original capacity (Harries, et. al., 2012). In the event that a damaged girder is assessed as a category severe III, or sufficient capacity cannot be obtained through any of the repair techniques

discussed, the best, yet most expensive and time consuming, course of action is to replace it (Kasan, 2009).

FRCM consists of a cementitious matrix and a fiber grid. The matrix is impregnated through the mesh to form a bond between the fabric strands and the girder. The grid geometry of FRCM gives it advantages when compared to FRP. One of the advantages to a grid geometry is bi-axial strength. This bi-axial strength allows for the system to provide shear resistance without requiring additional layers in the transverse direction as required by FRP. By reducing the amount of materials the number of applications, the FRCM will also reduce the risk of overdesign due to the necessity of additional layers to resist secondary stresses. The designer, however, must be aware of the potential to over design FRCM similar to FRP. Installation of FRCM requires skilled laborers and temperature during installation must be managed as much as possible to ensure that it does not affect long term performance (ACI Committee 549, 2013).

#### **2.4: Summary**

Based on the literature review, three repair methods were identified for experimental investigation: strand splice, bonded FRP, and FRCM. Strand splices were investigated because they are an active repair method which is economical and easy to install. Externally-bonded FRP was chosen as a passive repair because it is currently one of the primary methods being used in the industry and has a low life cycle cost. FRCM was chosen because it is a relatively new repair method and has benefits over FRP such as biaxial strength and not relying on epoxy to create a bond. Table 5 delineates the breakdown of responsibilities for investigating and reporting within the project.

**Table 5. Project Scope Responsibilities and Summary**

<b>Girder</b>	<b>Test</b>	<b>Description</b>	<b>Investigator</b>	<b># Severed Strands</b>
<b>A</b>	<b>1</b>	<b>Control Test</b>	Mark Jones, Justin Liesen	0
<b>B</b>	<b>2</b>	<b>8-Strand Spliced</b>	Mark Jones, Justin Liesen	8
<b>C</b>	<b>3</b>	<b>4-Strands Severed with FRP</b>	Justin Liesen	4
	<b>4</b>	<b>4-Strand Spliced</b>	Mark Jones, Justin Liesen	4
<b>D</b>	<b>5</b>	<b>4-Strands Severed with FRCM</b>	Mark Jones	4
	<b>6</b>	<b>4-Strand Spliced with FRCM</b>	Mark Jones	4

### **CHAPTER III: Experimental Testing Methods**

During this investigation three repair methods were evaluated by conducting six flexural tests on four AASHTO Type III girders. Flexural tests were conducted instead of shear tests because typical impact damage from overheight vehicles occurs around the mid-span and flexural strength dominated region of bridge girders. Figure 11 shows the cross section of the girder from the VDOT design drawings. Section A-A is a typical support cross section and section B-B is a typical section between strand harping points. Figure 12 shows a cross section of the AASHTO Type III girder with a section of deck as tested. The deck width varied across the length of the girder and varied between tests. The variation in the deck width resulted when the girder and deck sections were removed from the bridge by saw cutting through the deck along the edge of the prestressed girder top flange. The approximate deck width for girder A was 16 in and was 11 in for girders B and C.

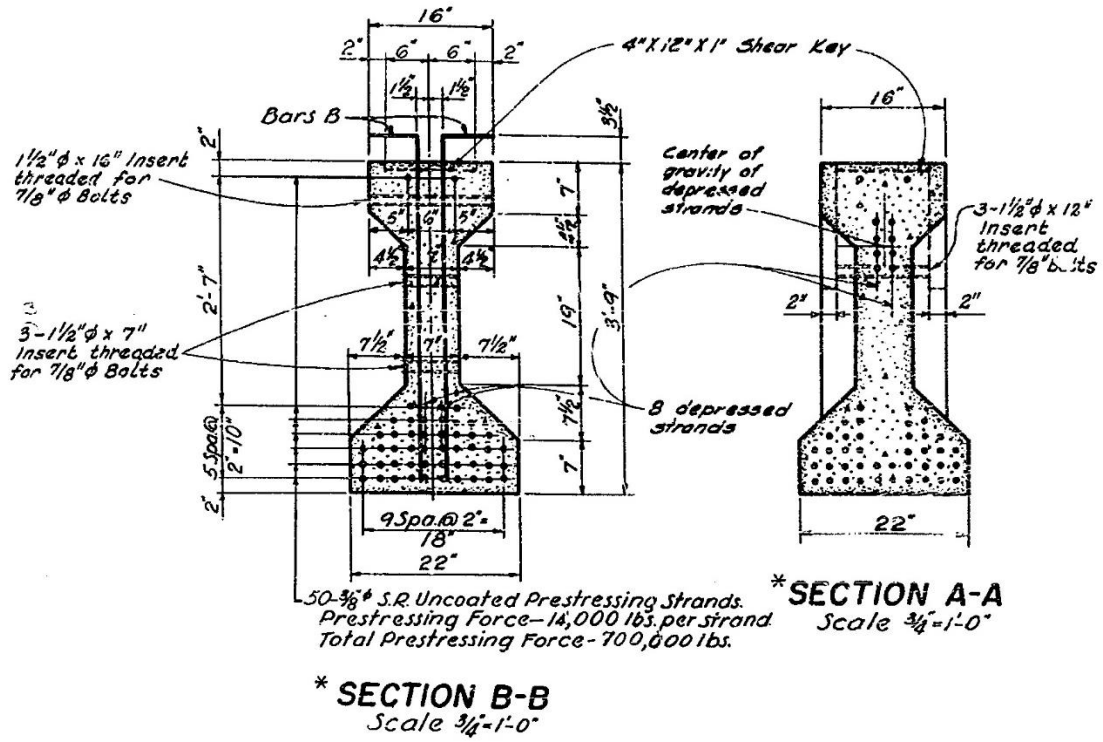
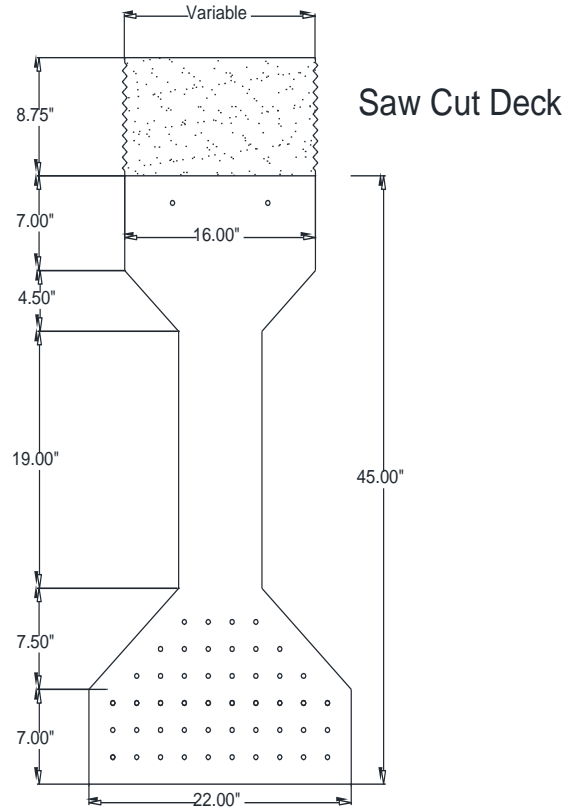


Figure 11. Girder Cross Section from Bridge Plans



**Figure 12. Typical AASHTO Type III Girder Cross Section Tested**

The shear reinforcement spacing of No 5 bars in the girder, shown in Figure 13, was analyzed during the set-up of each test in order to evaluate potential failure modes. The shear reinforcement type and spacing was identical in each of the test girders. The intent was to achieve a flexural failure in each test. The first test was a flexural test of a 44 ft long unrepaired section of Girder A to establish a baseline for comparison with the subsequent tests. The second test was a flexural test on a 60 ft girder, Girder B, which was damaged and repaired at midspan using the strand splice method. The third and fourth tests were flexural tests on one 60 ft girder, Girder C, which was damaged and repaired at the third points. This was done to maximize the number of tests conducted with the finite number of specimens. For this girder, the two repair techniques implemented were strand splice and Fiber Reinforced Polymer (FRP). The fourth and

fifth tests were flexural tests on one 60 ft girder, Girder D, which was damaged and repaired at the third points also. For this girder, the two repair techniques implemented were Fabric Reinforced Cementitious Matrix (FRCM) independently and FRCM in conjunction with strand splice.

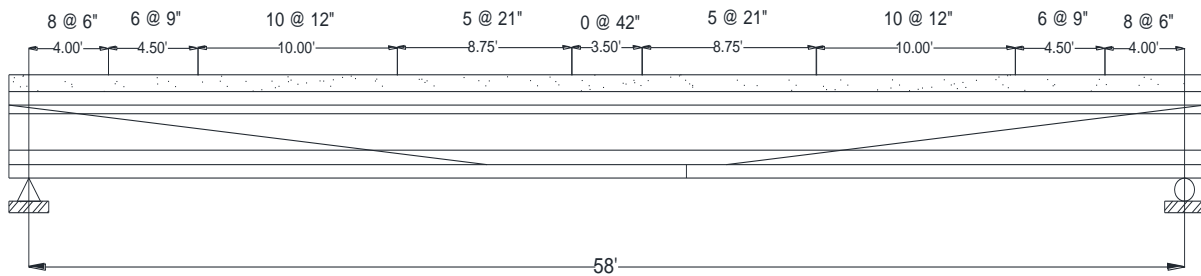


**Figure 13. Shear Reinforcement Spacing for No 5 Reinforcing Bars**

Table 6 delineates the testing schedule for this project, identifies the researcher responsible for investigating and reporting on each test, and summarizes the set-up. Tests one through four will be discussed in this report. Tests five and six are discussed by Jones (2015). Figure 14, Figure 15, Figure 17, Figure 18, Figure 19, Figure 20, Figure 21, and Figure 22 show the layouts for each test. Also shown in these figures is the instrumentation used which is discussed in subsequent sections.

**Table 6. Testing Schedule and Summary**

Girder	Test	Description	Investigator	# Severed Strands	Span Length (ft)	Distance to Load Point 1 (ft)	Distance to Load Point 2 (ft)
A	1	Control Test	Mark Jones, Justin Liesen	0	35	12.5	16.5
B	2	8-Strand Spliced	Mark Jones, Justin Liesen	8	58	25	33
C	3, Iteration 1	4-Strands Severed with FRP	Justin Liesen	4	48	17	21
	3, Iteration 2				53	17	21
	4, Iteration 1	4-Strand Spliced	Mark Jones, Justin Liesen	4	58	37	41
	4, Iteration 2				50	29	33
D	5	4-Strands Severed with FRCM	Mark Jones	4	52	31	35
	6	4-Strand Spliced with FRCM	Mark Jones	4	52	17	21

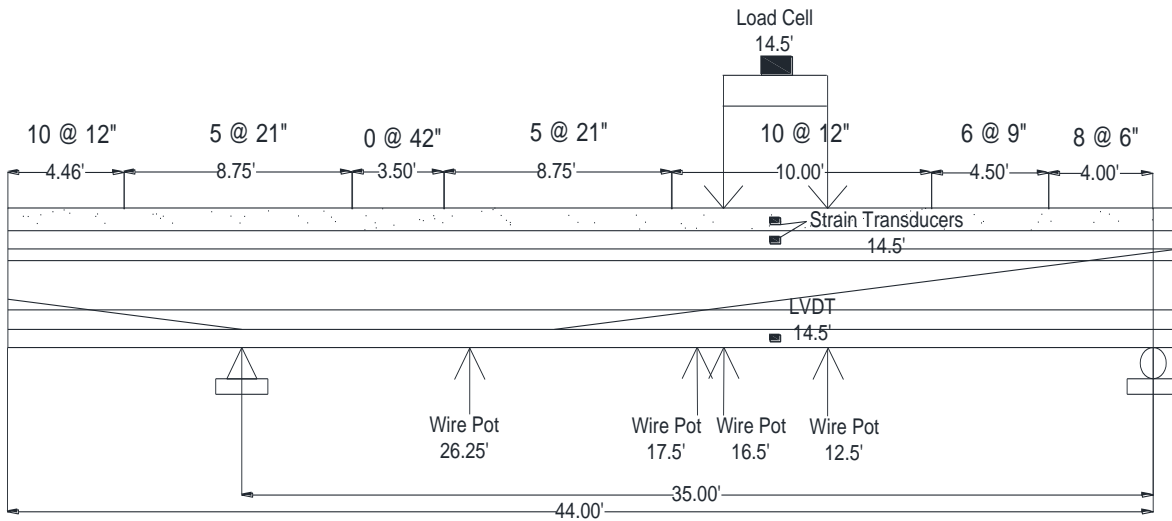


**Figure 14. Test 1 Set-up**

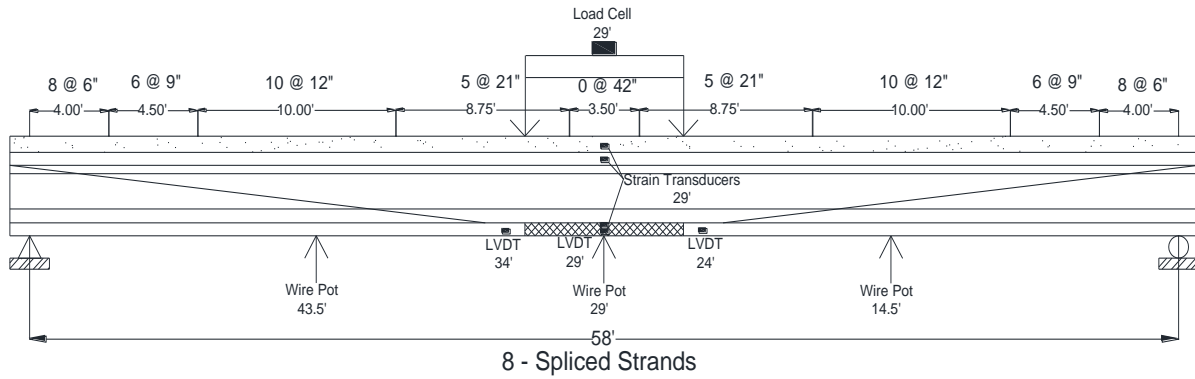


**Figure 15. Test 2 Set-up**

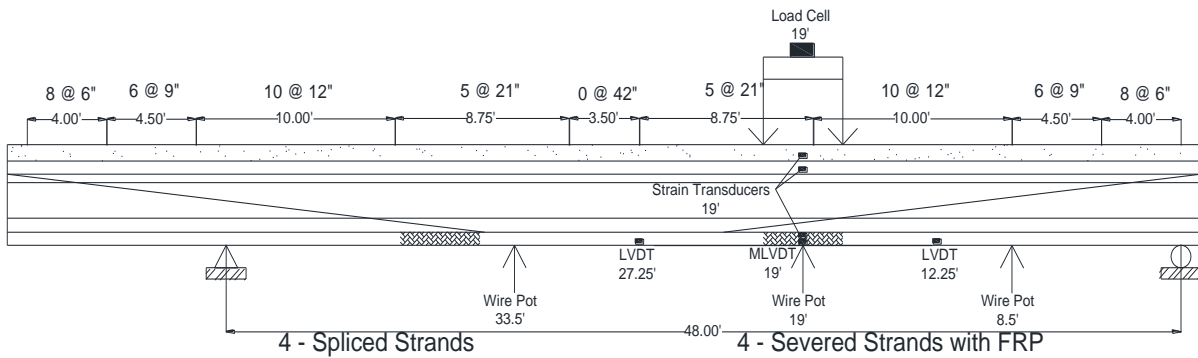


**Figure 16. Test 3, Iteration 1 Set-up**

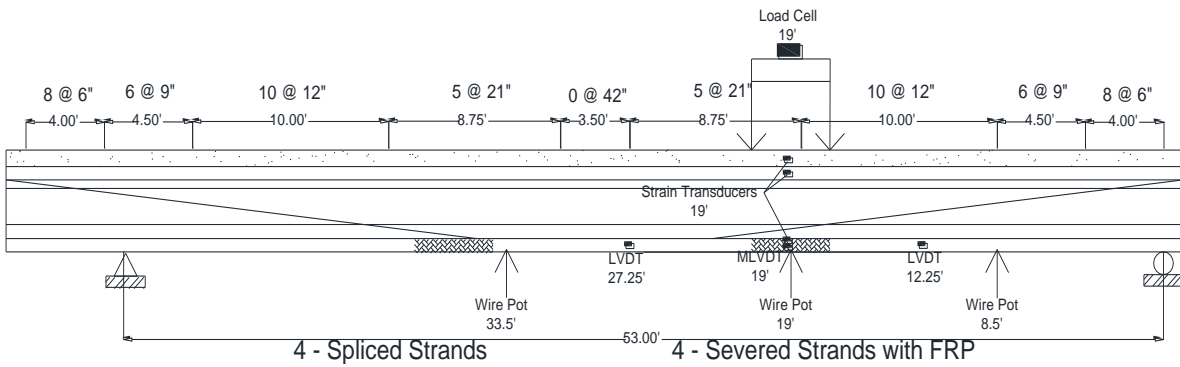


**Figure 17. Test 3, Iteration 2 Set-up**

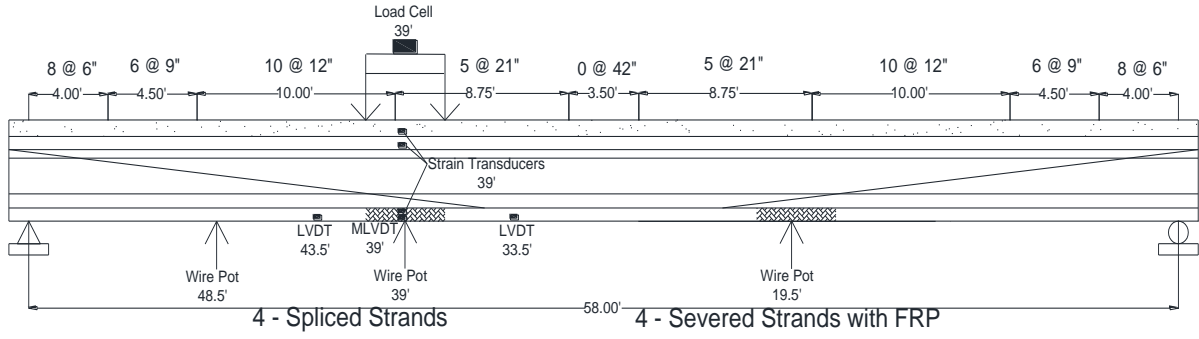


**Figure 18. Test 4, Iteration 1 Set-up**

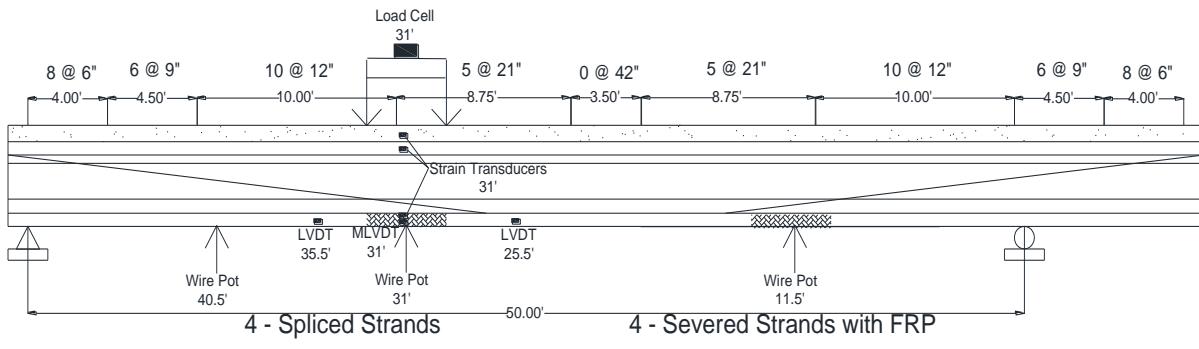


**Figure 19. Test 4, Iteration 2 Set-up**

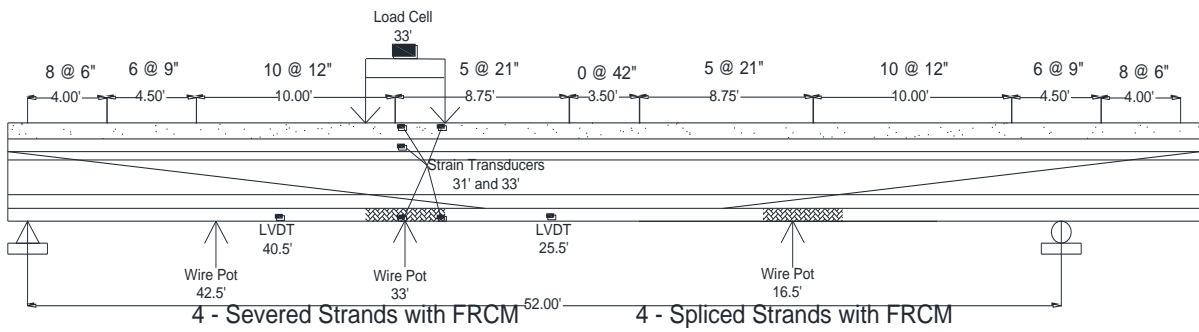


**Figure 20. Test 5 Set-up**

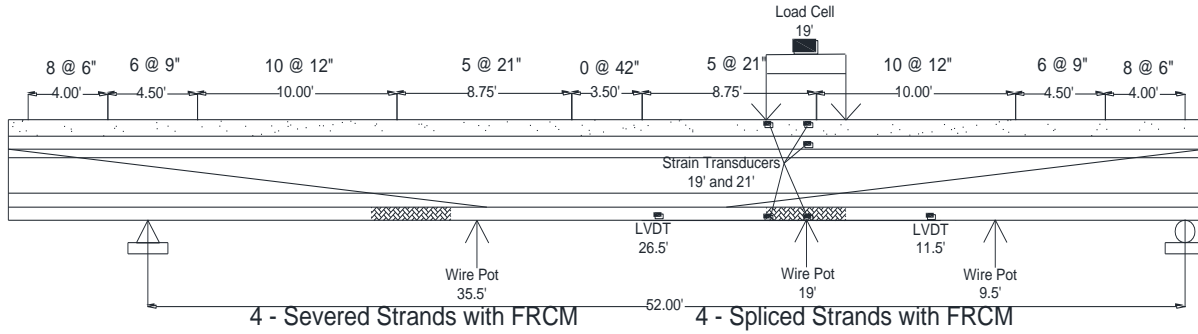


**Figure 21. Test 6 Set-up**

Girders B, C, and D were intentionally damaged in order to simulate the damage caused by overheight vehicle impact. The girders were laid on their sides and struck with a hydraulic hammer attached to a backhoe. After a representative section of concrete was removed several prestressing strands were severed.

After the girders were damaged, Structural Technologies provided personnel, materials, and expertise to repair the damaged locations. Structural Technologies is a member of Structural Group that specializes in the repair of damaged structures (Structural Group Incorporated, 2015). Girder B was a strand splice repair on eight severed strands and was used in Test 2. A strand splice repair was done on one end of Girder C on four severed strands and used in Test 3. On the other end of Girder C, a FRP repair was done with four severed strands and used in Test 4. Once the repairs were complete, the girders were set up for flexural tests to determine the effective strength regenerated by the repairs in comparison to the initial strength of the undamaged girder.

### **3.1: Materials Testing**

In order to accurately predict the experiment results and determine the contributing factors to the failure modes, material tests were conducted for the concrete in the girder, the concrete in the deck, the girder reinforcement, and the repair materials. Repair materials include the Grabb-it Strand Splice system (Prestress Supply Incorporated, 2010), the Tstrata Infuseable

Rapid Cure Restoration Material (Tstrata IRC) used to patch the damage, the V-Wrap C400 carbon fiber fabric, the V-Wrap 700 epoxy, and the V-Wrap composite system (Structural Group Incorporated, 2015). Compression tests as per American Society for Testing and Materials (ASTM) C42 were conducted on the concrete in the deck and girder, and as per ASTM C496 on the Tstrata IRC cylinders. Tensile tests were conducted on the prestress strands as per ASTM A416, reinforcing bars as per ASTM A615, and the concrete in the girder as per ASTM C496. Direct tension as per ASTM D3039, interlaminar shear as per ASTM D2344, tensile bond as per ASTM D7234, and glass transition temperature tests as per ASTM E1640 were conducted on the components of the V-Wrap composite system (Pino & Nanni, 2015). The Grabb-it cable splices were tested to determine the relationship between the torque applied on the turnbuckle to the tensile stress induced into the strands. Also, tensile strength tests were conducted on the Grabb-it cable splice and strands (Bao, 2015). In addition, when cutting strands during the damage phase of the tests, strain gauges were placed on the strands to attempt to quantify the effective prestress in the strands.

Tstrata IRC is a premixed, dry packaged, rapid cure, self-consolidating concrete mixture used for damage repair (Structural Group Incorporated, 2015). The V-Wrap C400 FRP composite system is comprised of the C400 FRP and the 700 epoxy. The C400 fabric is a unidirectional carbon fiber fabric that is 0.08 in thick. The 700 epoxy resin is a high strength bonding matrix used for adhering the FRP to the girder (Structural Group Incorporated, 2015).

A concrete core drill was used to remove four cylinders from the girder cross section and two cylinders from the deck of Girder A as shown in Figure 22. On June 11, 2014, two cylinders from the girder and two cylinders from the deck were used to conduct an ASTM C42 compression test (ASTM International, 2015). The cylinders were 2.75 in in diameter and

approximately 6 in long. The other two cylinders from the girder were used to conduct an ASTM C496 splitting tensile test (ASTM International, 2015).



**Figure 22. Concrete Core Removal (Photo used with permission of Mark Jones, 2015)**

During the repair of the damaged sections on July 16, 2014, six cylinders with a 4 in diameter were made from the Tstrata IRC repair concrete for compressive strength testing using the ASTM C39 compression test. On July 17, 2014, two cylinders were tested for their 24 hour compressive strength. On July 18, 2014, two cylinders were tested for their 48 hour compressive strength. On July 18, 2014, two cylinders were tested for their 48 hour compressive strength. On July 23, 2014, two cylinders were tested for their 7 day compressive strength.

Two sections of No 4 reinforcing bar approximately 3 ft long were removed from Girder A. Load was applied at a rate of 0.05 in per minute for the first 4 minutes and increased to 0.5 in per minute until the bars ruptured after a total of 8 minutes. The test was conducted on two separate pieces of reinforcement.

To determine the material properties of the prestressing steel, two 4 ft long pieces of prestressing strands were extracted from Girder A. The strands were prepared for testing following the procedures developed by Salomon (2014) and Loflin (2008). Copper tubing was used to pad the strands to mitigate the potential for a premature failure from a stress riser caused by the grips. The tubing had an interior diameter of 0.5 in. It was cut in half lengthwise and cut into approximately 10 in long sections. The sections were sand blasted to create a rough surface for the best condition to bond with the epoxy. The epoxy mix was made from West System 105A epoxy resin, West System 205 epoxy hardener, and 120 Aluminum Oxide Grit with a ratio of 5 fluid ounces of grit to 5 squirts each from the manufacturer provided pump of the epoxy resin and hardener. The epoxy and grit mixture was poured into each half of the copper tubing and each end of the strand was sandwiched between the tubing halves. The tubing was held together with clamps and the epoxy was allowed to dry for a minimum of 24 hours. The strands were placed in the SATEC universal machine and the hydraulic V-grips were used to grip the copper tubing on either end of the strand as shown in Figure 23. Data was recorded using the SATEC internal extensometer, the internal load cell, an external wire pot attached to the bottom of the SATEC loading platform, and an external extensometer placed on the strand. The tension test results indicate that the strands are grade 250 ksi (Nilson, 1987).



**Figure 23. Prestress Strand Tensile Test**

In order to determine the effective prestress in the strands, an extensometer was attached to the strands on Girder D as shown in Figure 24. The extensometer was used to measure the change in length of the strands when cut. The strands were cut with an electric grinder and steel cutting blade as shown in Figure 25. The extensometer was positioned on the strand more than 6 in from the location of the cut depending on the amount of damage around the strand as shown in

Figure 26. This distance was chosen to minimize the effects of temperature change during the cutting process. Six strands were cut with an extensometer attached to them. Based on these values, it can be determined that the extensometer slipped on the second, third, fourth, and sixth strands. The stress for the second, third, and sixth strands were past the yield stress and indicate that the elastic assumption associated with the stress-strain relationship is not valid. The fourth strand's stress indicated that it was in compression. In these cases, acknowledging the vibrations caused by the grinder while cutting the strands and the violent shortening of the strand as each wire was cut, the most likely cause of the variation was due to slipping of the instrumentation during testing. When averaging the first and fifth strands, the effective prestress force was 132 ksi.

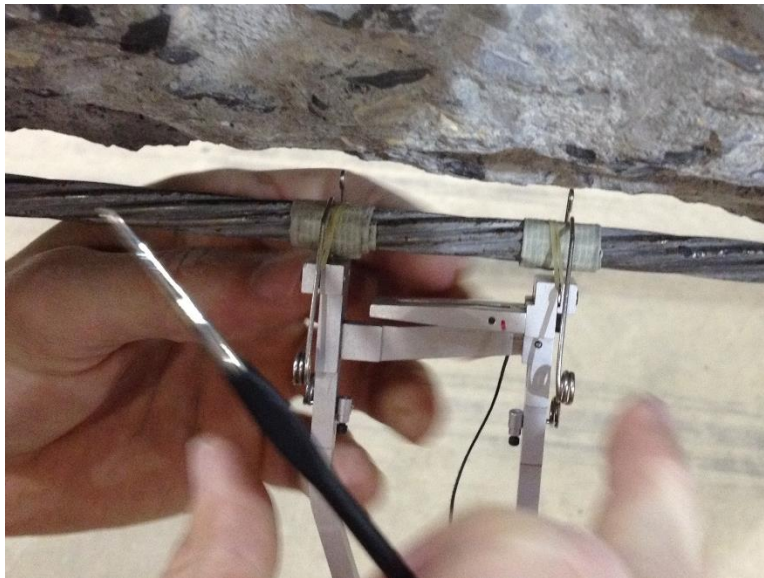


**Figure 24. Extensometer Attached to Strand (Photo taken by Mark Jones, used under fair use 2015)**



**Figure 25. Cutting of Strands (Photo taken by Mark Jones, used under fair use 2015)**



**Figure 26. Extensometer Location on Strand (Photo taken by Mark Jones, used under fair use 2015)**

Material property tests for the FRP were conducted at the University of Miami (Pino & Nanni, 2015). Two thicknesses of FRP were tested in direct tension. Tests were performed on V-Wrap C200 and V-Wrap C400 samples. C400 samples were used in this project. Direct tension tests were conducted on five single and five double ply samples of both C200 and C400 in ambient environmental conditions. These tests were used to determine the modulus of elasticity, ultimate tensile stress, and ultimate tensile strain (Pino & Nanni, 2015).

Tension tests of the Grabb-it splice device were conducted (Bao, 2015). Prestressing strands were anchored between two steel abutments with a strand splice between them. The abutments were placed 16 ft apart for the first test, 6 ft apart for the second test, and 4 ft apart for the third test. The strand was attached to a load cell and the splice was tightened using a calibrated torque wrench and readings were taken at specified torque values to compare to the theoretical value given by the manufacturer in Table 3. After completing the torque test, the strands were loaded to failure. In all tests, the strands reached failure before the splice chunk.

### **3.2: Instrumentation Types**

This section will discuss the different instruments used to monitor girder behavior during testing. The layout used in each test will be described in subsequent sections. The following instrumentation was used: Linear Variable Differential Transformers (LVDT), Miniature Linear Variable Differential Transformers (MLVDT), Strain Transducers, Potentiometers, Extensometers, and Load Cells. The LVDT, MLVDT, and strain transducers were used to measure the surface strain in the girder. The potentiometers were used to measure vertical deflection and lateral movement of the girder. The extensometers were used to measure the strain in the prestressing strands and reinforcing bar during material tests. The load cells were used to measure the applied loads during testing.

Linear Variable Differential Transformers were used to measure the concrete surface strain in the girders. They were calibrated to 0.001 in and zeroed prior to each test.

Mini Linear Variable Differential Transformers are a shorter version of the LVDT and were used to measure the concrete surface strain in the girders. They were calibrated to 0.001 in and zeroed prior to each test.

Strain transducers were used to measure length changes. The changes in length were used to calculate strain in the girder. They were calibrated to 0.001 in and zeroed prior to each test.

Potentiometers were used to measure vertical deflection and lateral movement of the girders. They were calibrated to 0.001 in and zeroed prior to each test. Potentiometers were also used to determine changes in length when conducting material tests on prestressing strands and reinforcing bars.

An extensometer was used to measure length during material tests on prestressing strands, reinforcing bars, and when determining effective prestress. It was calibrated to 0.001 in and zeroed prior to each test.

A load cell was used to measure the applied load to the girder. It was calibrated to 1000 lb and zeroed prior to each test. Load cells were also used to measure applied loads in material tests.

### **3.3: Test Procedures**

#### **3.3.1: Test 1 – Control Test**

Girder A had significant collision damage and sustained additional damage during removal and transportation from the bridge site to the laboratory. Due to this damage, a 16 ft section broke off and was used to provide samples for concrete, reinforcing bar, and strand

materials testing. The remaining 44 ft section of the girder was used as a control to determine the unrepaired girder flexural strength. The supports were located to create a 35 ft span length which avoided damaged areas near the girder's end. In addition, the load points were not at midspan, rather they were set at 12.5 and 16.5 ft from one support. This was done to minimize the potential of a shear failure and maximize the potential for a flexural failure based on the layout of the shear reinforcement and the strand harping point.

In order to develop the plan for the test set-up and decrease the probability of a shear failure while ensuring the desired flexural failure, the girder nominal moment and shear capacities were determined using provisions of AASHTO LRFD Bridge Design Specification (American Association of State Highway and Transportation Officials, 2012) and the girder material properties (Jones, 2015). The nominal moment capacity of this girder at the points of load application was 2940 k-ft. This corresponds to a calculated load of 348 kips. Figure 27 shows the nominal moment capacity of the tested section of Girder A and the maximum calculated moment resulting from a load of 348 kips. Figure 28 shows the absolute values of the nominal shear capacity of Girder A and the maximum shear force resulting from a load of 348 kips. As shown in Figure 28, the maximum shear force is close to, but less than, the nominal shear capacity at about 13 ft and around 18 ft from the left support. Other loading arrangements were investigated, however this loading arrangement was chosen to minimize the potential for a shear failure since the desired failure mode was flexural (Jones, 2015).

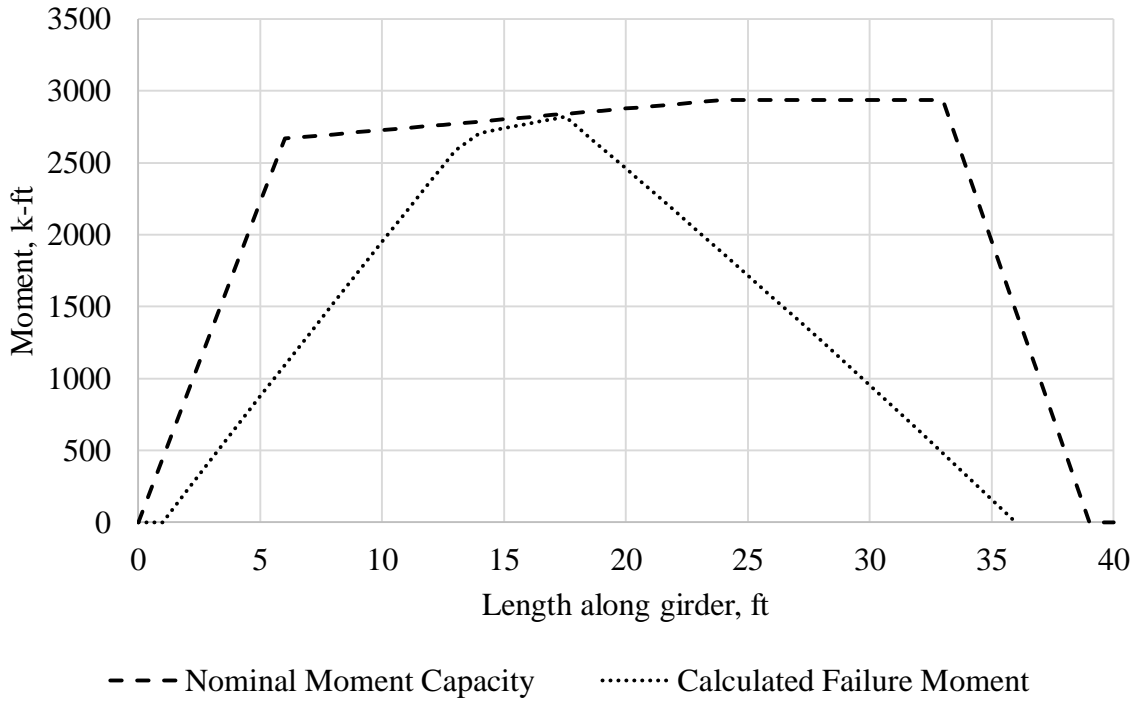


Figure 27. Nominal Moment Capacity versus Calculated Failure Moment for Test 1

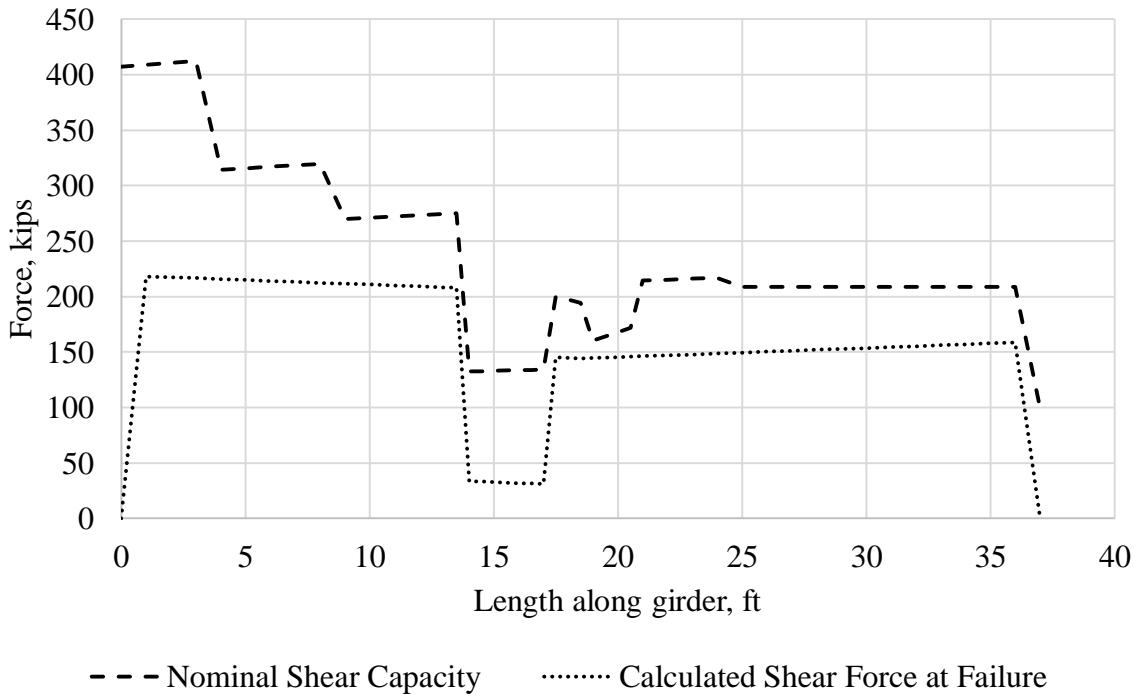


Figure 28. Nominal Shear Capacity versus Calculated Shear for Test 1

Test 1 was a flexural test of a 44 ft section of Girder A with a 35 ft simple span length. The section was supported on two W21x101 steel sections with a pin bearing on one steel section and a roller bearing on the other. The original sole bearing plate on the girder was placed on top of the roller bearing while rubber pads were used between the pin bearing and the bottom flange of the girder. Figure 29 and Figure 30 show the set-up of the pin and roller bearings. Two frames were used to prevent the girder from tipping from lateral deflection during the test. Figure 31 shows one side of a frame. A third frame was used to hold a 400 kip hydraulic actuator above the load points. The actuator exerted a force on a 6 ft long steel spreader beam resting on two neoprene and steel laminate bearings. The load points were chosen to create a constant moment region in the area that a flexural failure was desired. Figure 32 shows the loading system set-up with the actuator, spreader beam, load frame, and laminate bearings.



**Figure 29. Pin Bearing (Photo taken by Mark Jones, used under fair use 2015)**



**Figure 30. Roller Bearing (Photo taken by Mark Jones, used under fair use 2015)**



**Figure 31. Frame to Prevent Tipping**



**Figure 32. Control Test Loading System (Photo taken by Mark Jones, used under fair use 2015)**

Data was continuously recorded using a high speed data acquisition system. Figure 33 shows the instrumentation layout along the length of the girder. Four wire pots were attached to the bottom of the girder to measure vertical deflection during the test. Figure 34 shows the set-up for wire pots 2 and 3 located directly below the load points. Two LVDTs and two strain transducers were used to record a strain profile within the constant moment region during the test. They were all placed directly under the centerline of the load point. One LVDT was placed on each side of the bottom flange of the girder at 2 in from the bottom of the girder to measure the associated strain of the bottom prestress strand while the girder was still in the elastic range and strain compatibility could be assumed between the concrete and the strand. The strain transducers were placed on the side of the girder at 41 and 49 in from the bottom of the girder. A 400 kip load cell was placed between the actuator and the load frame to measure the applied load.

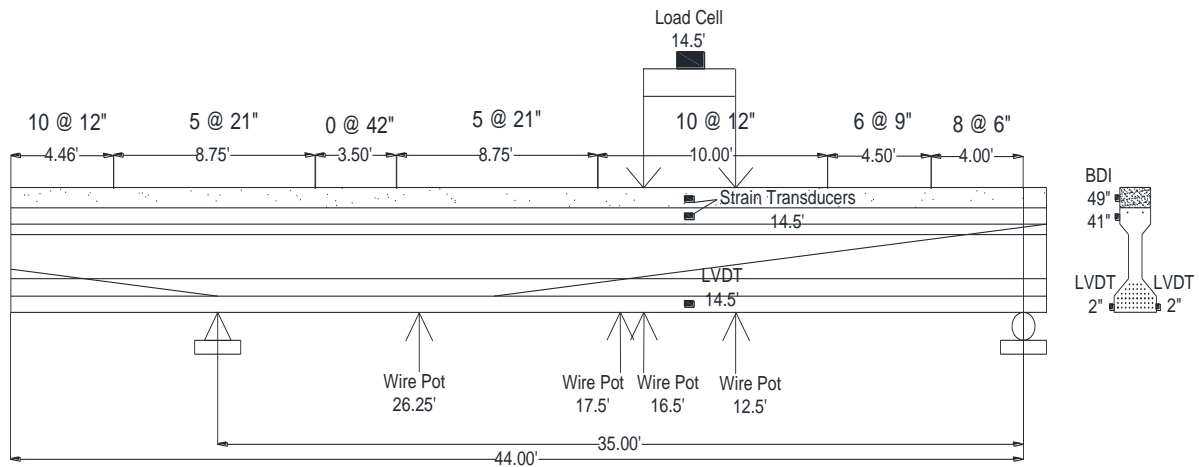


**Figure 33. Test 1 Set-up and Instrumentation Plan**



**Figure 34. Wire Pots below Load Point to Measure Deflection (Photo taken by Mark Jones, used under fair use 2015)**

The girder was tested on May 27, 2014 up to a load of 353 kips and a deflection of 1.43 in. Initially, the rate of loading was managed to ensure there were not effects from sudden or impact loading. The load was held at approximately 20 kip increments to allow the girder to settle under the load before it was inspected. At each pause, the girder was inspected and cracks

were highlighted and marked. This pace of loading was used from 0 to 280 kips of total load. After 280 kips (for safety reasons), the strain transducers were removed and inspection ceased. The hydraulic pump malfunctioned at 353 kips and a second test was conducted on June 2, 2014 after the pump was replaced. During the second test, the girder was re-loaded. The test was conducted in a similar manner. The load was increased at 50 kip increments from 0 to 250 kips. The rate of increase was reduced to 20 kips until the load reached 401 kips and was stopped because it exceeded the design capacity of the test frame.

### **3.3.2: Test 2 – Girder with Eight Severed/Re-tensioned Strands**

Girder B was a 60 ft long girder that was damaged for 4 ft on either side of midspan. Of the 48 prestressing strands in the bottom flange of the girder, eight were intentionally severed during damaging. The location of the damage is shown in Figure 35. The locations of the strands that were severed are shown in Figure 36. Eight ft was chosen as the length for the damage on Girder B based on data from the YRC Freight Company indicating the average width of a semi-trailer as approximately 8 ft (YRC Worldwide, 2015).

Wipf, Klaiber, Rhodes, and Kempers (2004a) reported that some departments of transportation replace a girder if any strand is damaged from the impact of overheight vehicles. Other departments of transportation reported that a prestressed girder is replaced when 10% of strands were damaged. The maximum number of damaged prestress strands allowed to be repaired by any state before the damaged girder would be replaced was 25%. In addition, based on results in Table 4, eight damaged strands on an AASHTO Type III girder is the maximum number of strands to efficiently repair using externally bonded FRP (Harries, et. al., 2012). Considering this information, damaging 17% of strands or eight strands was chosen. Subsequent girders were inflicted with less damage so the data from tests could be scaled to compare results.

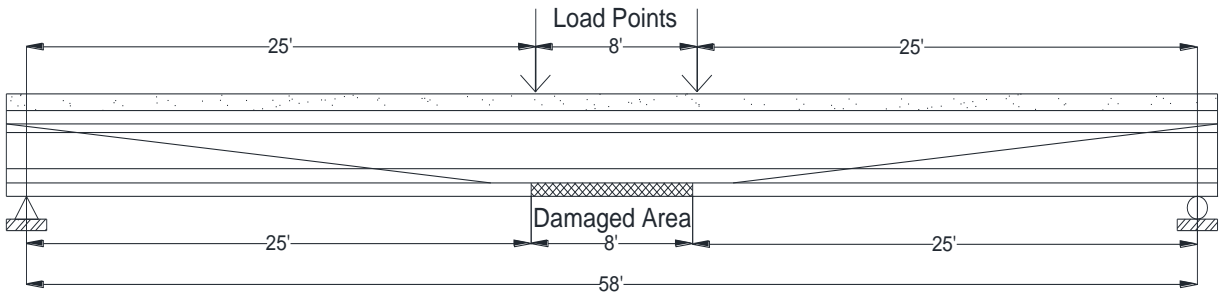


**Figure 35. Girder B Damage Location**

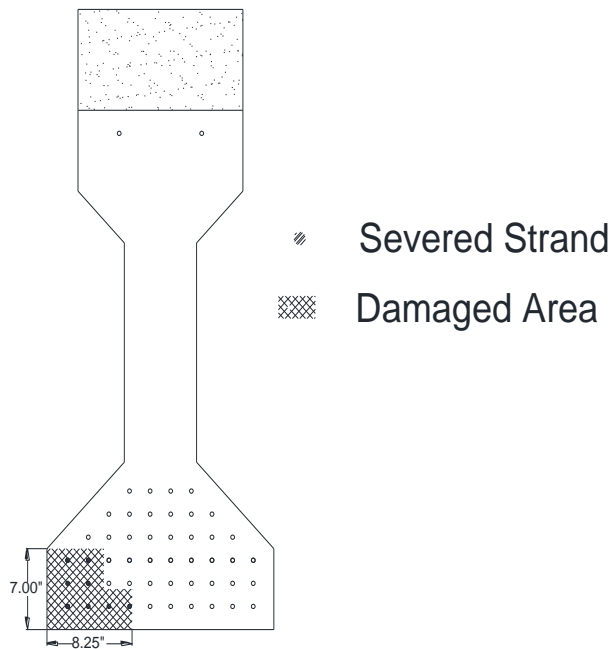


**Figure 36. Girder B Cross Section through Damaged Area with Severed Strand Locations Shown**

Structural Technologies conducted the repair of the eight severed strands on Girder B with Grabb-It strand splices. The splices were tightened with a torque wrench to 150 ft-lbs which corresponds to 80% of ultimate strength or 160 kips based on the Table 3 provided by the manufacturer (Prestress Supply Incorporated, 2010). After the strands were spliced, they were encased in Tstrata IRC high strength, quick cure concrete. APPENDIX H: gives the repair procedures followed for the repair concrete. APPENDIX I: Installation of Strand Splices gives the repair procedures followed for the strand splices.

In order to develop the plan for the test set-up and decrease the probability of a shear failure while ensuring the desired flexural failure, the girder nominal moment and shear capacities were determined using the provisions of AASHTO LRFD Bridge Design Specifications (American Association of State Highway and Transportation Officials, 2012) and the tested girder material properties (Jones, 2015). The nominal moment capacity of this girder at the points of load application was 2620 k-ft. This corresponds to a load of 176 kips. Figure 37 shows the nominal moment capacity of Girder B and the maximum calculated moment resulting from a load of 176 kips. Figure 38 shows the absolute values of the nominal shear capacity of Girder B and the maximum calculated shear force resulting from a load of 176 kips. Other loading arrangements were investigated, however this loading arrangement was chosen to minimize the potential for a shear failure since the desired failure mode was flexural (Jones, 2015).

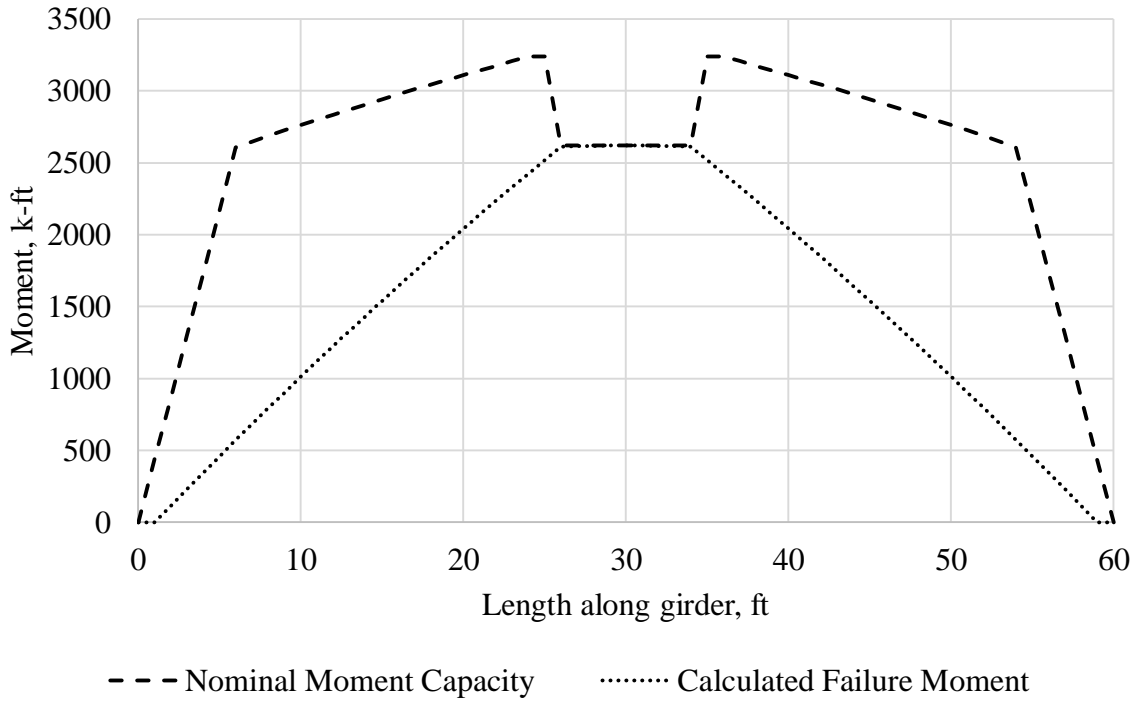


Figure 37. Nominal Moment Capacity versus Calculated Failure Moment for Test 2

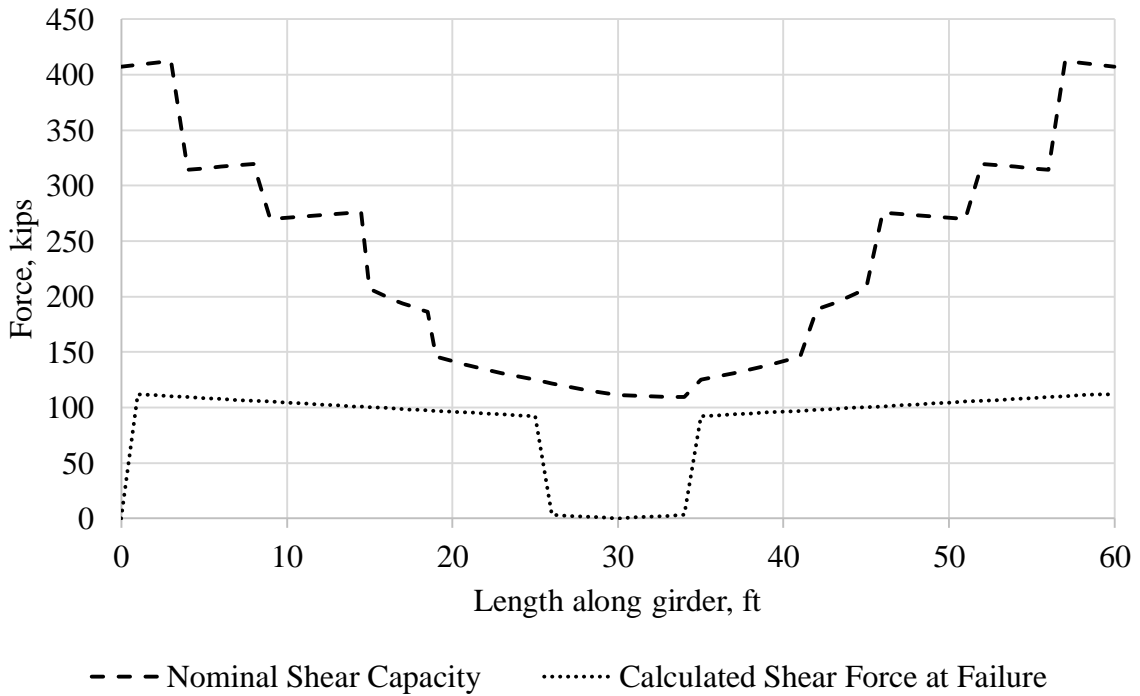


Figure 38. Nominal Shear Capacity versus Applied Shear for Test 2

Test 2 was a flexural test of a 60 ft girder with a 58 ft simple span length. The girder was supported on two W21x101 steel sections with a pin bearing on one steel section and a roller bearing on the other. The original sole bearing plates on the girder were placed on top of the bearings. The original sole bearing plates on the girder were placed on top of the bearings. Figure 39 and Figure 40 show the set-up of the pin and roller bearings. Two frames were used to prohibit the girder from tipping from lateral deflection during the test. A third frame was used to hold a 400 kip hydraulic actuator above the load points. The actuator exerted a force on a 12 ft long steel spreader beam resting on two neoprene and steel laminate bearings. The two load points created a constant moment across the repaired section. The loading system is shown in Figure 41. The location of the load points was chosen to contain all of the repaired strand sections and splice chucks within the constant moment region. Figure 42 is a picture along the length of the beam showing an overview of the set-up.



**Figure 39. Roller Bearing (Photo taken by Mark Jones, used under fair use 2015)**



**Figure 40. Pin Bearing (Photo taken by Mark Jones, used under fair use 2015)**



**Figure 41. Test 2 Loading System (Photo taken by Mark Jones, used under fair use 2015)**



**Figure 42. Test 2 Set-up**

Data was continuously recorded using a high speed data acquisition system. Figure 43 shows the instrumentation layout. Three wire pots were attached to the bottom of the girder to measure vertical deflection during the test. Wire pot 1 is shown in Figure 44. A fourth wire pot was attached to the side of the girder at the load point to record lateral movement. Two LVDT and six strain transducers were used to record a strain profile during the test. They were all placed directly under the centerline of the load point as shown in Figure 45. One LVDT was placed on each side of the bottom flange of the girder at 2 in from the bottom of the girder to measure the associated strain of the bottom prestress strand while the girder was still in the elastic range and strain compatibility could be assumed between the concrete and the strand. Strain transducers were placed at midspan on each side of the girder at 6, 41, and 49 in from the bottom of the girder. Four LVDT gauges were placed at the interfaces of the repair concrete and the original concrete on the bottom flange of the girder. They were placed 2 in from the bottom

of the girder as shown in Figure 46. The gauges on the unrepaired side of the girder were used as a baseline to evaluate with the gauges on the repaired side and determine if there was a significant slip along the interface of the repair section and original concrete. A 400 kip load cell was placed between the actuator and the load frame to measure the applied load.

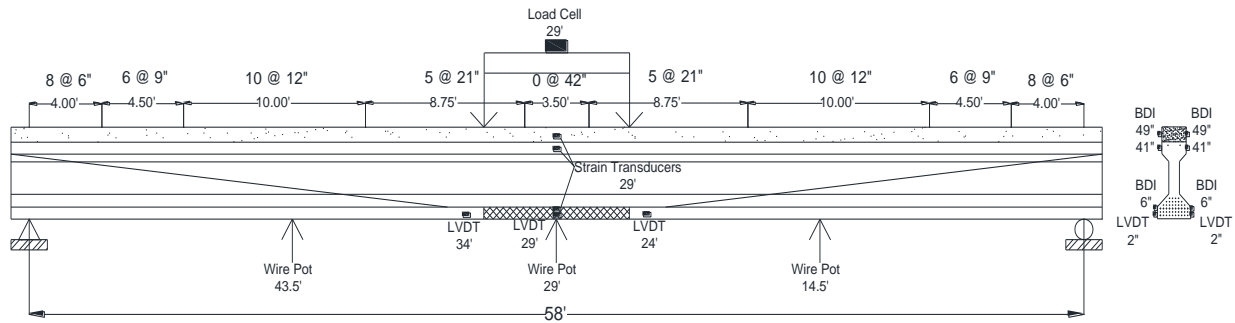


**Figure 43. Test 2 Set-up and Instrumentation Plan**



**Figure 44. Wire Pot 1 at 14.5 Ft from Roller (Photo taken by Mark Jones, used under fair use 2015)**

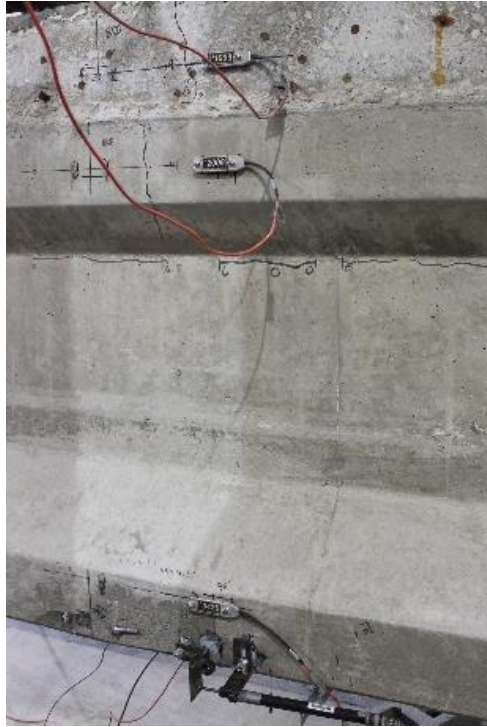


**Figure 45. Strain Profile Instrumentation Set-up (Photo taken by Mark Jones, used under fair use 2015)**



**Figure 46. LVDT at Repair Interface**

The girder was tested on August 21, 2014. Initially, the rate of loading was managed to ensure there were not effects from sudden or impact loading. The load was held at approximately 40 kip increments to allow the girder to settle under the load before it was

inspected. At each pause, the girder was inspected and cracks were highlighted and marked. This pace of loading was used from 0 to 100 kips of total load. The load increment between pauses for inspection was decreased to 20 kips from 100 to 160 kips of total load. The load increment was then decreased to 10 kips from 160 to 195 kips of total load. After 170 kips (for safety reasons), the strain transducers were removed and close-up inspection and marking of cracks ceased. The load was increased to 195 kips and 3.39 in of deflection when one of the prestressing strands failed. The load fell to 191 kips and was increased again to 193 kips when a second strand failed causing the load to fall to 184 kips. At this point, the test was determined to be a flexural tension failure.

### **3.3.3: Test 3 – FRP Repaired Girder with Four Severed Strands**

For test 3, Girder C, a 60 ft girder, was damaged for 2 ft on either side of both third points. Of the 48 prestressing strands in the bottom flange of the girder, four were intentionally severed at each location during damaging. Four feet was chosen as the length for damage to allow Girder C to be damaged in two locations as shown in Figure 47. The two damage locations allowed two repair techniques to be tested on the same girder without one repair influencing the other repair's test results. In addition to reducing the length of damage, the number of severed prestressing strands was reduced to four strands. Figure 48 shows the locations of the strands that were severed during the damaging process.

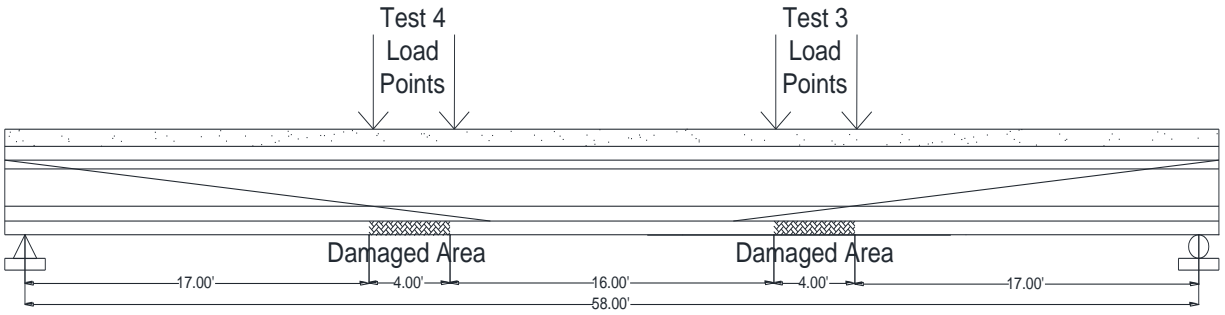


**Figure 47. Girder C Damage Locations**

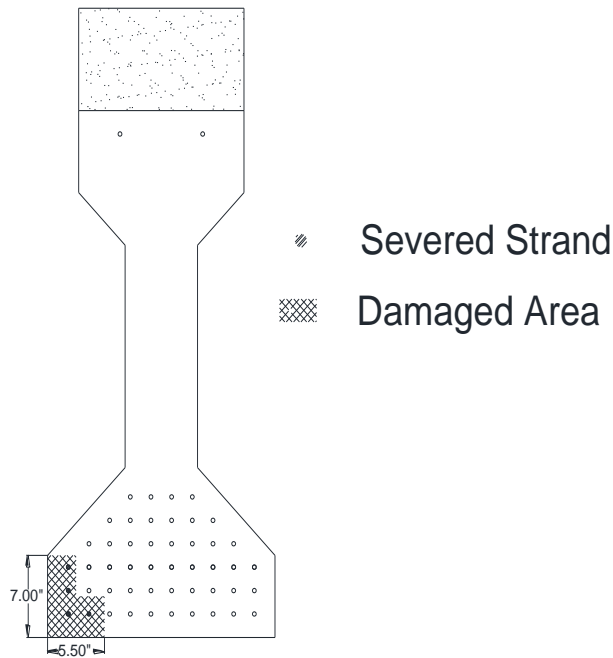


**Figure 48. Girder C Cross Section through Damaged Area with Severed Strand Locations Shown**

Structural Technologies conducted the repair of the damaged location on Girder C for Test 3 with Tstrata IRC as a patch and V-Wrap C400 FRP composite. V-Wrap C400 FRP is a 0.08 in thick fabric with V-Wrap 700 ambient cure epoxy resin provided by Structural Technologies (International Code Council Evaluation Service, 2014). After the concrete patch was placed and allowed to cure, the FRP was installed. APPENDIX H: Common Repair Procedures gives the repair procedures followed for the repair concrete. APPENDIX J: Fiber

Reinforced Polymer Repair Procedures gives the repair procedures followed for the FRP application.

Two iterations of Test 3 were conducted. During the first iteration, flexural cracking was observed in vicinity of the second repair to be tested during Test 4. In addition, shear cracking was observed in the midspan region where there is no shear reinforcement. In order to ensure that Test 4's results were not adversely affected, test iteration one was stopped until after Test 4 was completed. At that time, test iteration two was conducted. In order to develop the plan for the test set-up and decrease the probability of a shear failure while ensuring the desired flexural failure, the girder nominal moment and shear capacities were determined using the provisions of AASHTO LRFD Bridge Design Specifications (American Association of State Highway and Transportation Officials, 2012) and the tested girder material properties (Jones, 2015).

The nominal moment capacity of this girder at the points of load application was 3410 k-ft. This corresponds to a load of 293 kips for iteration 1 and 268 kips for iteration 2. Figure 49 shows the nominal moment capacity of Girder C and the maximum calculated moment resulting from a load of 293 kips. Figure 51 shows the nominal moment capacity of Girder C and the maximum calculated moment resulting from a load of 268 kips. Figure 50 shows the absolute values of the nominal shear capacity of Girder B and the maximum calculated shear force resulting from a load of 293 kips. Figure 52 shows the absolute values of the nominal shear capacity of Girder B and the maximum calculated shear force resulting from a load of 268 kips. Other loading arrangements were investigated, however this loading arrangement was chosen to minimize the potential for a shear failure since the desired failure mode was flexural (Jones, 2015).

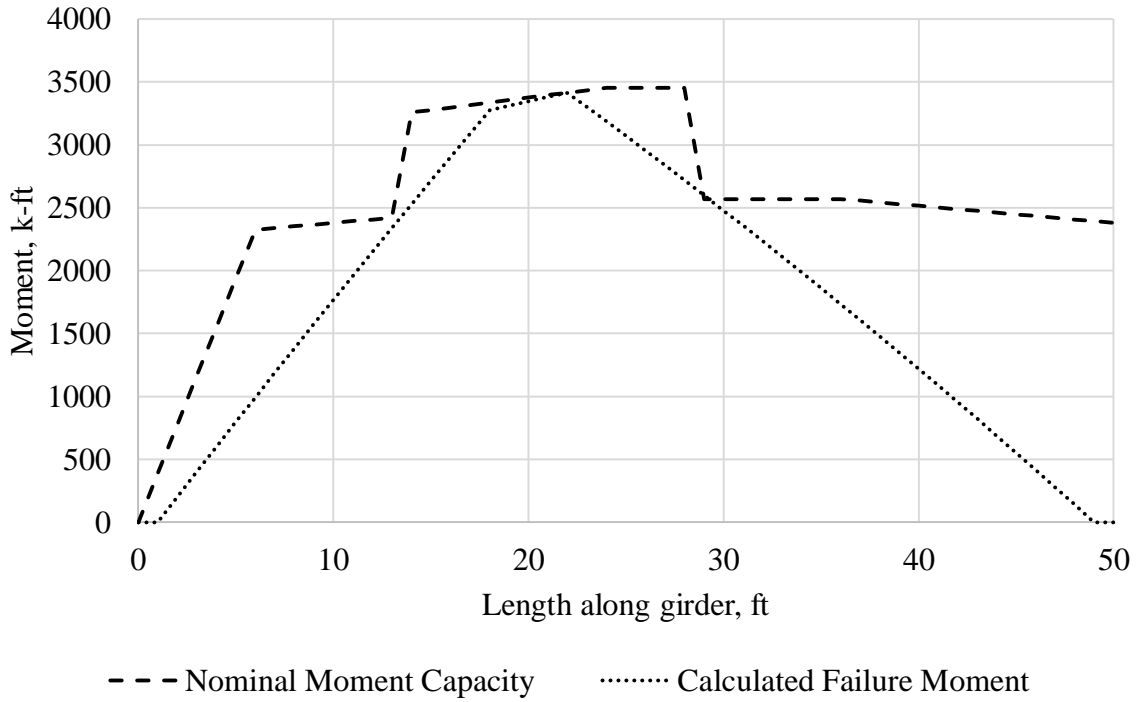


**Figure 49. Nominal Moment Capacity versus Calculated Failure Moment for Test 3, Iteration 1**

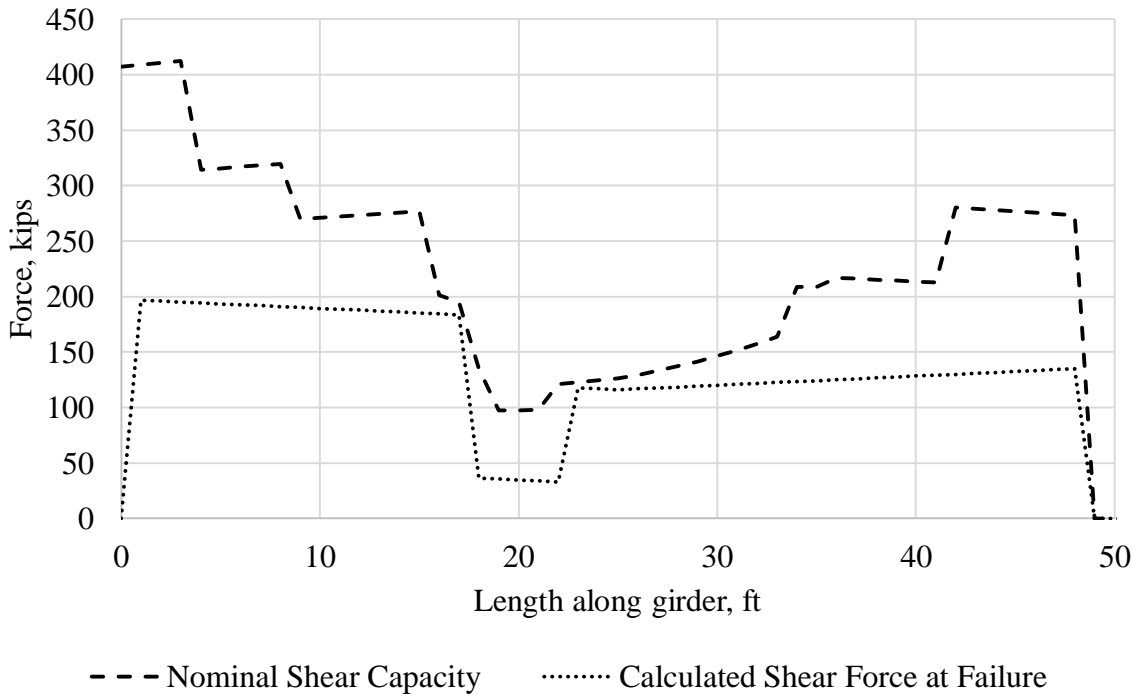


**Figure 50. Nominal Shear Capacity versus Calculated Shear for Test 3, Iteration 1**

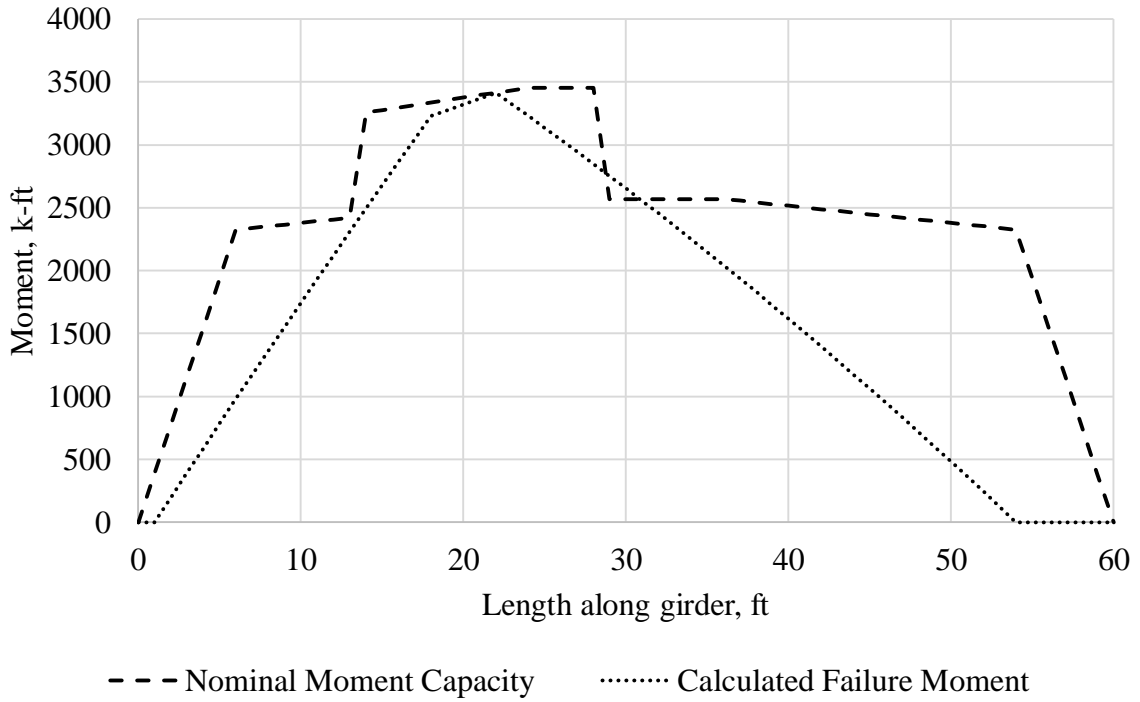


**Figure 51. Nominal Moment Capacity versus Calculated Failure Moment for Test 3, Iteration 2**

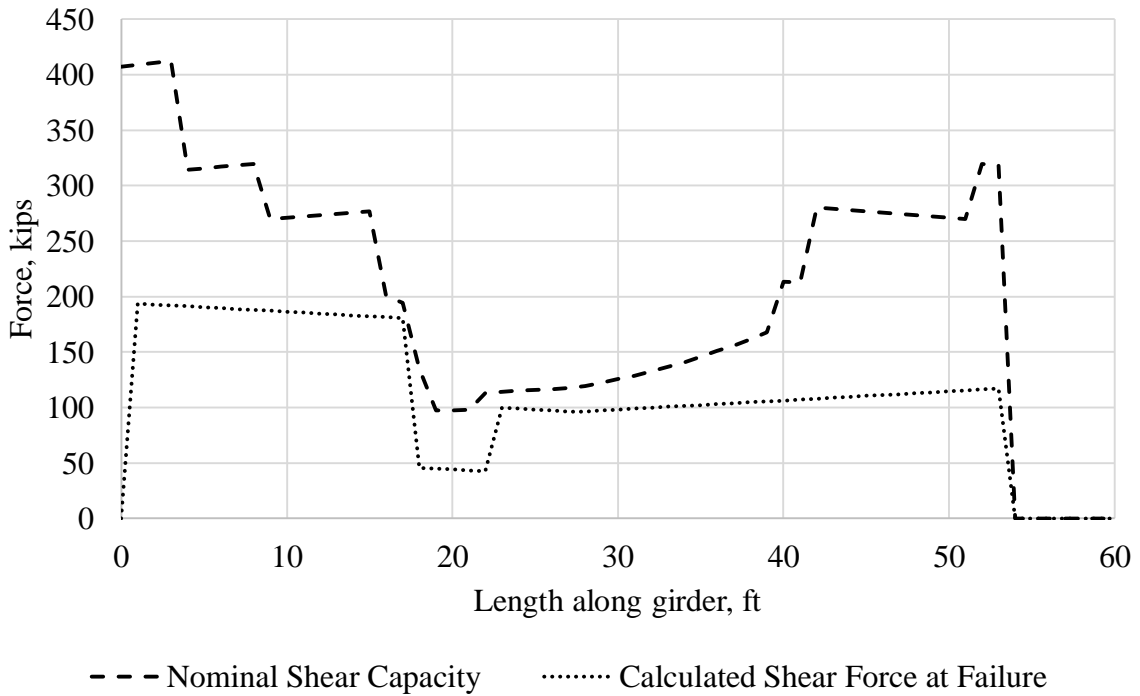


**Figure 52. Nominal Shear Capacity versus Calculated Shear for Test 3, Iteration 2**

Test 3 was a flexural test of a 60 ft girder with a 48 ft simple span length for the first iteration and a 53 ft simple span length for the second iteration. The girder was supported on two W21x101 steel sections with a pin bearing placed on one steel section and a roller bearing placed on the other. The original sole bearing plate on one end of the girder was placed on top of the roller bearing while rubber pads were used between the pin bearing and the bottom flange of the girder. The span length was extended for the second iteration to reduce shear force in the midspan region of the girder where there is less shear reinforcement. Figure 53 shows the test set-up along the length of the girder. Figure 54 shows the pin for the first iteration. Figure 55 shows the pin location for the second iteration. Figure 56 shows the roller location for both iterations. Two frames were used to prohibit the girder from tipping from lateral deflection during the test. A third frame was used to hold a 400 kip hydraulic actuator above the load points. The actuator exerted a force on a 6 ft long steel spreader beam resting on two neoprene and steel laminate bearings that translated the load into a constant moment region between two load points. The load points were chosen so all of the severed strand sections within the constant moment region. The set-up of the loading system is shown in Figure 57.



Figure 53. Test 3 Set-up

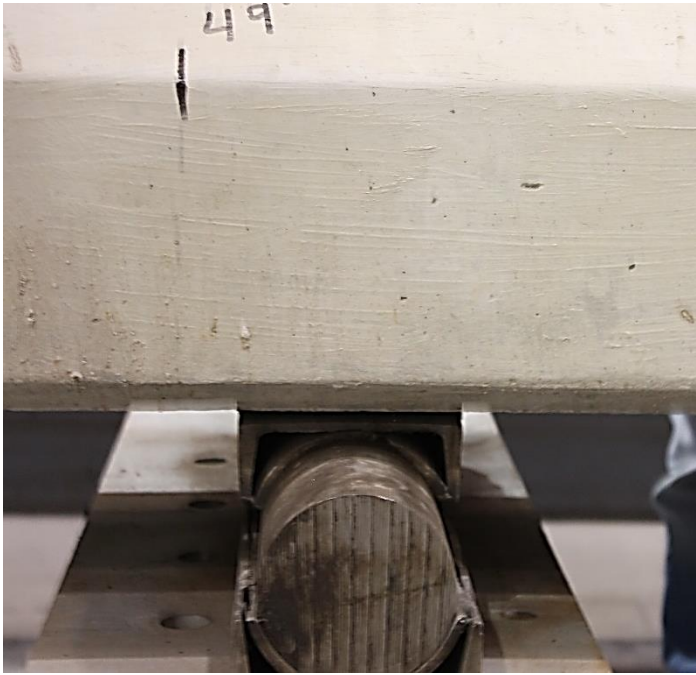


Figure 54. Test 3, Iteration 1 Pin Location (Photo taken by Mark Jones, used under fair use 2015)



**Figure 55. Test 3, Iteration 2 Pin Location (Photo taken by Mark Jones, used under fair use 2015)**



**Figure 56. Test 3 Roller Location (Photo taken by Mark Jones, used under fair use 2015)**



**Figure 57. Test 3 Load Point**

Data was continuously recorded using a high speed data acquisition system. Figure 58 shows the instrumentation layout along the length of the girder for the first iteration and Figure 59 shows the instrumentation layout along the length of the girder for the second iteration. Three wire pots were attached to the bottom of the girder to measure vertical deflection during the test. A fourth wire pot was attached to the side of the girder at the load point to measure any lateral movement. Two MLVDTs and six strain transducers were used to record a strain profile during the test. They were all placed directly under the centerline of the load point. One MLVDT was placed on either side of the bottom flange for the girder at 2 in from the bottom to try to measure the associated strain of the bottom prestress strand while the girder was still in the elastic range and strain compatibility could be assumed between the concrete and the strand. The strain

transducers were placed on either side of the girder at 6, 41, and 49 in from the bottom of the girder. Figure 60 and Figure 61 show the layout of the strain transducers on each side of the girder. One LVDT was placed on each side of the girder at both interfaces between the FRP and the girder as shown in Figure 62. These were used to measure any slip along the interface that may indicate a failure with the adhesive. A 400 kip load cell was placed between the actuator and the load frame to measure the applied load.

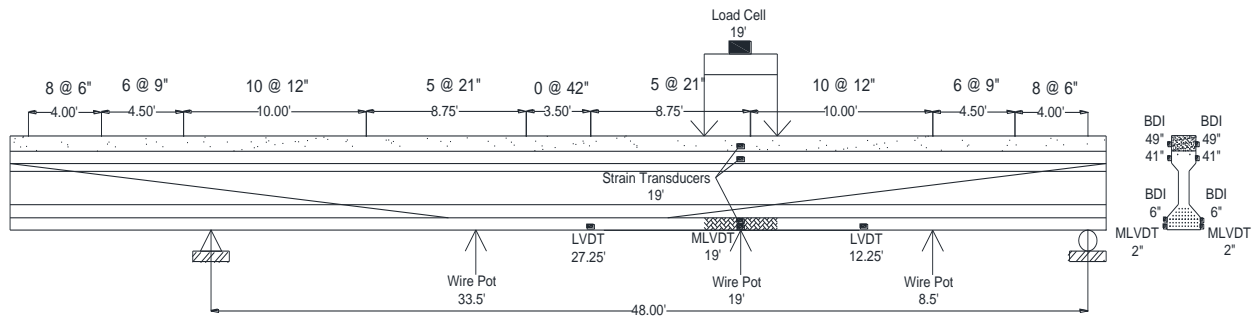


**Figure 58. Test 3, Iteration 1 Test and Instrumentation Set-up**

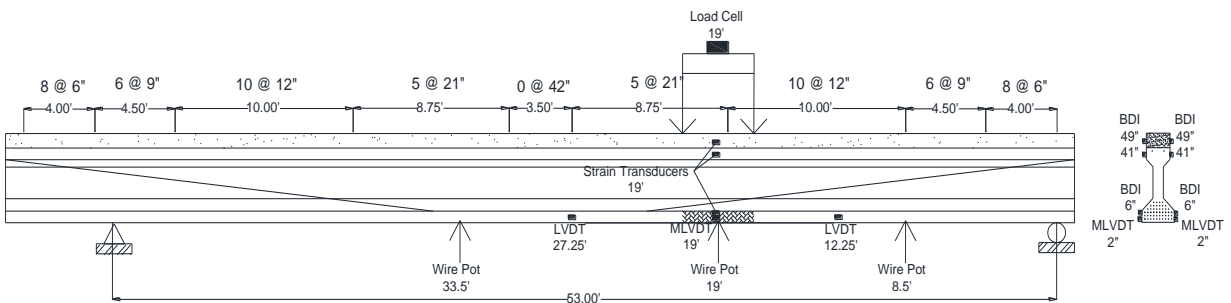


**Figure 59. Test 3, Iteration 2 Test and Instrumentation Set-up**



**Figure 60. Strain Transducers on Damaged/Repaired Side of Girder (Photo taken by Ioannis Koutromanos, used under fair use 2015)**



**Figure 61. Strain Transducers on Undamaged Side of Girder**



**Figure 62. LVDT at FRP and Concrete Interface**

The girder was tested on October 21, 2014. Initially, the rate of loading was managed to ensure there were not effects from sudden or impact loading. The load was held at approximately 20 kip increments to allow the girder to settle under the load before it was inspected. At each pause, the girder was inspected and cracks were highlighted and marked. After 260 kips (for safety reasons), the strain transducers were removed and up close inspection ceased. The load was increased to 312 kips and 3.16 in of deflection when the flexural cracking approached the four strand splice repair section to be tested in Test 4. In addition, shear cracks in the web of the girder started to form in locations with minimal shear reinforcement as shown in Figure 63. In order to avoid damaging the four strand splice repair section, propagating shear cracking, and adversely affecting the results of Test 4, the test was stopped and a second test to load the girder to failure was scheduled for after the completion of Test 4. Figure 64 shows the cracking observed at the load point near the peak load prior to stopping the test. The second iteration was conducted on December 18, 2014. At 180 kips, the actuator slipped and was no

longer exerting a consistent vertical force on the girder. A frame to hold the actuator level used in the second iteration of Test 4 was used to try to keep the actuator from slipping. The frame is shown in Figure 65. After the third attempt to load the girder to failure, the concrete in the constant moment region between the load points showed evidence indicating a flexural compression failure similar to Test 4 and the test was determined to be complete.



**Figure 63. Shear Cracking in Midspan Region during Iteration 1 (Photo taken by Ioannis Koutromanos, used under fair use 2015)**



**Figure 64. Cracking Near Peak Load for Iteration 1 (Photo taken by Ioannis Koutromanos, used under fair use 2015)**



Figure 65. Brace for Actuator (Photo taken by Mark Jones, used under fair use 2015)

### **3.3.4: Test 4 – Girder with Four Severed/Re-tensioned Strands**

For Test 4, Girder C, a 60 ft girder, was damaged for 2 ft on either side of the third point. Of the 48 prestressing strands in the bottom flange of the girder, four were intentionally severed during damaging. Four feet was chosen as the length for damage to allow Girder C to be damaged in two locations. The two damage locations allowed two repair techniques to be tested on the same girder without one repair influencing the other repair's test results. In addition to reducing the length of damage, the number of severed prestressing strands was reduced to four strands.

Structural Technologies conducted the repair of the four severed strands on Girder C for Test 4 with Grabb-it strand splices. The splices were tightened with a torque wrench to 150 ft-lbs which corresponds to 80% of ultimate strength or 160 kips based on the Table 3 provided by the manufacturer (Prestress Supply Incorporated, 2010). After the strands were spliced, they were encased in Tstrata IRC, a high strength, quick cure concrete. APPENDIX H: gives the

repair procedures followed for the repair concrete. APPENDIX I: Installation of Strand Splices gives the repair procedures followed for the strand splices.

Two iterations of Test 4 were conducted. During the first iteration, the actuator slipped longitudinally in relation to the girder. For the second iteration, the span length was decreased to reduce the curvature of the beam at the load point and reduce the potential of the actuator slipping. In order to develop the plan for the test set-up and decrease the probability of a shear failure while ensuring the desired flexural failure, the girder nominal moment and shear capacities were determined using the provisions of AASHTO LRFD Bridge Design Specifications (American Association of State Highway and Transportation Officials, 2012) and the tested girder material properties (Jones, 2015).

The nominal moment capacity of this girder at the points of load application was 2660 k-ft. This corresponds to a load of 187 kips for iteration 1 and 216 kips for iteration 2. Figure 66 shows the nominal moment capacity of Girder C and the maximum calculated moment resulting from a load of 187 kips for iteration 1. Figure 68 shows the nominal moment capacity of Girder C and the maximum calculated moment resulting from a load of 216 kips. Figure 67 shows the absolute values of the nominal shear capacity of Girder B and the maximum calculated shear force resulting from a load of 187 kips. Figure 69 shows the absolute values of the nominal shear capacity of Girder B and the maximum calculated shear force resulting from a load of 216 kips. Other loading arrangements were investigated, however this loading arrangement was chosen to minimize the potential for a shear failure since the desired failure mode was flexural. In addition, it minimized the potential for slipping from the actuator (Jones, 2015).

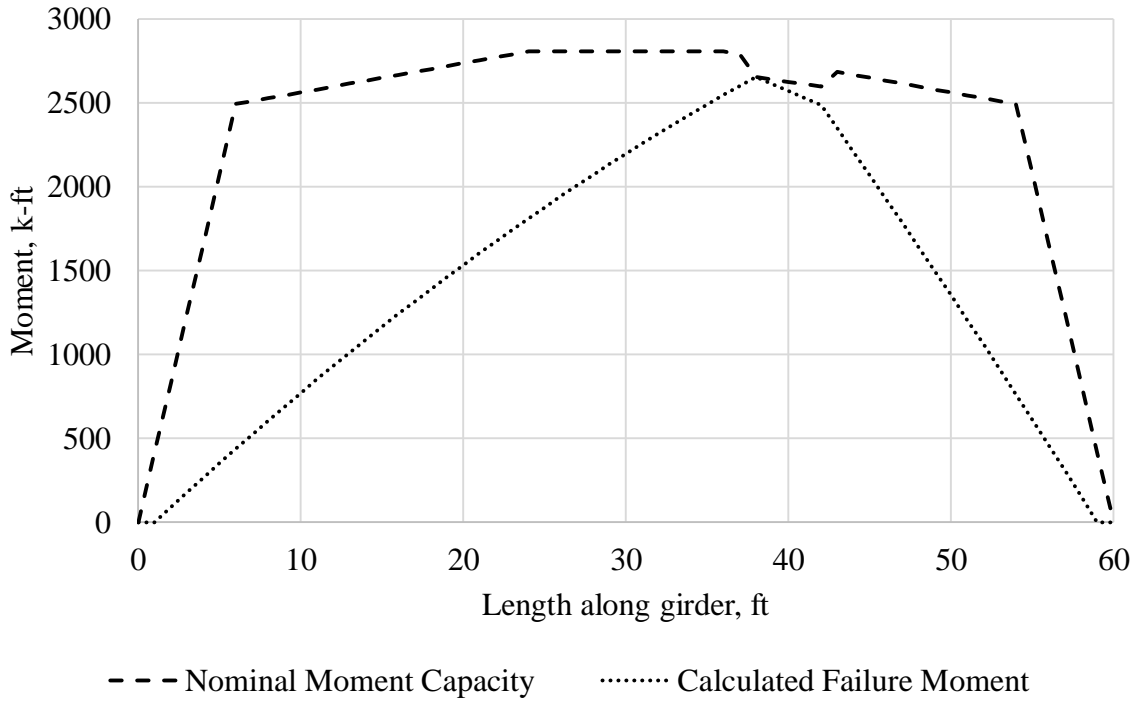


**Figure 66. Nominal Moment Capacity versus Calculated Failure Moment for Test 4, Iteration 1**

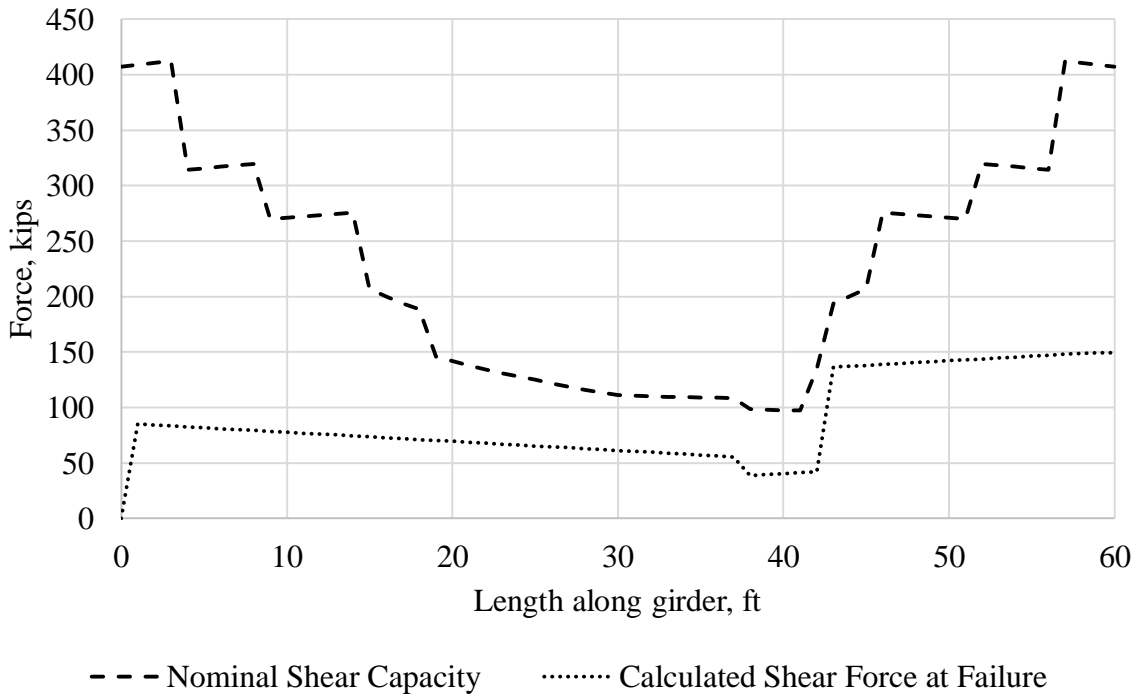


**Figure 67. Nominal Shear Capacity versus Calculated Shear for Test 4, Iteration 1**

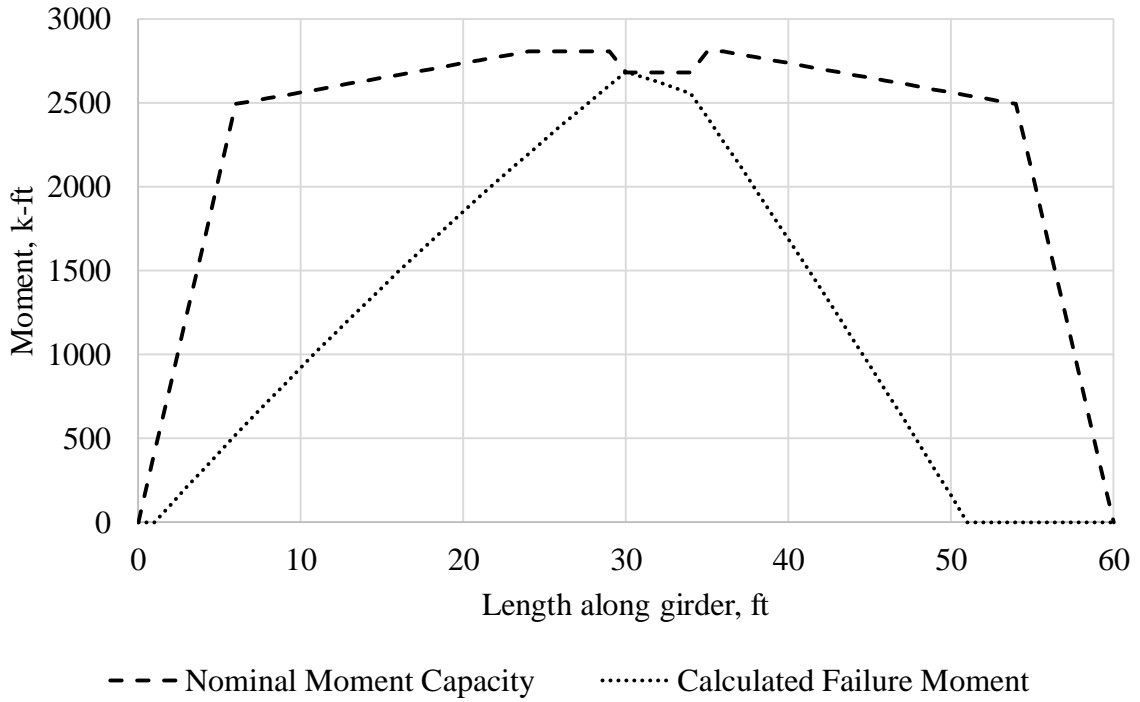


**Figure 68. Nominal Moment Capacity versus Calculated Failure Moment for Test 4, Iteration 2**

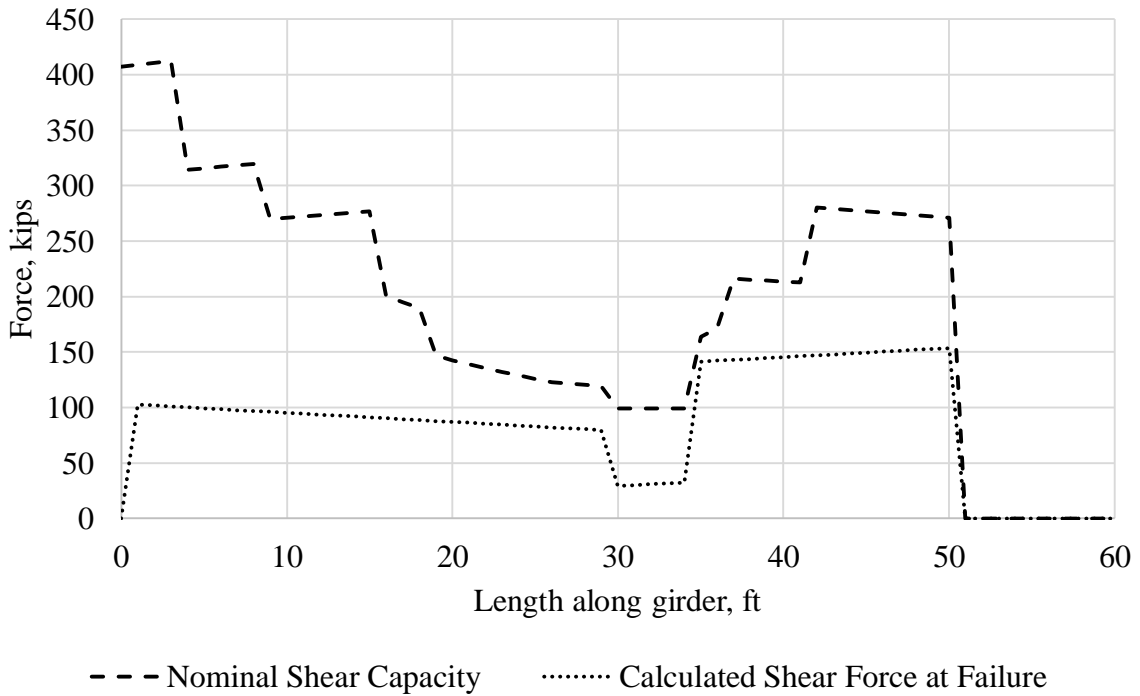


**Figure 69. Nominal Shear Capacity versus Calculated Shear for Test 4, Iteration 2**

Test 4 was a flexural test of a 60 ft girder conducted in two iterations with a 58 ft simple span length for the first iteration and a 50 ft simple span length for the second iteration. The girder was supported on two W21x101 steel sections with a pin bearing placed on one steel section and a roller bearing placed on the other. The original sole bearing plates on the girder were placed on top of the bearings for the first iteration. For the second iteration, rubber pads were placed between the roller bearing and the bottom of the girder. Figure 70 shows the location of the roller for the first iteration. Figure 71 shows the location of the roller for the second iteration. Figure 72 shows the location of the pin for both iterations. Two frames were used to prohibit the girder from tipping from lateral deflection during the test. A third frame was used to hold a 400 kip hydraulic actuator above the load points. The actuator exerted a force on a 6 ft long steel spreader beam that translated the load into a constant moment region between the two load points. The load points were chosen so all of the repaired strand sections and splice chucks within the constant moment region. During this iteration, the curvature of the girder caused the actuator to appear that it would slip out of plumb. In order to reduce the impact of the curvature, the span length was decreased from 58 ft to 50 ft for the second iteration by moving the roller bearing 8 ft closer to the pin.



**Figure 70. Test 4, Iteration 1 Roller Location (Photo taken by Mark Jones, used under fair use 2015)**



**Figure 71. Test 4, Iteration 2 Roller Location (Photo taken by Mark Jones, used under fair use 2015)**



**Figure 72. Test 4 Pin Location (Photo taken by Mark Jones, used under fair use 2015)**

Data was continuously recorded using a high speed data acquisition system. Figure 73 shows the instrumentation layout for the first iteration. Figure 74 shows the instrumentation layout for the second iteration. Three wire pots were attached to the bottom of the girder to measure vertical deflection during the test. A fourth wire pot was attached to the side of the girder at the load point to measure any lateral movement. Two MLVDTs and six strain transducers were used to record a strain profile during the test. They were all placed directly under the centerline of the load point. One MLVDT was placed on either side of the bottom flange of the girder at 2 in from the bottom to try to measure the associated strain of the bottom prestress strand while the girder was still in the elastic range and strain compatibility could be assumed between the concrete and the strand. The strain transducers were placed on either side of the girder at 41 and 49 in from the bottom of the girder. One strain transducer was placed at 6 in from the bottom of the girder on the near side of the girder and one was placed at 4 in from the bottom of the girder. These were offset due to damage to the surface of the girder that did not

allow them to be placed directly across from each other. The damage is shown in Figure 75. The set-up of the strain transducers is shown in Figure 76. Four LVDT strain gauges were placed at the repair interface. One was placed on each end of the repair with one on the opposite side of the girder. The two on the undamaged side were used to compare the strain at the interface to indicate any slipping between the new and the old concrete. A 400 kip load cell was placed between the actuator and the load frame to measure the applied load.

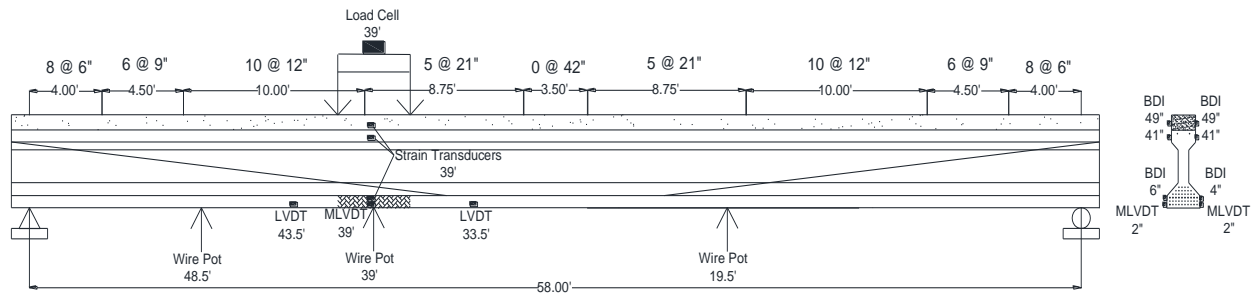


**Figure 73. Test 4, Iteration 1 Set-up and Instrumentation Plan**

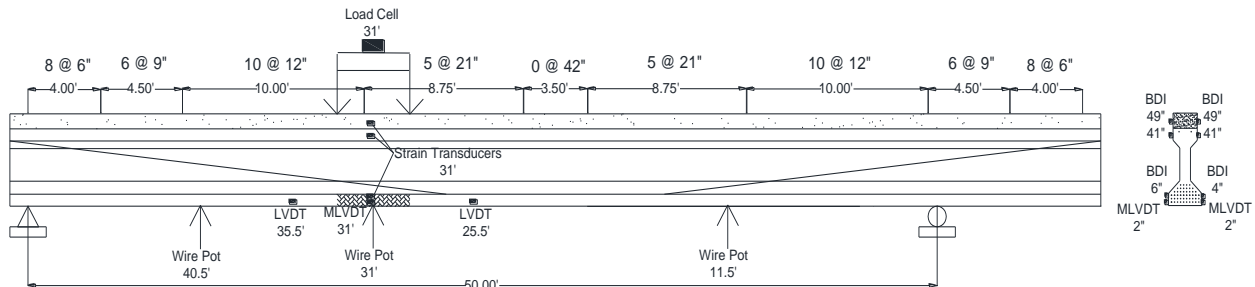


**Figure 74. Test 4, Iteration 2 Set-up and Instrumentation Plan**



**Figure 75. Damage on Girder near Strain Transducer Location (Photo taken by Ioannis Koutromanos, used under fair use 2015)**

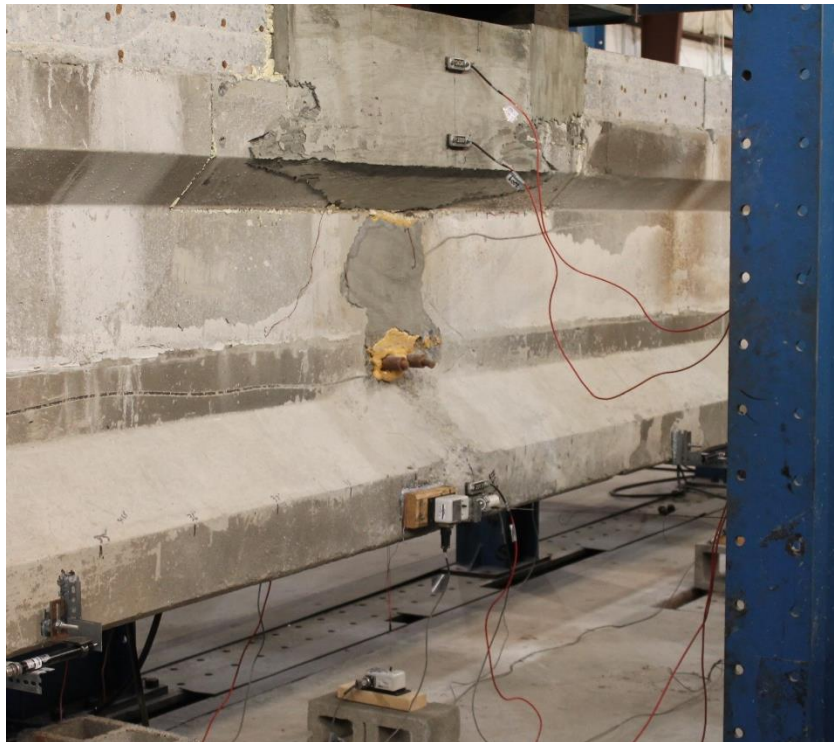


**Figure 76. Strain Transducer Set-up Below Load Point**

The girder was tested on 20 November 2014. Initially, the rate of loading was managed to ensure there were not effects from sudden or impact loading. The load was held at approximately 25 kip increments to allow the girder to settle under the load before it was inspected. At each pause, the girder was inspected and cracks were highlighted and marked. This pace of loading was used from 0 to 100 kips of total load. The load increment between pauses for inspection was decreased to 20 kips from 100 to 180 kips of total load. After 200 kips (for safety reasons), close visual inspection and marking of cracks ceased. The load increment between pauses was decreased to 10 kips. During pauses, inspections were made from a safe distance to see if there were any early indications of failure or safety issues. The load was increased to 241 kips and 4.12 in of deflection when the actuator appeared as though it would slip out of plumb with the girder. The span length was decreased to reduce the curvature of the beam when loaded. In addition, a frame was constructed to hold the piston in place so it would continue to impose a downward force throughout the test. A second test was conducted on 25 November 2014. The load was increased at 50 kip increments until it reached 200 kips of total load. It was then increased at 10 kip increments to allow for visual inspection of the actuator for signs of slip. At 265 kips, the concrete in the constant moment region between the load points crushed resulting in a flexural compression failure.

## CHAPTER IV: Results and Discussion

### 4.1: Introduction

This section compares the tested and calculated data from the reported tests. The cracking and failure moments for each test are evaluated and compared to predictions of the girder's behavior using AASHTO calculations, a moment-curvature diagram, and non-linear finite element modeling. In addition, it looks at how well the strand splices and FRP repairs to restore the girders strength is investigated.

### 4.2: Material Properties

#### 4.2.1: Girder Concrete

Table 7 summarizes the failure loads, compressive strengths, and average compressive strength of the cores collected from the girder and the deck. Table 8 summarizes the failure loads, tensile strength, and average tensile strength of the cores collected from the girder. The average compressive strength in the girder was 6,650 psi, which is greater than 5,000 psi as required by the bridge plans which are provided in APPENDIX A: Arcadia Bridge Blueprints. The average compressive strength in the deck was 6,020 psi, which is greater than the typical required bridge deck concrete compressive strength of 4,000 psi. The average tensile strength was 424 psi. Figure 77 shows the concrete core sample after the tensile splitting test.

**Table 7. Girder and Deck Concrete Compressive Strength**

Sample	Cylinder #	Load (lbs)	Diameter (in)	Area (in <sup>2</sup> )	Strength (psi)	Average (psi)
Girder	1	39,000	2.75	5.94	6570	6650
	2	40,000	2.75	5.94	6730	
Deck	3	35,000	2.75	5.94	5890	6020
	4	36,500	2.75	5.94	6150	

**Table 8. Girder Concrete Tensile Strength**

Cylinder #	Load (lbs)	Diameter (in)	Length (in)	Strength (psi)	Average (psi)
5	7,500	2.75	4.50	386	424
6	10,000	2.75	5.00	463	



**Figure 77. Girder Concrete Tensile Test**

#### **4.2.2: Tstrata IRC Repair Concrete**

Table 9 summarizes the failure loads, compressive strength, and average compressive strength for the cylinders collected from the repair concrete. The average compressive strength at 24 hours was 4,060 psi, which does not meet the advertised design strength of 4500 psi (Structural Group Incorporated, 2015). The average compressive strength was 5,730 psi at 48 hours. The design strength for 48 hours was not advertised. The average compressive strength

was 6,250 psi at 7 days, which does not meet the advertised design strength of 7700 psi (Structural Group Incorporated, 2015).

**Table 9. Repair Concrete Compressive Strength**

Cylinder #	Test Age (days)	Load (kips)	Diameter (in)	Area (in <sup>2</sup> )	Strength (psi)	Average (psi)	Design (psi)
1	24 hr	45	4	12.6	3580	4060	4500
2		57	4	12.6	4540		
3	48 hr	69	4	12.6	5490	5730	-
4		75	4	12.6	5970		
5	7 day	82	4	12.6	6530	6250	7700
6		75	4	12.6	5970		

#### **4.2.3: Girder Reinforcement**

Table 10 summarizes the failure loads, tensile strengths, and average tensile strength of the reinforcing steel samples collected from the girder. The average tensile strength was 78.5 ksi. The average failure tensile strength is consistent with grade 40 reinforcing steel (Nilson, 1987). Figure 78 shows the stress strain relationships for both tests.

**Table 10. Reinforcing Bar Failure Tensile Strength**

Bar #	Load (kips)	Diameter (in)	Area (in <sup>2</sup> )	Yield (ksi)	Average Yield (ksi)	Strength (ksi)	Average Strength (ksi)
1	16,000	0.5	0.20	52.3	49.3	81.4	78.5
2	14,900	0.5	0.20	46.2		75.6	

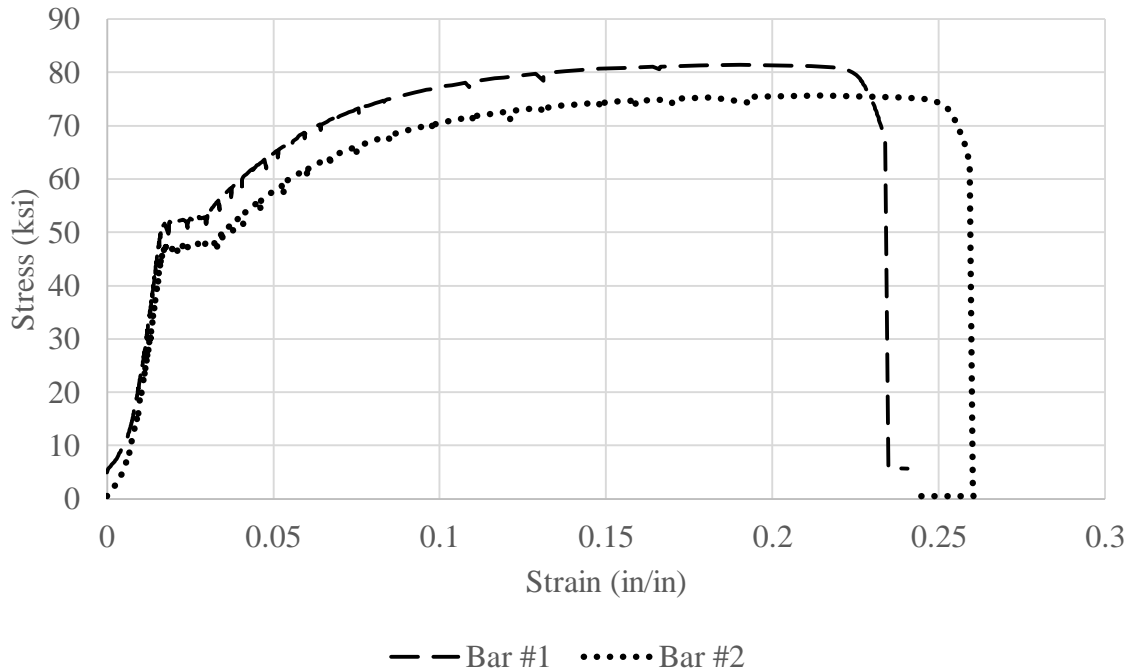


Figure 78. Reinforcing Bar Stress Strain Relationship

#### **4.2.4: Prestressing Strand**

Table 11 summarizes the failure loads, tensile strengths, and average tensile strength of the prestressing strand samples collected from the girder. The average tensile strength was 262 ksi. The average tensile strength indicates 250 grade prestressing strands (Nilson, 1987) which is consistent with the bridge plans shown in APPENDIX A: Arcadia Bridge Blueprints. Figure 79 shows the failure of the prestress strand with one wire rupturing. Figure 81 shows the stress strain relationship from the prestress strand tensile tests and the bilinear approximation used during analytical analysis.

**Table 11. Prestress Strand Strength**

Strand #	Load (lbs)	Diameter (in)	Area (in <sup>2</sup> )	Yield (ksi)	Average Yield (ksi)	Strength (ksi)	Average Strength (ksi)
1	20,500	0.375	0.08	218	214	257	262
2	21,400	0.375	0.08	210		267	



**Figure 79. Prestress Tensile Test Strand Rupture (Photo taken by Mark Jones, used under fair use 2015)**

Table 12 summarizes the initial length, change in length, strain, and effective prestress force for each strand from the effective prestress tests. As discussed, the results of the second, third, fourth, and sixth strands indicate that the extensometer slipped. When averaging only the first and fifth strands, the effective prestress force was 132 ksi. Using AASHTO equation 5.9.5.3-1 to estimate time-dependent losses, the approximate effective prestress force after losses is 143 ksi. The calculated result of 132 ksi is within 8 % of the stress calculated using the AASHTO approximation.

**Table 12. Effective Prestress Force**

<b>Strand #</b>	<b>Initial Length (in)</b>	<b>Length Change (in)</b>	<b>Strain (in/in)</b>	<b>Effective Prestress Force (ksi)</b>
<b>1</b>	2.0104	0.0102	0.0051	137
<b>2</b>	2.0085	0.0191	0.0095	257
<b>3</b>	2.0057	0.031	0.0155	417
<b>4</b>	2.0131	-0.0012	-0.0006	-16.1
<b>5</b>	2.0071	0.0095	0.0047	128
<b>6</b>	2.0059	0.0254	0.0127	342

#### **4.2.5: V-Wrap C400 FRP Repair System Materials**

FRP composite samples were tested at the University of Miami for tensile strength (Pino & Nanni, 2015). The tensile strength tests provided ultimate strength, modulus of elasticity, and ultimate strain. Table 13 shows the results of the V-wrap C400H FRP 1-ply and 2-ply tension tests. The results show that the average strength of a single ply of FRP is 188 ksi and a double ply is 136 ksi, which are both greater than the advertised design value of 121 ksi (Structural Group Incorporated, 2015). The average modulus of elasticity for the single ply was 11000 ksi, which is less than the advertised design modulus of elasticity of 11900 ksi (Structural Group Incorporated, 2015). The average modulus of elasticity for the double ply is 12100 ksi, which is greater than the advertised modulus of elasticity. The average ultimate strain was 0.017 for the single ply and 0.011 for the double ply, which are both greater than the advertised ultimate strain of 0.0085 (Structural Group Incorporated, 2015).

**Table 13. FRP Tensile Test Results**

<b>Sample #</b>	<b>Ply #</b>	<b>Ultimate Load (kips)</b>	<b>Ultimate Strength (ksi)</b>	<b>Ultimate Strain (in/in)</b>	<b>Modulus of Elasticity (ksi)</b>
<b>1</b>	1	14400	185	0.017	11100
<b>2</b>	1	15000	196	0.018	11000
<b>3</b>	1	13600	178	0.016	11000
<b>4</b>	1	13800	187	0.018	10700
<b>5</b>	1	14400	191	0.017	11400
<b>Averages:</b>			<b>188</b>	<b>0.017</b>	<b>11000</b>
<b>6</b>	2	23400	140	0.012	12000
<b>7</b>	2	22600	135	0.011	12000
<b>8</b>	2	22300	133	0.010	12900
<b>9</b>	2	21900	132	0.010	12800
<b>10</b>	2	22700	138	0.013	10800
<b>Averages:</b>			<b>136</b>	<b>0.011</b>	<b>12100</b>

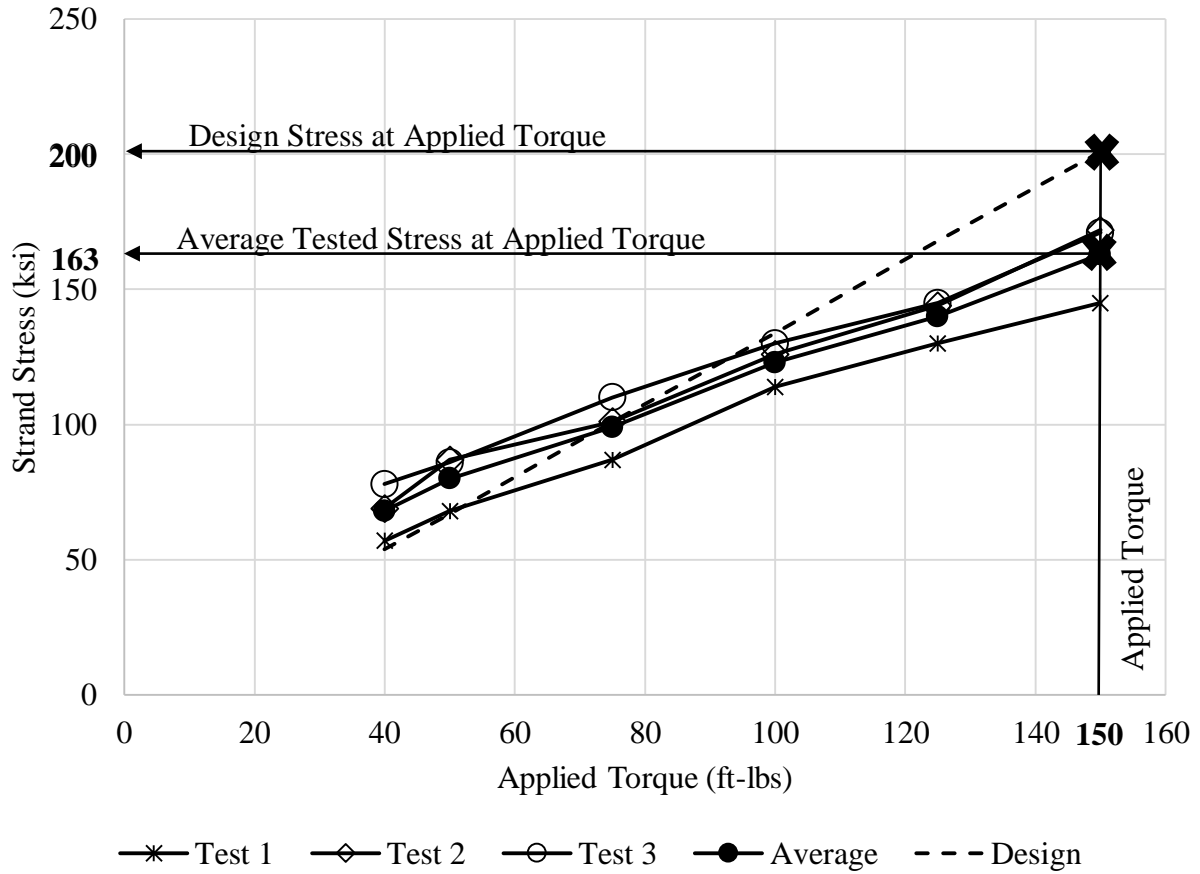
#### **4.2.6: Grabb-It Splice Chuck**

Table 14 shows the results from the splice chuck torque tests (Bao, 2015). The table relates the design stress applied to the strand at a given torque to the tested stress applied to a strand. The design stress is found using Table 3 provided by the splice chuck manufacturing company to correlate a desired stress with the required torque to achieve that stress (Prestress Supply Incorporated, 2010). The test averages are also reported as a percentage of the design stress. As the splice reached higher tensile strengths, the results failed to reach the theoretical values as shown in Figure 80 (Bao, 2015). The applied torque during the installation of the strand splices for tests two and four was 150 ft-lbs for a design stress of 200 ksi. However, based on the torque splice chuck tests, the strand stress corresponding to a torque of 150 ft-lbs was 163 ksi. For the AASHTO calculations, the 163 ksi was used in the tested material property calculations and 200 ksi was used for the design material property calculations. For the moment-curvature calculations, the tested value of 163 ksi was used. In the finite element models, the

design value of 200 ksi was used. The AASHTO calculations were completed with both values to compare the nominal moment using design values to the tested moment in the event actual material properties cannot be determined through testing. In addition, the calculations were done with the tested values to compare the accuracy of the equations to the tested values. Table 15 shows the results from the tensile tests on the spliced strand. In all three test, the strands failed prior to the splice chuck. In addition, the strand used for these tests was 270 grade prestressing strands while the strands tested in the girder were 250 grade. Based on these results, the strands should fail in tension before the splice chuck (Bao, 2015). The effective stress provided by the splice chuck as tested is lower than the design stress. The lower stress would lower the cracking moment and allow cracks to form earlier which could increase the potential for corrosion.

**Table 14. Strand Splice Chuck Torque Test Results**

<b>Torque (ft-lbs)</b>	<b>Test 1 (ksi)</b>	<b>Test 2 (ksi)</b>	<b>Test 3 (ksi)</b>	<b>Average (ksi)</b>	<b>Design (ksi)</b>	<b>% Average Tested vs. Design</b>
40	57	69	78	68	54	127
50	68	87	86	80	67	120
75	87	101	110	99	101	99
100	114	126	130	123	134	92
125	130	144	145	140	168	83
150	145	172	171	163	200	81



**Figure 80. Strand Splice Torque-Tension Relationship**

**Table 15. Spliced Strand Tension Test**

Test #	Load (lbs)	Length Chuck-to-Chuck (ft)	Stress (ksi)	Failure
1	23300	16	291	Strand Fracture
2	22800	6	285	Strand Fracture
3	24000	4	299	Strand Fracture
<b>Average:</b>	<b>23300</b>		<b>292</b>	

### **4.3: Analytical Modeling**

#### **4.3.1: Calculations Based on AASHTO Guidelines**

This method for calculated nominal moment capacity of prestressed concrete bridge girders presented in AASHTO (American Association of State Highway and Transportation Officials, 2012) uses equilibrium across the girder cross section to determine the neutral axis depth and the resulting forces in the concrete and in the strands. The force in the strands is assumed to act at a single location at the strand centroid and is calculated using AASHTO equation 5.7.3.1.1-1. The compression force in the concrete was determined using a rectangular approximation of the stress distribution. Once the neutral axis was determined, the nominal moment was calculated using AASHTO equation 5.7.3.2.2-1. The cracking moment was calculated using AASHTO equation 5.7.3.3.2-1. Table 16 summarizes the cracking and nominal moments. The equations used in the AASHTO nominal and cracking moments are found in APPENDIX B: AASHTO Calculations.

The design values given in the original bridge plans of 5,000 psi for the concrete in the girder and 4,000 psi for the concrete in the deck were used to calculate the design nominal moment capacity. In addition, the nominal moment capacity was calculated based on tested material properties of 6650 psi for the concrete in the girder and 6020 psi for the concrete in the deck. The tensile strength of the concrete in the girder used for calculations was the tested value of 424 psi. To calculate the effective prestress force, the results of the effective prestress tests one and five were averaged based on the inconclusive results obtained from the other tests. This gave an effective prestress force of 132 ksi. The tested average of 163 ksi was used to predict the effective prestress restored by the strand splice. The prestressing ultimate strength for calculations was based on the tested ultimate strength of 262 ksi. The values for the FRP

composite system used in the calculations were based on the tested values for double ply samples of 12100 ksi for the modulus of elasticity, 0.011 in/in as the ultimate strain, and 136 ksi as the ultimate strength.

In order to simulate the damage to the girder for tests two, three, and four, the total area of prestress strands was reduced by the number of severed strands associated with that test at the damaged area of the girder. This reduced the effective prestress force where the strands had been severed. Next, to simulate the repair, the effective strengths were added back in as an additional tensile force. For the strand splices (tests two and four), the ultimate and yield stresses in the spliced strands were calculated as a weighted average. During strand splice testing, the strands failed prior to the splice chucks, therefore, the calculations using tested properties assumed 100% of the ultimate and yield stresses of 262 ksi and 242 ksi. For the design values, the ultimate stress was approximated at 90%, or 225ksi, based on manufacturing tables as presented in Table 3 (Prestress Supply Incorporated, 2010).

For Test 3, the FRP was modeled as additional tensile reinforcement. In order to determine the neutral axis, the tested ultimate stress for 2-ply of 136 ksi was used in the tested material properties calculations and design ultimate stress of 121 ksi was used in the design material properties calculations. In order to calculate the effective force in the FRP at failure, the strain in the fabric was calculated by relating it proportionally to the additional strain in the prestressing strand at failure and the neutral axis. The initial strain in the strand was calculated to be 0.00489 in the moment-curvature calculations and was subtracted from the yield strain of 0.01 to calculate the change in strain in the FRP. The tested modulus of elasticity of 12,100 ksi was used to determine the stress in the fabric and the tensile force in the tested calculations and

the design modulus of 11,900 ksi was used in the design calculations. Example calculations are presented in APPENDIX B: AASHTO Calculations.

**Table 16. AASHTO Mn Calculation Summary**

Test	Description	# Severed Strands	L (ft)	Design Material Properties		Tested Material Properties	
				$M_{cr,AASHTO}$ (k-ft)	$M_n,AASHTO$ (k-ft)	$M_{cr,AASHTO}$ (k-ft)	$M_n,AASHTO$ (k-ft)
1	Control Test	0	35	1780	2720	1770	3260
2	8-Strand Spliced	8	58	181	2380	181	3060
3, Iteration 1	4-Severed Strands with FRP	4	48	201	2960	201	3540
3, Iteration 2			53				
4, Iteration 1	4-Strand Spliced	4	58	189	2350	189	3030
4, Iteration 2			50				

#### **4.3.2: Moment-Curvature Based on Strain Compatibility**

In order to predict the complete load cycle, a moment-curvature analysis of each girder was performed (Michael, 2010). The analysis included six points: no applied moment, decompression of concrete around strand, first flexural cracking, top concrete fiber strain of 0.0015 in/in, prestress strand yield strain of 0.009 in/in, and top concrete fiber strain of 0.003 in/in. The failure mode assumed for each scenario was concrete crushing. The strand tensile stress strain behavior used in these calculations is given in Figure 81. The idealized stress-strain diagram was developed by Gangi (2015) and used in the finite element modeling as a bilinear approximation of the stress-strain results obtained during the prestress strand tests (Gangi, 2015). For the concrete stress versus strain relationship, the modified Hognestad model was used (Hognestad, 1956). Asymmetrical bending was not considered in these calculations. Biaxial bending analysis determined that the strand centroid moved laterally 1.6 in when eight strands

were severed and 0.77 in when four strands were severed. In addition, each strand provided approximately two percent of the prestress force and when compared to the overall load, the load from the individual strands was relatively small. The nominal capacity of the girders when accounting for biaxial bending changed from 2390 k-ft to 2260 k-ft for the eight strand splice which is a difference of less than 6%. Because of the relatively small change in nominal capacity between the uniaxial and biaxial loading cases, biaxial bending was not considered.

Example moment-curvature calculations are found in APPENDIX C: Strain-Compatibility Moment-Curvature Calculations. The nominal moment capacity was calculated based on tested material properties of 6650 psi for the concrete in the girder and 6020 psi for the concrete in the deck. The tensile strength of the concrete in the girder used for calculations was the tested value of 424 psi. To calculate the effective prestress force, the results of the effective prestress tests one and five were averaged based on the inconclusive results obtained from the other tests. This gave an effective prestress force of 132 ksi. The tested average of 163 ksi was used to predict the effective prestress restored by the strand splice. The prestressing ultimate strength for calculations was based on the tested ultimate strength of 262 ksi. The values for the FRP composite system used in the calculations was based on the tested values for double ply samples of 12100 ksi for the modulus of elasticity, 0.011 in/in as the ultimate strain, and 136 ksi as the ultimate strength.

Table 17 summarizes the results of the nominal moment calculated using moment-curvature. It shows the moments for the damaged and repaired girders for each test. Included are the moments at decompression, cracking, a strain in the concrete top fiber of 0.0015, a yield strain in the strands of 0.009 in/in, and a compressive failure strain in the concrete top fiber of 0.003 in/in. Also presented is the percent of nominal strength when compared to the control test.

Figure 82 shows the moment-curvature behavior for Test 1, the damaged girders, and the repaired girders. Also, the maximum nominal moments based on the moment-curvature calculations are labeled.

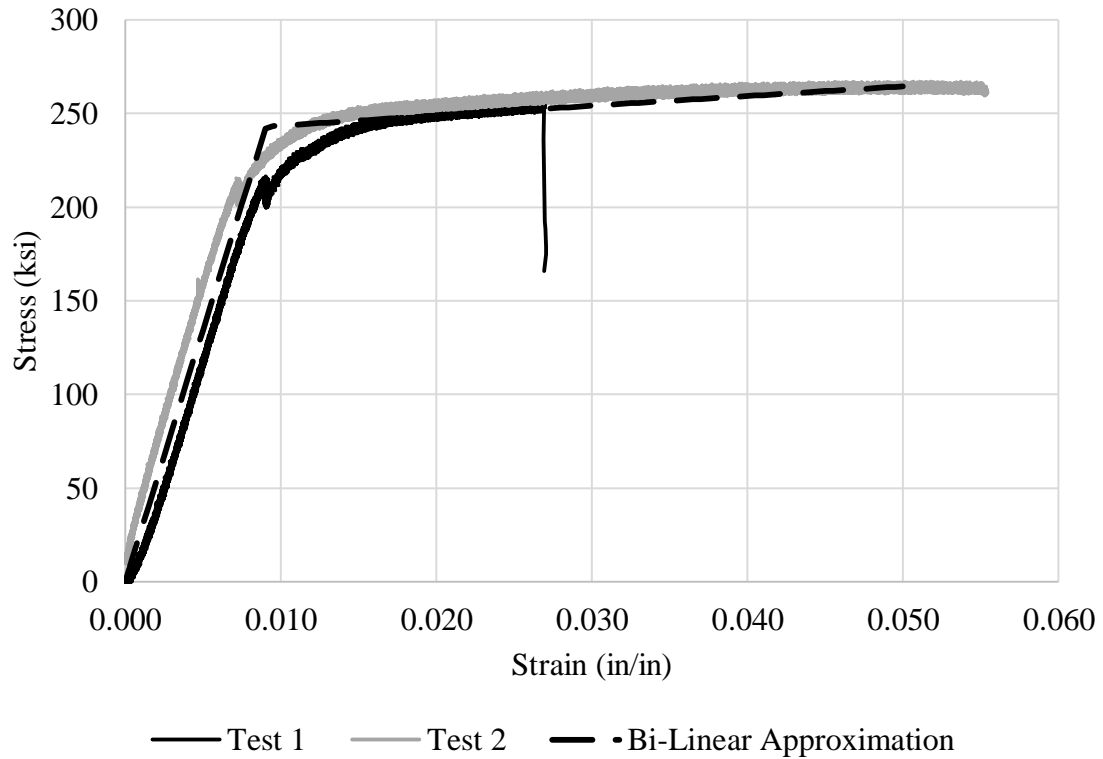


**Figure 81. Prestress Steel Stress - Strain Relationship Gangi, M. (2015). Nonlinear Beam Modeling of the Repair of Impact-Damaged Prestressed Bridge Girders. Virginia Polytechnic and State University, Department of Civil and Environmental Engineering. Blacksburg: Virginia Center for Transportation Innovation and Research, Used under fair use, 2015**

Table 17. Moment-Curvature Calculation Summary

Test	Description	# Severed Strands	$M_{decomp,mp}$ (k-ft)	$M_{cr,mp}$ (k-ft)	$M_{0.0015,mp}$ (k-ft)	$M_{y,mp}$ (k-ft)	$M_{n,mp}$ (k-ft)	% of $M_n$ Control
1	Control Test	0	1660	1770	2880	3270	3350	-
2	8-Strand Splice	Damage	1350	1510	2290	2750	2820	84
		Repair	1620	137*	2510	3220	3270	97
3	4-Strand FRP	Damage	1480	1610	2440	2950	3000	90
		Repair	1480	132*	2880	3460	3580	107
4	4-Strand Splice	Damage	1480	1610	2440	2950	3000	90
		Repair	1620	118*	2470	3170	3220	96

\*First Cracking Occurred in the Repair Section

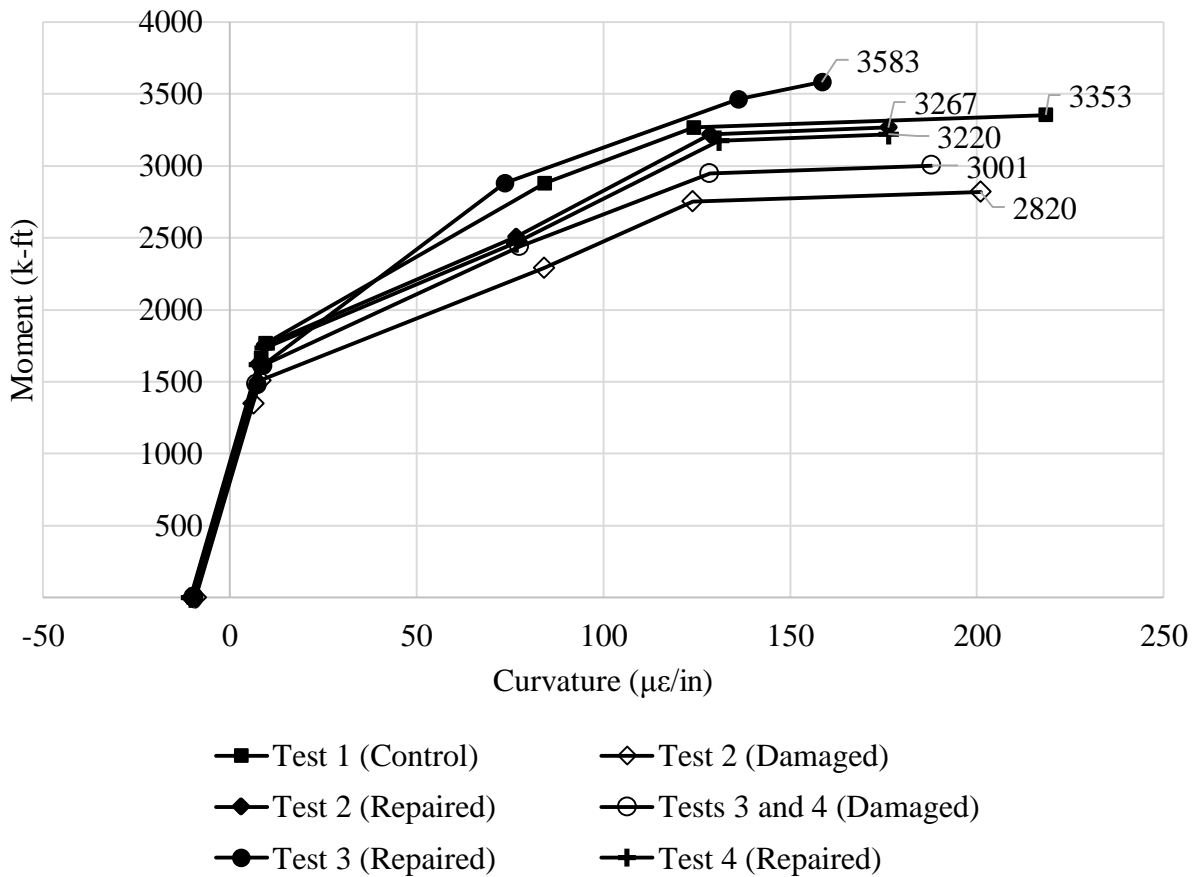


Figure 82. Calculated Moment-Curvature Behavior

Calculations for the repaired girders were made by adding the repaired sections as an additional force acting on the girder cross section and using strain compatibility to determine the stress in the repair. First, the strength of the damage girder was calculated by reducing the

effective prestressing force by the number of severed strands. Next, the repairs were added back in as an additional force. The manufacturing tables were used to determine the amount of effective stress to add from the strand splices. The force from the strand splices was added at the centroid of the prestressing strands. The FRP was added as an additional force at the centroid of the fabric repair and strain compatibility was used to calculate the effective force provided by the fabric at each point along the moment-curvature diagram.

The cracking moment for the repaired section was calculated for the repair concrete. The cracking moment in these locations is much lower than in the original concrete because the patch was not precompressed by the prestressing strands. This is important for serviceability because cracking in the repair can allow moisture to reach the repaired strands and can cause corrosion and deterioration.

#### **4.3.3: Non-Linear Finite Element**

OpenSees was used to build a non-linear finite element model of the girder (Gangi, 2015). The two dimensional model of the girder was built using beam elements that could be analyzed in two dimensions rather than three dimensional elements. This is possible because of the relative length of the girder when compared to its height and width. Also, the load is applied along the axis perpendicular to the length allowing a two dimensional analysis.

The deck width of 16 in and thickness of 8.75 in were assumed to be constant along the length of the girders for all models. A compressive strength of 5 ksi was used for both the girder and deck concrete. The stress-strain relationship of the concrete was approximated using a Hognestad model with a peak compressive strength of 6.65 ksi for the girder and 6.02 ksi for the deck. The tensile strength was assumed to be 10% of the compressive strength, or 0.665 ksi for the girder and 0.602 ksi for the deck. The prestress strands were modeled as having an ultimate

strength of 250 ksi and an initial strain of 0.00519 which corresponded to an effective prestress of 140 ksi. The stress-strain relationship used for the prestressing strand model as shown in Figure 81 is the bilinear approximation of the tested stress-strain relationship for the prestressing strands. The FRP was modeled with the design modulus of elasticity of 10,700 ksi, a debonding strain of 0.00517, and a design rupture strain of 0.014.

Simulations were run for the undamaged, damaged and repaired girder for each repair method. The finite element simulations for Test 2 and Test 4 considered in this report assumed 90% of the ultimate strength, or 225 ksi, was restored by the strand splices and that the repaired section of concrete remained bonded to the original concrete in the girder. Table 18 shows the maximum nominal moment capacities determined by the finite element modeling (Gangi, 2015). Also in Table 18 is the percentage of predicted strength regenerated when compared to the nominal moment from the control test and the failure mode used in each finite element model as prescribed by AASHTO. The girder failed in flexure with a concrete compressive strain in the top fiber of the deck of 0.003 in/in for test 1, test 3, and test 4. The simulation was also run with a FRP debonding failure in test 3 at a strain of 0.0052 in/in as per ACI provisions. Test 2 had a flexural tension failure in which a spliced strand ruptured at a stress of 225 ksi or 90% of the ultimate strength (Gangi, 2015).

**Table 18. Finite Element Analysis Results**

Test	Tested Repair	# Severed Strands	$M_{n,FE}$ (k-ft)	% of $M_{nControl}$	Failure Mode
1	Control Test	0	3190	-	Concrete Crush at 0.003 in/in
2	8-Strand Splice	8	2750	86	Spliced Strand Rupture at 225 ksi
3	4-Strand FRP	4	3870	121	Concrete Crush at 0.003 in/in
					FRP Debond at 0.0052 in/in
4, Iteration 1	4-Strand Splice	4	2910	91	Concrete Crush at 0.003 in/in
4, Iteration 2			2910	91	

#### **4.4: Laboratory Tests**

##### **4.4.1: Test Results Overview**

As previously discussed, the width of the deck varied from Girder A to Girders B and C. This variance caused a variation in the self-weight. Table 19 shows the different deck widths, the self-weight from the deck and girder as a distributed load, and the applied moment from just the self-weight at the point of the maximum applied moment. Table 20 summarizes the results of the girder flexural tests. Included in the table are number of damaged strands, span length, calculated nominal moment capacities ( $M_{n,AASHTO}$ ,  $M_{n,m\phi}$ ,  $M_{n,FE}$ ), and failure moment ( $M_{a,fail}$ ) of the tests covered in this report. Table 21 summarizes the results of the tests and the calculated cracking moments.

**Table 19. Girder Self-Weight Moments**

Girder	Test	Description	Deck Width (in)	Self-Weight (k/ft)	Self-Weight Moment (k-ft)
A	1	Control Test	16	0.729	111
B	2	8-Strand Spliced	11	0.684	282
C	3	4-Strands Severed with FRP	11	0.684	194
	4	4-Strand Spliced	11	0.684	265

**Table 20. Nominal and Failure Moment Summary**

Test	Description	# Severed Strands	L (ft)	$M_{n,AASHTO}$ (k-ft)	$M_{n,m\phi}$ (k-ft)	$M_{n,FE}$ (k-ft)	$M_{a,fail}$ (k-ft)
1	Control Test	0	35	3260	3350	3190	3180
2	8-Strand Spliced	8	58	3060	3270	2750	2750
3, Iteration 1	4-Strands Severed with FRP	4	48	3540	3580	3870	3540
3, Iteration 2			53				3410
4, Iteration 1	4-Strand Spliced	4	58	3030	3220	2910	3190
4, Iteration 2			50				3140

**Table 21. Cracking Moment Test Results Summary**

Test	Description	# Severed Strands	L (ft)	$M_{cr,AASHTO}$ (k-ft)	$M_{cr,m\phi}$ (k-ft)	$M_{a,crack}$ (k-ft)
1	Control Test	0	35	1770	1770	2160
2	8-Strand Spliced	8	58	181	137	782
3	4-Strands Severed with FRP	4	48	201	132	2750*
4	4-Strand Spliced	4	58	189	118	510

\*Applied moment when cracks were detected in the web – no cracks were detected in the FRP

The data from the LVDTs along the repair sections and the original girder did not indicate slip at the interface for the repairs in Tests 2, 3, and 4. The data from the strain transducers between the two load points were used to develop a strain profile and build a moment-curvature diagram for each test which are presented in the subsequent sections.

#### **4.4.2: Test 1 – Control Test**

The control test reached a load of 401 kips and a deflection of 1.85 in. The span for this test was 35 ft. The calculated moment capacity of the girder based on the maximum load applied during the test was 3180 k-ft. The cracking load was 267 kips for an applied cracking moment of 2160 k-ft.

The control test did not reach failure because the actuator reached its maximum capacity before the girder failed. Cracking was observed along the bottom flange and in the web. Crack patterns between the load points were consistent with impending flexural or shear failures, but were more indicative of a flexural failure. Non-linear finite element failure analysis predicted a flexural failure (concrete crushing) at a total load of 403 kips with a deflection of 1.81 in (Gangi, 2015). Figure 83 compares the calculated moments versus deflection curves with the measured moment versus deflection curve for test 1. The test closely resembled the finite element predictions. The flattened response curve of the second trial shows the loss of elasticity after the girder was loaded beyond the elastic range during the first trial. The moment versus deflection response shows plastic behavior as the girder approached its nominal moment.

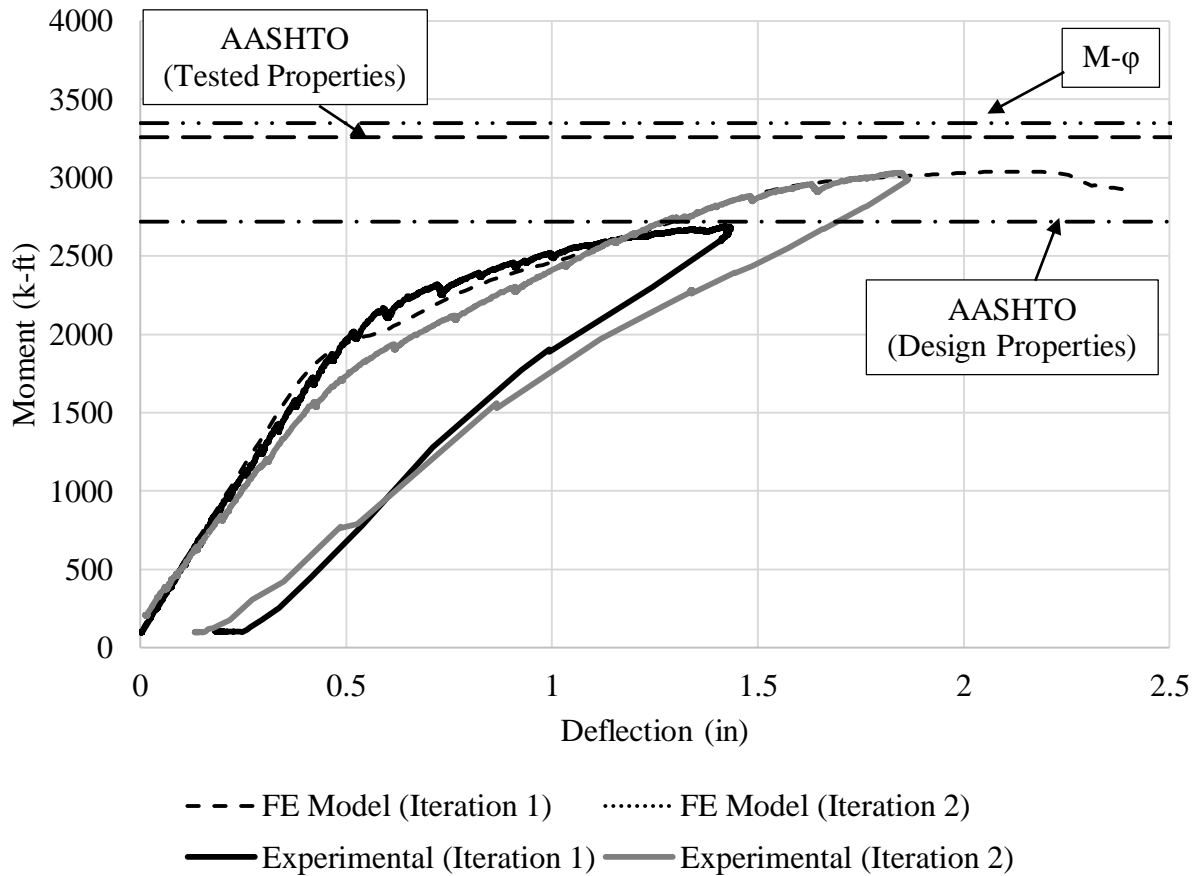


**Figure 83. Test 1 Moment Deflection Behavior**

The cracking and increased rate of deflection provided ample warning of failure as the girder approached its nominal load. The predicted moments for cracking and capacity were compared to the tested moments. For the cracking moments, both AASHTO and the moment-curvature calculations were conservative. For the nominal moment capacity, moment-curvature calculations overestimated the strength of the girder, while AASHTO calculations and finite element modeling were conservative. Table 22 compares the nominal cracking and nominal moments with the applied cracking and failure moments. The ratio was determined by dividing the predicted cracking and nominal moments by the tested cracking and nominal moments. The

nominal moment calculated from this test and the failure mode were used as a basis for comparison between an undamaged girder and the damaged girders in subsequent tests.

**Table 22. Experimental and Calculated Cracking and Nominal Moment Capacities for Test 1**

	<b>Cracking Moment (k-ft)</b>	<b>Nominal Moment (k-ft)</b>	<b>M<sub>cr</sub> Ratio</b>	<b>M<sub>n</sub> Ratio</b>
<b>Tested</b>	2160	3180	-	-
<b>AASHTO (Tested Properties)</b>	1770	3260	0.82	1.02
<b>AASHTO (Design Properties)</b>	1780	2720	0.82	0.86
<b>Moment-Curvature</b>	1700	3350	0.79	1.05
<b>Finite Element</b>	-	3190	-	1.00

Figure 84 shows the predicted moment-curvature relationship and the experimental moment-curvature relationship calculated using the measurements from the strain gauges at 41 and 2 in from the bottom of the girder during Test 1. The strain profile graphed using the data from the strain gauges was not linear. Upon inspection, the neutral axis graph between the 41 in gauge and the 2 in gauge was consistent with the neutral axis calculated during the moment-curvature calculations. The incompatibility indicated by the gauge on the deck at 49 in could be a result of slipping between the deck and the girder due to non-composite behavior. Therefore, the curvature was calculated using the gauges in the top and bottom flanges. The instrumentation was removed prior to the ultimate moment, therefore the full relationship is not presented. The portion that is presented gives a representation to which the moment-curvature relationships of subsequent tests is compared.

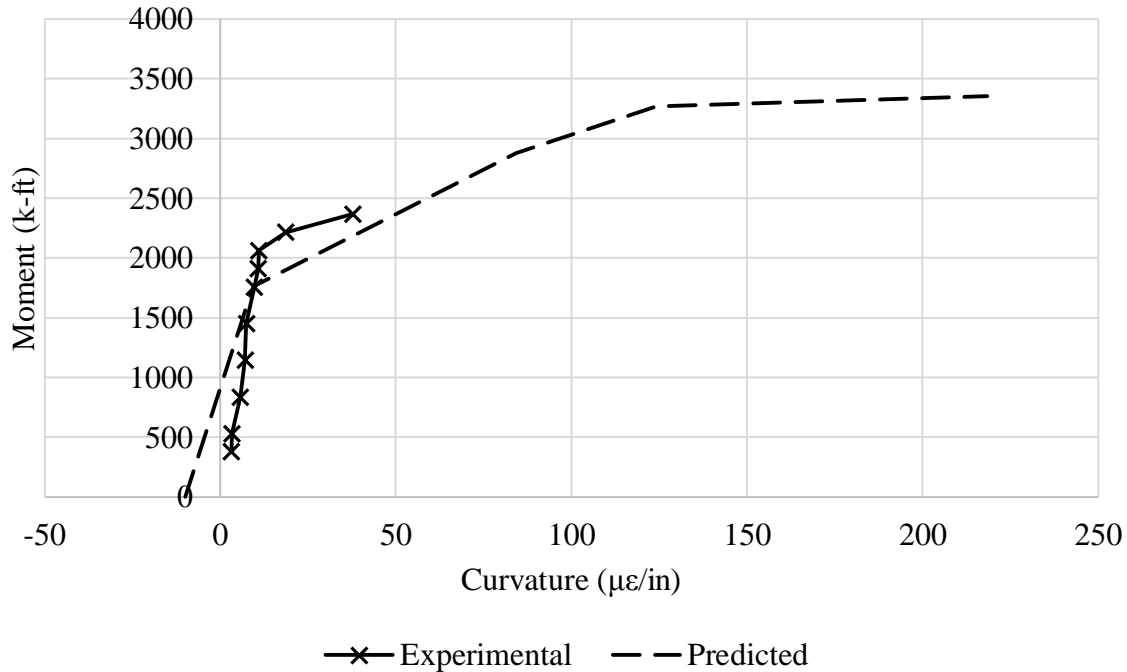


Figure 84. Test 1 Moment-Curvature Relationship

#### **4.4.3: Test 2 – Girder with Eight Severed/Re-tensioned Strands**

Test 2 reached a load of 197 kips and a deflection of 3.84 in. The span for this test was 58 ft. The calculated moment capacity of the girder based on the maximum load applied during the test was 2750 k-ft. The cracking load was 40 kips for an applied cracking moment of 782 k-ft.

The girder showed signs of failure prior to reaching the nominal load. The final failure mode was a tensile flexural failure in which one strand slipped out of the splice chuck and one strand ruptured. Figure 85 compares the nominal moment versus deflection curves with the applied moment versus deflection curve for Test 2. Table 23 compares the calculated cracking and nominal moments with the applied cracking and failure moments. The ratio is determined by dividing the calculated values by the tested values. The AASHTO and moment-curvature calculations overestimated the cracking moment because the first cracks formed in the repaired

section where the concrete was not compressed from the prestressing strands. The AASHTO and moment-curvature calculations overestimated the nominal capacity of the girder while the finite element model was accurate in its prediction of the failure moment.

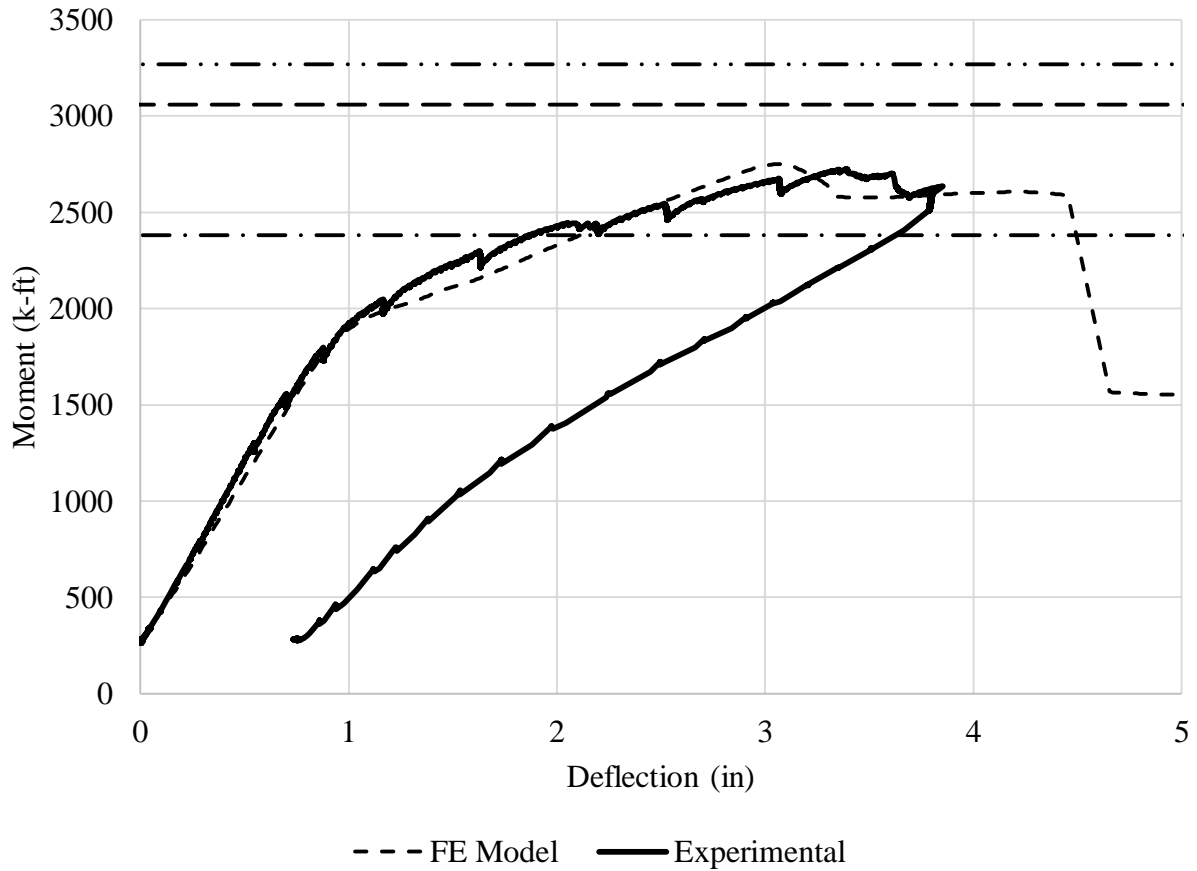


Figure 85. Test 2 Moment Deflection Behavior

Table 23. Experimental and Calculated Cracking and Nominal Moment Capacities for Test 2

	Cracking Moment (k-ft)	Nominal Moment (k-ft)	$M_{cr}$ Ratio	$M_n$ Ratio
<b>Tested</b>	782	2750	-	-
<b>AASHTO (Tested Properties)</b>	181	3060	0.23	1.11
<b>AASHTO (Design Properties)</b>	181	2380	0.23	0.87
<b>Moment-Curvature</b>	137	3270	0.18	1.19
<b>Finite Element</b>	-	2750	-	1.00

As the moment increased, cracking consistent with a flexural failure was observed along the bottom flange as shown in Figure 86. Figure 85 illustrates plastic behavior consistent with a flexural failure as the girder approached its nominal capacity. The cracking and deflection provided ample warning of the girder's failure. Figure 87 shows the predicted moment-curvature relationship and the moment-curvature relationship calculated using the measurements from the strain gauges at 41 and 2 in from the bottom of the girder. The strain profile graphed using the data from the strain gauges was not linear. Upon inspection, the neutral axis graph between the 41 in gauge and the 2 in gauge was consistent with the neutral axis calculated during the moment-curvature calculations. The incompatibility indicated by the gauge on the deck at 49 in could be a result of slipping between the deck and the girder due to non-composite behavior. Therefore, the curvature was calculated using the gauges in the top and bottom flanges. The graph of the tested moment-curvature relationship did not provide conclusive results.



**Figure 86. Flexural Cracks in Patch Concrete near Failed Strand Splice (Photo taken by Ioannis Koutromanos, used under fair use 2015)**

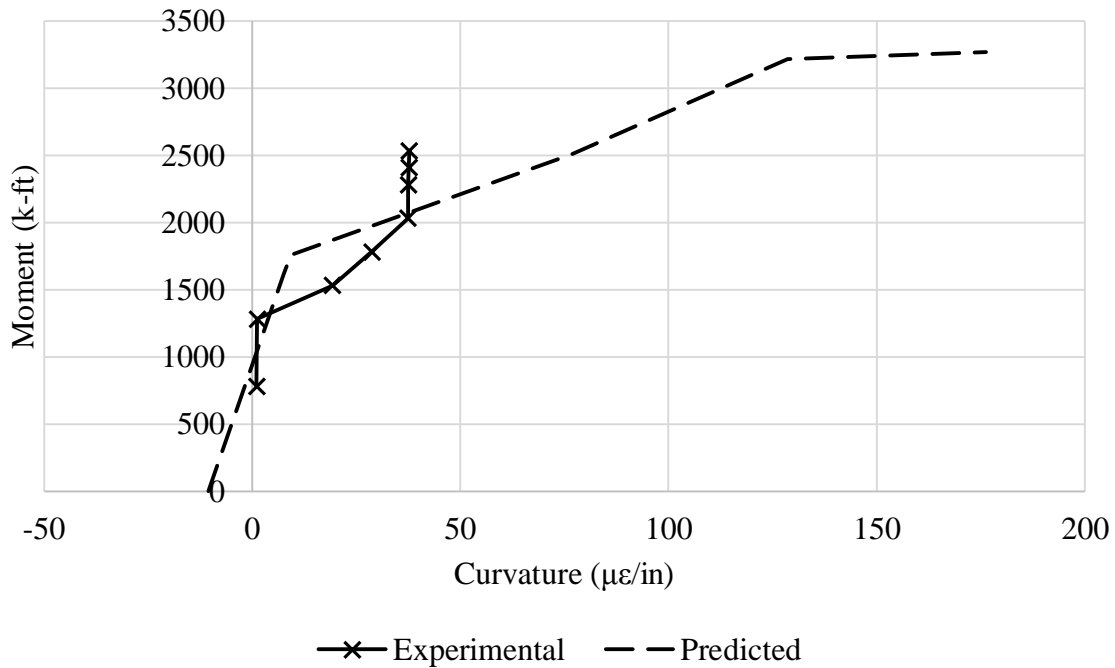


**Figure 87. Test 2 Moment-Curvature Relationship**

The repair concrete was removed after the test was complete to investigate the failure and it was discovered that one of the prestressing strands slipped out of the splice chuck and one of the prestressing strands fractured as shown in Figure 88. This picture was taken after the girder was removed from the testing bay, the strands were not rusted during testing.

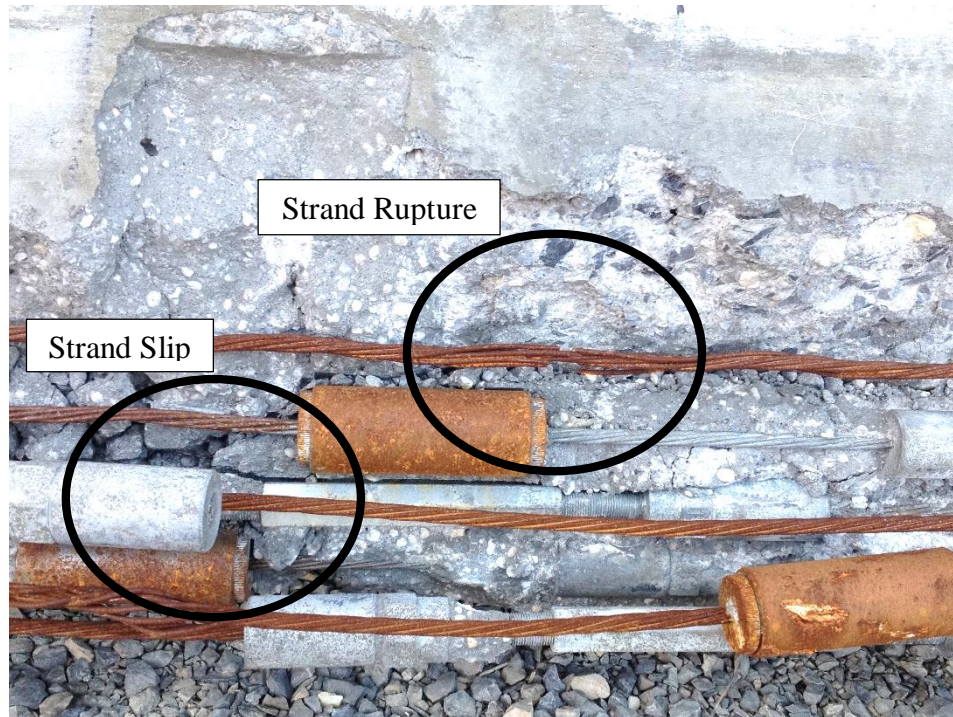


**Figure 88. Test 2 Failed Splice and Ruptured Strand (Photo taken by Mark Jones, used under fair use 2015)**

#### **4.4.4: Test 3 – FRP Repaired Girder with Four Severed Strands**

Test 3 reached a load of 313 kips and a deflection of 3.16 in for the first iteration and a load of 277 kips and a deflection of 3.35 in for the second iteration. The span was 48 ft for the first iteration and 53 ft for the second iteration. The calculated nominal moment capacity of the girder based on the maximum load applied during the first iteration was 3540 k-ft and 3410 k-ft for the second iteration. The average capacity from the two iterations was 3480 k-ft. Cracking in the concrete was first identified as it propagated from under the FRP at a load of 220 kips for a cracking moment of 2750 k-ft. Cracking was noted in the epoxy of the FRP composite system prior to this, but any cracking in the concrete was hidden by the FRP.

The girder showed signs of a flexural failure prior to the end of the test. The cracking pattern in the deck between the load points indicated a compression failure was imminent.

Figure 89 depicts the predicted nominal moment versus deflection curves with the applied

moment versus deflection curve for Test 3. Table 24 compares the calculated cracking and nominal moments with the applied cracking and failure moments. The ratios are found by dividing the calculated moments by the tested moments. The AASHTO and moment-curvature calculations for the cracking moment appear very conservative. However, the variation can be explained when considering that initial cracking most likely occurred prior to when it was visible above the FRP. AASHTO calculations, moment-curvature calculations, and finite element modeling over predicted the moment capacity of the girder.

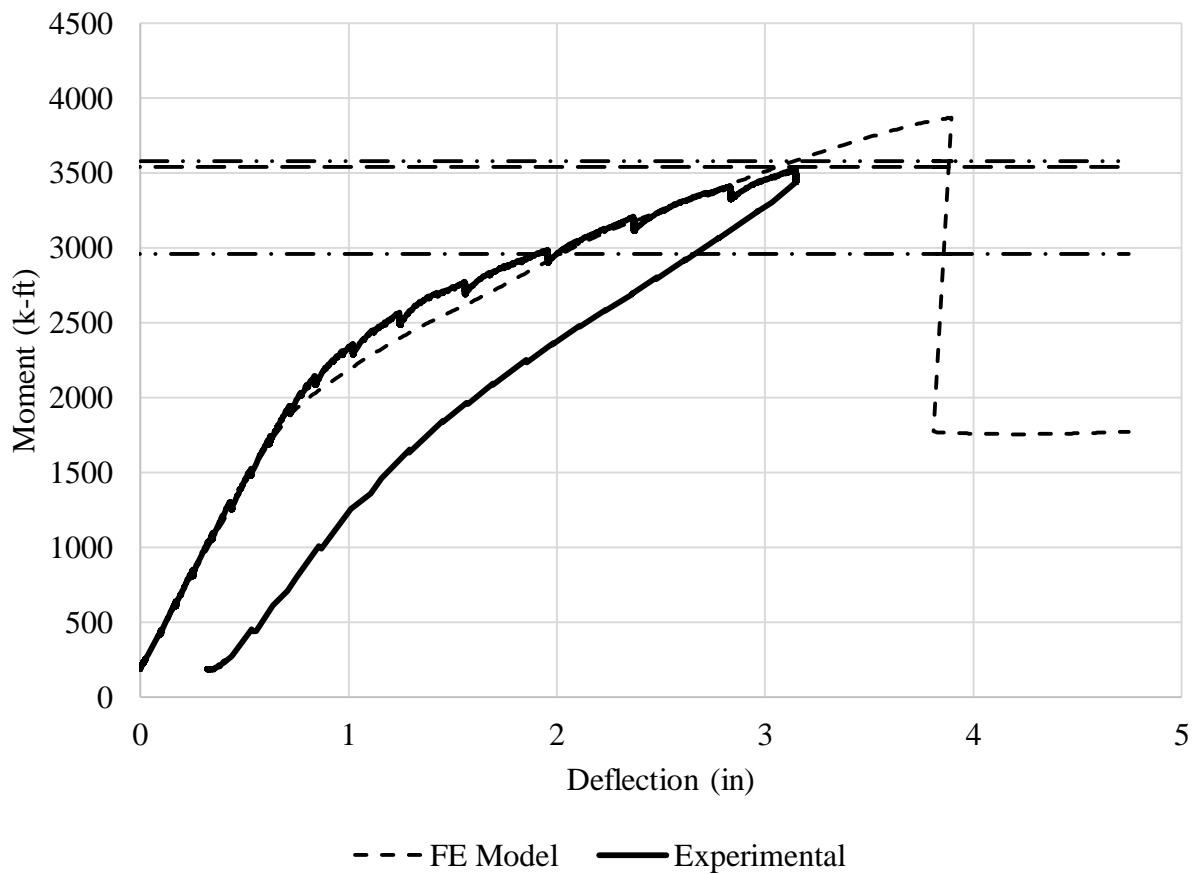


**Figure 89. Test 3 Moment Deflection Behavior**

**Table 24. Experimental and Calculated Cracking and Nominal Moment Capacities for Test 3**

	<b>Cracking Moment (k-ft)</b>	<b>Nominal Moment (k-ft)</b>	<b>M<sub>cr</sub> Ratio</b>	<b>M<sub>n</sub> Ratio</b>
<b>Tested</b>	2750	3540	-	-
<b>AASHTO (Tested Properties)</b>	201	3540	0.07	1.00
<b>AASHTO (Design Properties)</b>	201	2960	0.07	0.84
<b>Moment-Curvature</b>	132	3580	0.05	1.01
<b>Finite Element</b>	-	3870	-	1.09

Figure 90 shows the calculated moment-curvature relationship and the moment-curvature relationship calculated using the measurements from the strain gauges at 41 and 2 in from the bottom of the girder. The strain profile graphed using the data from the strain gauges was not linear. Upon inspection, the neutral axis graph between the 41 in gauge and the 2 in gauge was consistent with the neutral axis calculated during the moment-curvature calculations. The incompatibility indicated by the gauge on the deck at 49 in could be a result of slipping between the deck and the girder due to non-composite behavior. Therefore, the curvature was calculated using the gauges in the top and bottom flanges. The instrumentation was removed prior to the ultimate moment was reached, but the tested moment-curvature relationship along with the calculated curvature-ductility ratio presented in subsequent sections show that the ductile behavior was not diminished by the FRP.

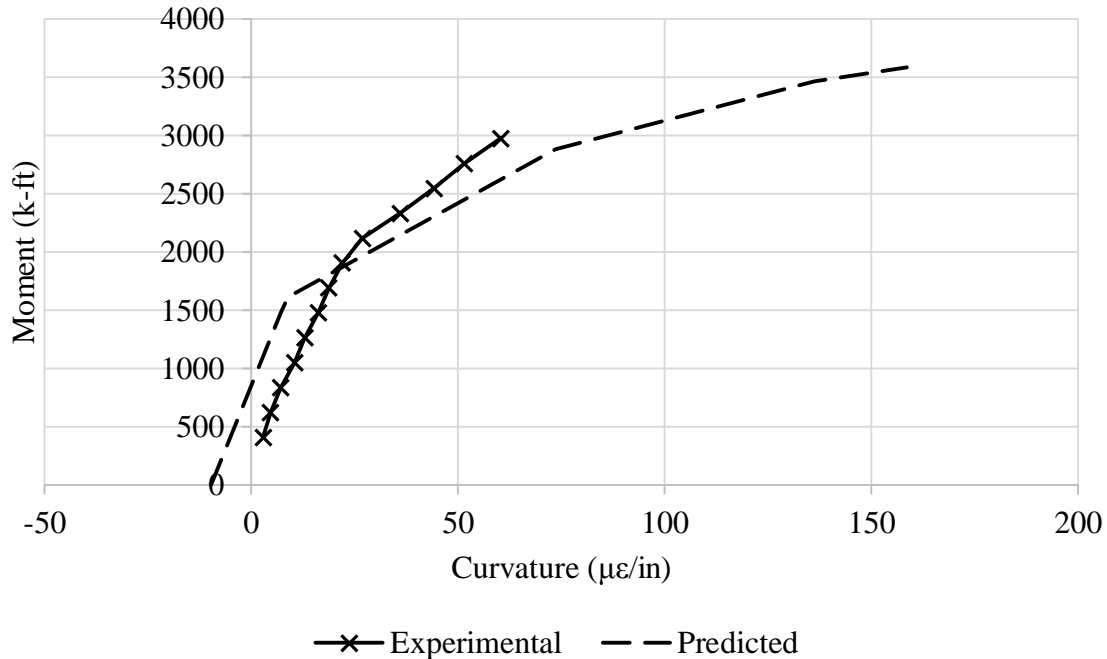


**Figure 90. Test 3 Moment-Curvature Relationship**

The epoxy bonding the FRP to the bottom flange of the girder cracked throughout the loading process. As the load approached the nominal capacity of the girder, the cracking propagated from the epoxy into the web of the girder as shown in Figure 91. Cracking developed at the end of the repair section along the interface between the epoxy and the concrete, however, it did not indicate a bond failure between the FRP and the substrate. Cracking in the concrete in the deck was indicative of a compression failure. In addition, the shallow slope of the load deflection curve and the reduced plastic behavior illustrated in Figure 89 is associated with a more brittle and sudden compression failure. The cracking in the epoxy provided a visual and auditory warning as the girder approached its nominal capacity. In addition, the cracks propagated into the web providing additional warning prior to the failure.

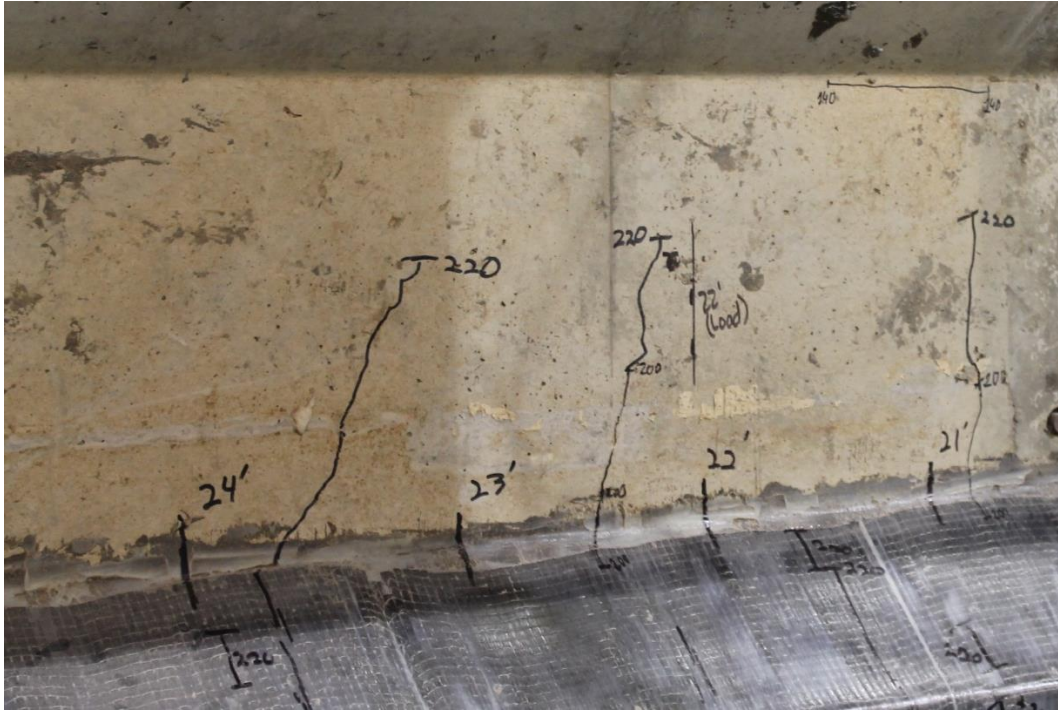


Figure 91. Crack Propagation from FRP into Web (Photo taken by Ioannis Koutromanos, used under fair use 2015)

#### **4.4.5: Test 4 – Girder with Four Severed/Re-tensioned Strands**

Test 4 reached a load of 241 kips and a deflection of 4.12 in for the first iteration and a load of 266 kips and a deflection of 3.61 in for the second iteration. The span was 58 ft for the first iteration and 50 ft for the second iteration. The calculated moment capacity of the girder based on the maximum load applied during the first iteration was 3190 k-ft. The moment capacity for the second iteration was 3140 k-ft. The average capacity from the two iterations was 3170 k-ft. Cracking was noted at an applied load of approximately 20 kips for a cracking moment of 510 k-ft.

The girder failed in compression when the concrete in the deck between the load points crushed. Figure 92 compares the predicted nominal moment versus deflection curves with the measured applied moment versus deflection curve for iteration 1 of Test 4. Figure 93 compares

the predicted moment versus deflection curves with the measured moment versus deflection curve for iteration 2 of Test 4. Table 25 compares the predicted cracking and nominal moments with the applied cracking and failure moment. The ratios are determined by dividing the calculated moments by the tested moments. The AASHTO and moment-curvature calculations over predicted the cracking moment of the girder. The AASHTO nominal moment calculation was conservative when compared to the applied failure moment. The moment-curvature calculations and the finite element model over predicted the failure moment.

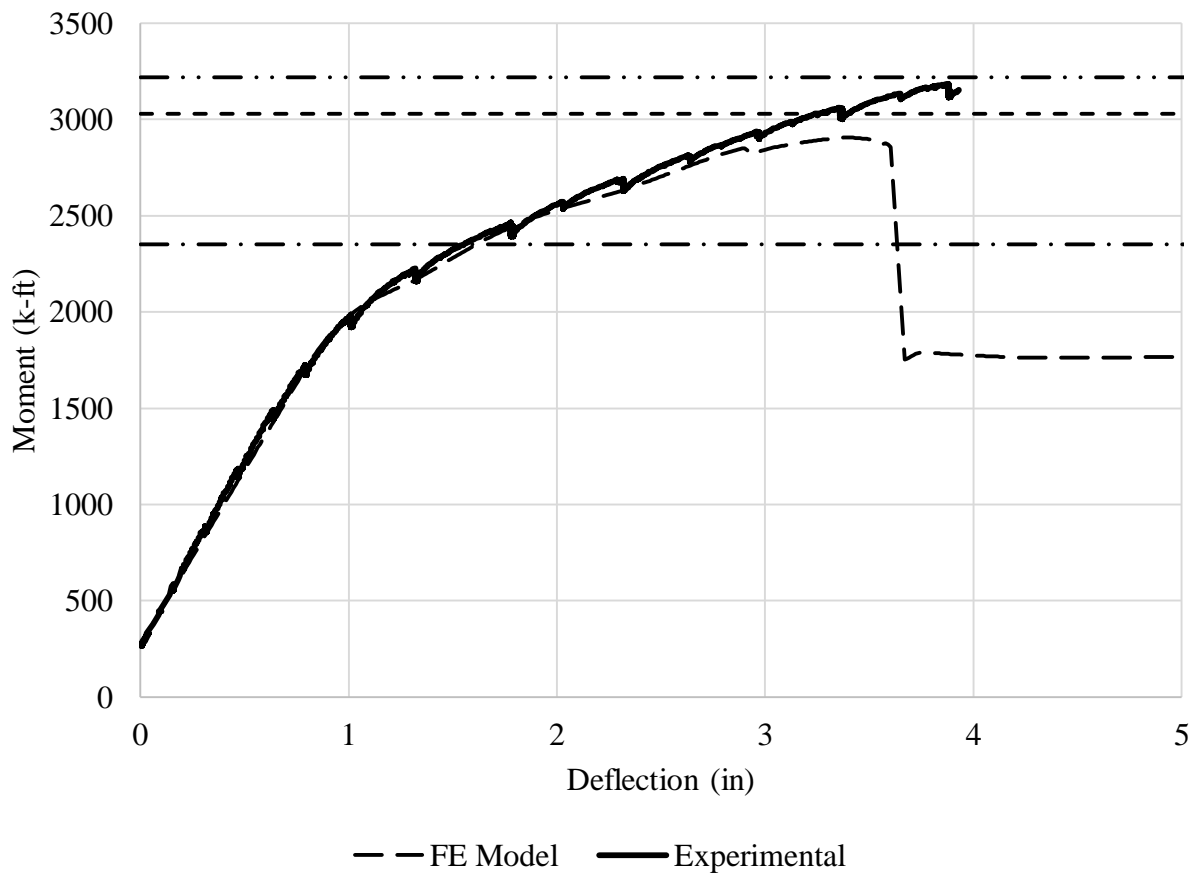


**Figure 92. Test 4, Iteration 1 Moment Deflection Behavior**

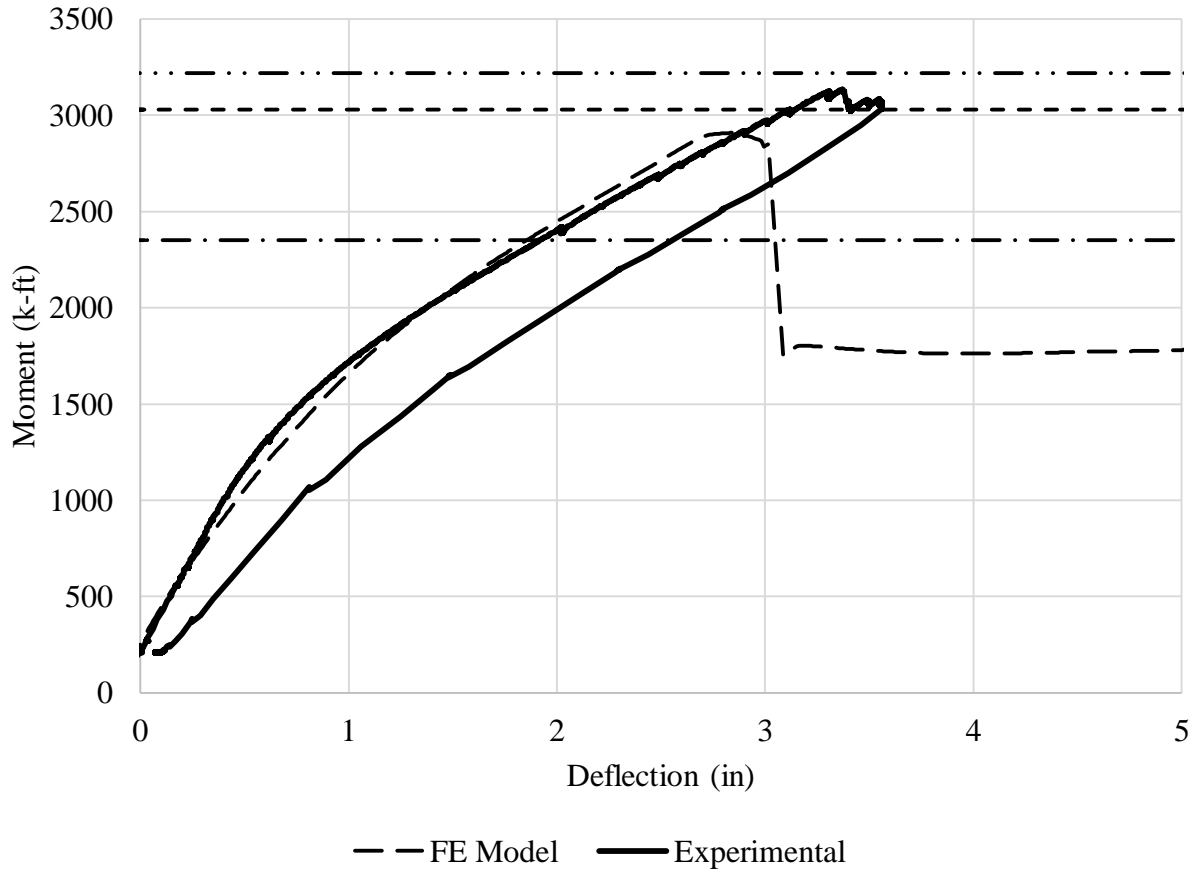


**Figure 93. Test 4, Iteration 2 Moment Deflection Behavior**

**Table 25. Experimental and Calculated Cracking and Nominal Moment Capacities for Test 4**

	Cracking Moment (k-ft)	Nominal Moment (k-ft)	$M_{cr}$ Ratio	$M_n$ Ratio
<b>Tested</b>	510	3190	-	-
<b>AASHTO (Tested Properties)</b>	189	3030	0.37	0.95
<b>AASHTO (Design Properties)</b>	189	2350	0.37	0.74
<b>Moment-Curvature</b>	118	3220	0.23	1.01
<b>Finite Element</b>	-	2910	-	0.91

Figure 94 shows the predicted moment-curvature relationship and the moment-curvature relationship calculated using the measurements from the strain gauges at 41 and 2 in from the bottom of the girder. The strain profile graphed using the data from the strain gauges was not linear. Upon inspection, the neutral axis graph between the 41 in gauge and the 2 in gauge was

consistent with the neutral axis calculated during the moment-curvature calculations. The incompatibility indicated by the gauge on the deck at 49 in could be a result of slipping between the deck and the girder due to non-composite behavior. Therefore, the curvature was calculated using the gauges in the top and bottom flanges. The tested moment-curvature relationship along with the calculated curvature-ductility ratio presented in subsequent sections show that the ductile behavior was not diminished by the strand splices.

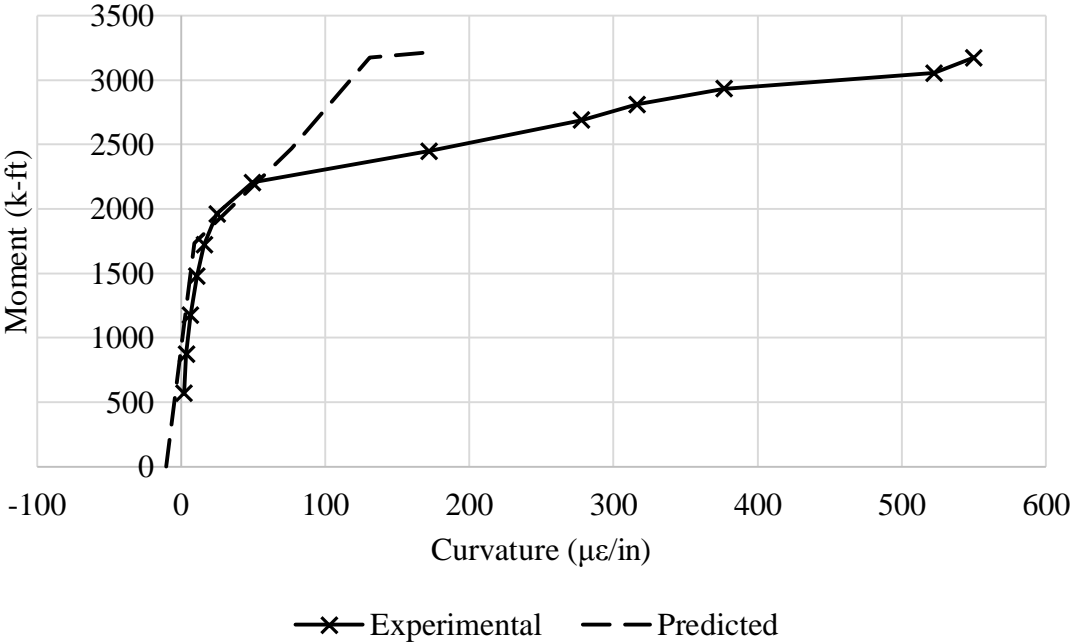


**Figure 94. Test 4 Moment-Curvature Relationship**

Cracking consistent with a flexural failure was observed along the bottom flange as shown in Figure 95 and Figure 96. The flattened response curve of the second trial seen in Figure 93 shows the loss of elasticity after the girder was loaded beyond the elastic range during the first trial. The second iteration also did not have as clearly defined plastic behavior as indicated in Figure 92 for the first trial. There was an increased rate of deflection as the load approached the nominal capacity of the girder, but the less defined plastic behavior is consistent

with a compression failure. The girder failed in compression when the concrete in the deck crushed as shown in Figure 97.



**Figure 95. Cracking Pattern at Load Point at Final Load for Iteration 1 (Photo taken by Ioannis Koutromanos, used under fair use 2015)**



**Figure 96. Cracking Patterns near Maximum Applied Load (Photo taken by Ioannis Koutromanos, used under fair use 2015)**

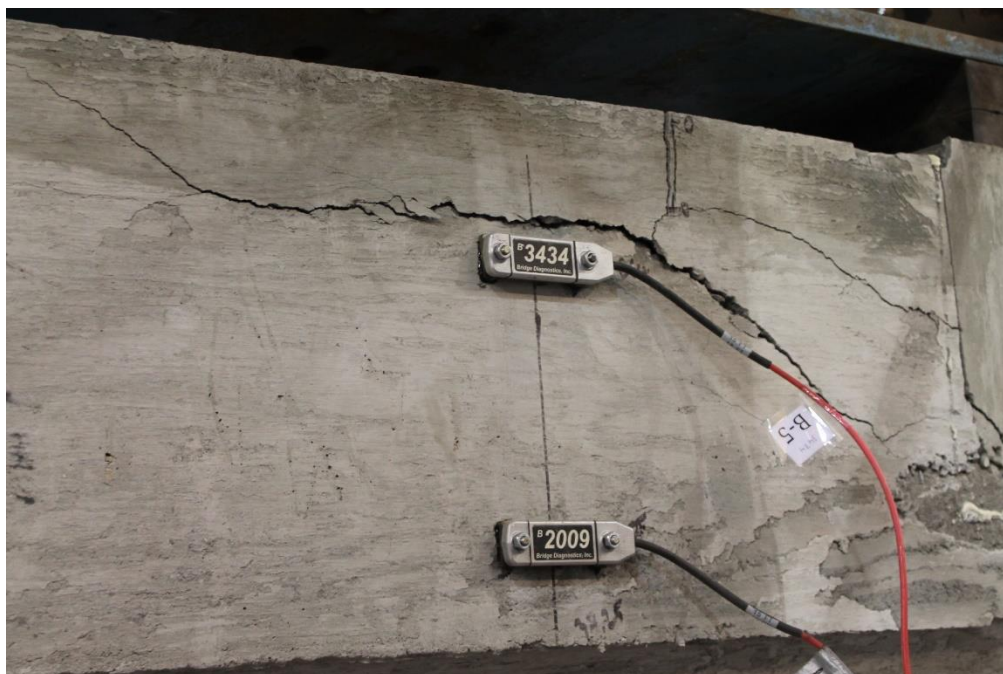


**Figure 97. Flexural Compression Failure in the Deck (Photo taken by Ioannis Koutromanos, used under fair use 2015)**

#### **4.6: Data Analysis**

In addition to calculating the nominal moment capacity for each repair, the undamaged capacity for each girder was found using the three analysis methods. Table 26 compares the original nominal capacity of the undamaged girders as calculated using each analytical methods to the repaired girder capacity. It also gives a percentage of the strength regenerated by dividing the tested strength by the nominal strength of the undamaged girder for each analytical method. Table 27 compares the same data using the cracking moment.

**Table 26. Nominal versus Tested Strength Regained**

Test	Description	# Severed Strands	Tested	Undamaged $M_n$ (k-ft)			Strength Regained (%)			
			$M_{a,fail}$ (k-ft)	$M_{n,AASHTO}$	$M_{n,m\phi}$	$M_{nFE}$	AASHTO	$m\phi$	FE	Tested
1	Control Test	0	3180	3260	3350	3190	N/A	N/A	N/A	N/A
2	8-Strand Spliced	8	2750	3060	3270	2930	90	84	94	86
3	4-Strands Severed with FRP	4	3540	3030	3220	3030	111	110	117	111
4	4-Strand Spliced	4	3190	3030	3220	2990	105	99	108	100

**Table 27. Cracking versus Tested Strength Regained**

Test	Description	# Severed Strands	Tested	Undamaged $M_{cr}$ (k-ft)		Strength Regained (%)		
			$M_{cr,fail}$ (k-ft)	$M_{cr,AASHTO}$	$M_{cr,m\phi}$	AASHTO	$m\phi$	Tested
1	Control Test	0	2160	1770	1770	N/A	N/A	N/A
2	8-Strand Splice	8	782*	1610	1760	31	28	36
3	4-Strands Severed with FRP	4	2750	1610	1610	146	146	127
4	4-Strand Splice	4	510*	1590	1730	91	84	24

\* Cracking observed in the repaired section

As shown in the previous sections, the moment-curvature relationship was calculated using the data from the strain transducers and using a strain compatibility relationship. As previously discussed, the strain transducers were removed prior to the ultimate moment for safety reasons. In addition, the strain in the strands was not measured directly and it is difficult to determine the point when the strands yielded. Also, because of the small cracking moment in the repaired section of the concrete for Tests 2 and 4, a curvature-ductility ratio was not able to be determined using the tested data. From the calculated moment-curvature relationships, a

curvature-ductility ratio was calculated comparing the ultimate curvature to the yield curvature as shown in APPENDIX G: Curvature-Ductility Calculations.

Table 28 compares the curvature-ductility ratio ( $\mu$ ) for the moment-curvature analysis. This relationship is a measure of the girder’s ability to deflect without losing significant flexural capacity (Park & Ruitong, 1988). The ratio compares the calculated curvature at ultimate to the calculated curvature at yielding using the moment-curvature calculations. The ratio is then related to the control curvature ductility ratio.

**Table 28. Curvature-Ductility Comparison**

<b>Test</b>	<b>Description</b>	<b># Severed Strands</b>	<b><math>\mu_{m\phi}</math></b>	<b>% of Control</b>
<b>1</b>	<b>Control Test</b>	0	1.8	-
<b>2</b>	<b>8-Strands Spliced</b>	8	4.2	233
<b>3</b>	<b>4-Strand Severed with FRP</b>	4	1.2	67
<b>4</b>	<b>4-Strands Spliced</b>	4	1.3	72

**4.6.1: Strand Splice Repair**

Lessons learned during the instillation process include the procedure for clearing damaged concrete a minimum of 1 in from the surface of the girder to include any cracked or debonded concrete. The process included using a grinder with a diamond cutting blade to cut approximately 0.5 in into the girder from the surface of the concrete. The remaining 0.5 in of concrete was removed using an electric chipping hammer. Approximately 0.5 in of concrete was removed from around any exposed strand to allow the repair concrete mix to consolidate around the strands and improve the bond. When removing concrete from around the strands, the operator must ensure that the strands are not nicked or damaged by the chipping hammer. After the loose and damaged concrete was removed, the area was cleaned and hydrated to ensure a proper bond is created between the original and the new concrete.

Figure 98 shows second order polynomial trends for the percent of original strength regained by the strand splice repair method as tested. There is an inverse relationship between the number of damaged strands and the percent of predicted capacity that was regenerated. Based on these trends and interpolating between results, it can be seen that strand splices are able to regenerate approximately 90% of strength for four to six damaged strands or 80% of strength for seven to nine damaged strands. These approximations include all three analysis methods and the percent is also a function of which method is used to calculate the original strength of the girder. The predictions are also limited to AASHTO Type III girders with impacted severed strands and a deck that is the width of the top flange of the girder. In addition, there were only two data points to interpolate the predictions.

When compared to the nominal capacity of the girder calculated using the design material strengths and the AASHTO equations, the strand splices restored 96% of the design nominal moment capacity of the original girder for the repair of four severed strands. The strand splices restored 81% of the AASHTO design nominal moment capacity of the original girder for the repair of eight severed strands.

Based on load requirements, selecting strand splices as the primary repair method may be feasible as long as the number of damaged strands is a low percentage of the total number of strands. If the number of damaged strands is greater than which can be restored through strand splices alone, another repair method should be considered with strand splices as a supplementary option. Strand splices can be installed quickly and provide relatively early repair strength resulting in decreased down time for the structure. When installing the strand splices, if a negative moment can be applied and removed after the installation is complete, it may allow the splice to reintroduce a larger percent of the effective prestress force than was lost when the

strands were severed. By doing this, it would increase the moment before cracking in the repaired section. Decreasing the probability of cracking is important to the serviceability of the girder.

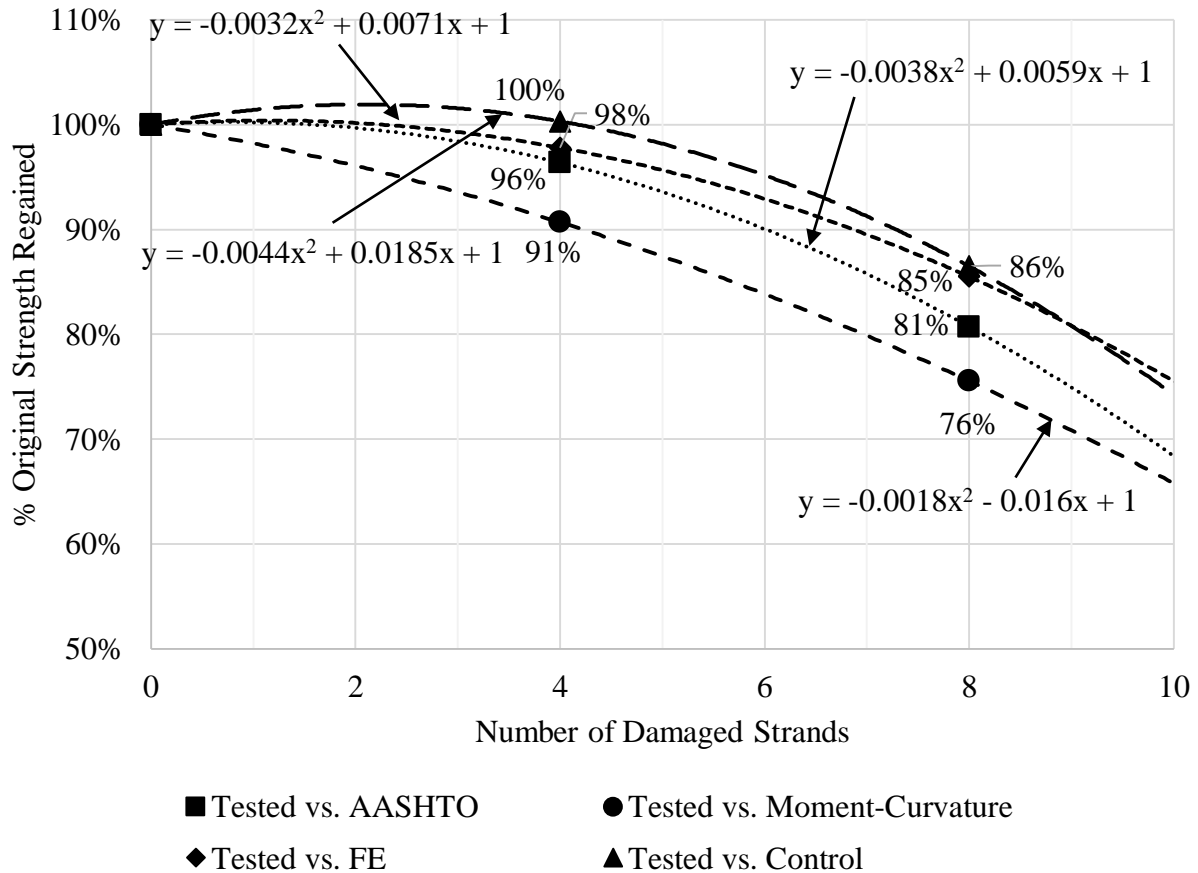


Figure 98. Strand Splice Strength Regenerated Trend Lines

#### 4.6.2: FRP Repair

Lessons learned during the repair process include the site preparation lessons discussed in the previous section for the strand splice repair. The lessons specific to the FRP repair include the requirement for trained personnel for the installation. The correct mix proportion of the epoxy was important to ensure it cured and bonded properly. In addition, it was important to ensure that the epoxy saturated the fibers of the fabric to avoid inconsistencies in the composite

matrix. The consistency of the repair was tested at 24 hrs to using hammer to check for inconsistent sounds that would indicate improper bonding. In order to reduce the potential of debonding of the FRP from shear stresses at the interface, the repair should be installed along the entire length of the girder.

The analysis methods were able to predict the strength of the repair within 10% of the actual repair. When compared to the AASHTO calculations, the ratio of calculated to tested moment was 1.00. When compared to the moment-curvature calculations, the ratio of calculated to tested moment was 1.01. When compared to the finite element model, the ratio of calculated to tested moment was 1.09.

Table 4 gives a guide for the type of FRP repair method that is best for an associated maximum number of damaged strands (Harries, et. al., 2012). It indicates that the maximum number of damaged strands for externally bonded FRP on an AASHTO Type III girder is eight. The results of this project, as shown in Table 24, validated that when four strands are severed, properly designed and installed externally bonded FRP can restore 110% of the original girder strength and is a sufficient repair technique. Designers of repairs must take into account that the relationship between stress and strain for FRP does not have the same plastic behavior that is associated with steel which in turn diminishes the plastic behavior of the girder. The warning associated with a tensile flexural failure on an overloaded girder is reduced when FRP is used instead of steel.

Based on Test 3, however there was still enough capacity in the undamaged strands to provide sufficient warning through increased deflection as the girder approached failure. This deflection and the cracked epoxy provided sufficient warning of the failure load. However, the concrete in the deck of the girder showed signs of crushing similar to the compression failure in

Test 4 which can be a sudden failure. In addition, cracking in the concrete in the bottom flange was hidden by the FRP until the cracks propagated into the web. Applying FRP to the exterior of the girder is a way to increase serviceability by containing the evidence of cracking. It is important to consider the potential of creating the conditions for a sudden failure when designing an FRP repair and ensure that it is not overdesigned. FRP does not restore any of the prestress lost by the severed strands. Therefore, supplementing the FRP repair with the relatively inexpensive strand splices would allow the designer to regain some of the force lost by the severed strands. Another option is to load the girder during the repair. If a positive moment is introduced while the repair concrete patch is being placed, it will compress when the moment is removed. This will assist in increasing the cracking moment and reducing serviceability problems.

The installation of FRP is more intensive than the installation of strand splices. It requires skilled labor that is trained in the handling of the materials. In addition, the concrete in the repair patch must be allowed to cure long enough to allow the epoxy to develop a sufficient bond. When compared to strand splices, the increased down time for the structure must be considered.

#### **4.6.3: Analysis Methods**

Several analysis methods were employed for the tests, including AASHTO equations, moment-curvature analysis using strain compatibility, and finite element modeling. Table 29 compares the results of each analysis tool to predict the cracking and failure moments. This table indicates the ratio of calculated moment to applied moment. In addition, it shows the average ratio and standard deviation for each method. The analytical models did not accurately predict the cracking moment. Both models used to predict the cracking moment had a standard

deviation greater than 0.30. AASHTO calculations and finite element modeling were able to predict the nominal failure moment capacity on average to about one percent difference. The finite element and AASHTO standard deviations were 0.07 and based on the results of these tests, they were the most accurate method to predict results. The repair methods were all able to restore more than the calculated nominal moment using the design material properties with the AASHTO equations with a standard deviation of 0.06. Figure 99 shows a plot of the ratio of the nominal moment calculated using each analytical method investigated to the tested failure moment from each test. As can be seen on the chart, the AASHTO with tested material properties, AASHTO with design material properties, and finite element methods are more accurate than the moment-curvature. The AASHTO calculations and the finite element method under predicted the strength of the final design. When compared to the AASHTO predictions using the design material properties, all repair tests were able to exceed the design nominal moment capacity.

**Table 29. Ratio of Predicted to Measured Moment Capacity**

	Cracking Moment Predictions			Failure Moment Capacity Predictions			
	AASHTO Design	AASHTO	Moment-Curvature	AASHTO Design	AASHTO	Moment-Curvature	Finite Element
<b>Test 1</b>	0.82	0.82	0.86	0.86	1.02	1.05	1.00
<b>Test 2</b>	0.23	0.23	0.18	0.87	1.11	1.19	1.00
<b>Test 3</b>	0.07	0.07	0.05	0.84	1.00	1.01	1.09
<b>Test 4</b>	0.37	0.37	0.23	0.74	0.95	1.01	0.91
<b>Average</b>	0.37	0.37	0.33	0.83	1.02	1.07	1.00
<b>Standard Deviation</b>	0.32	0.32	0.36	0.06	0.07	0.08	0.07

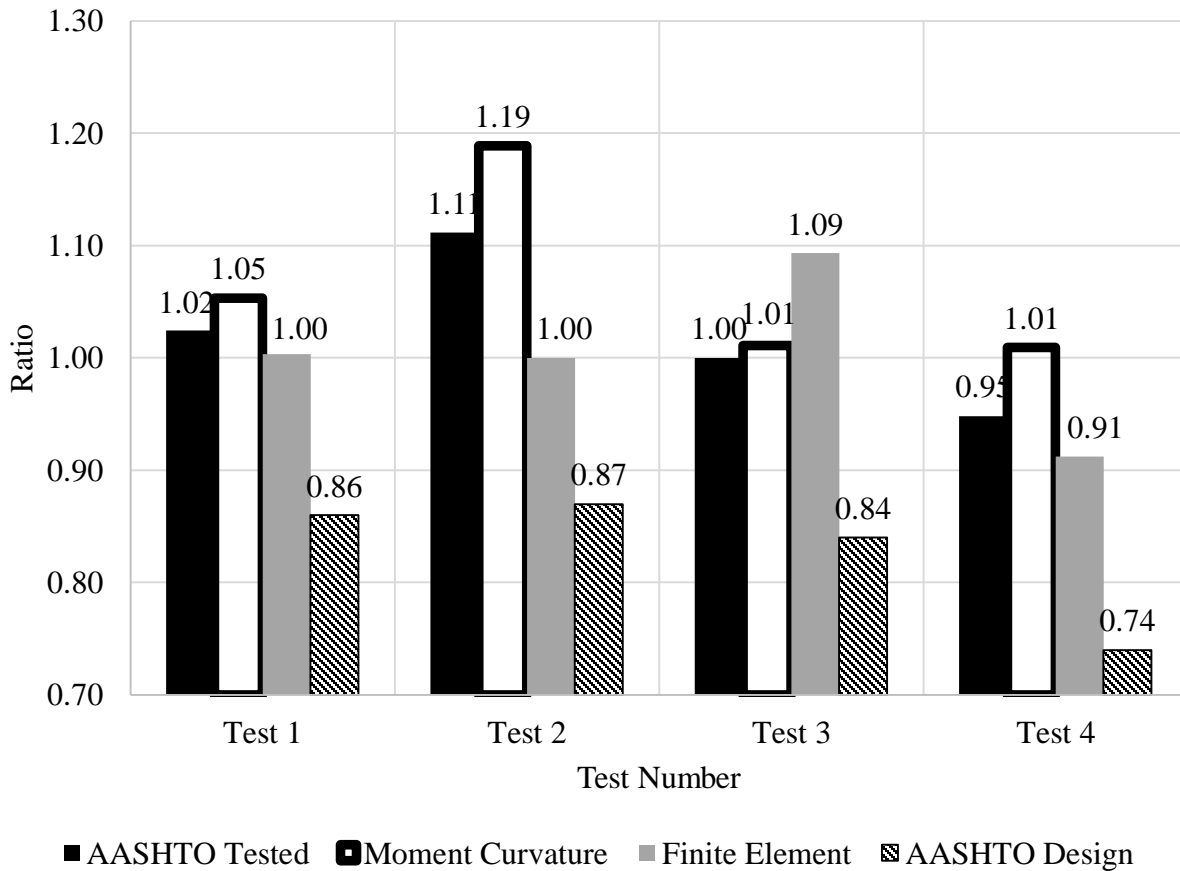


**Figure 99. Nominal to Tested Ratio**

The cracking moment for Test 2, Test 3, and Test 4 were significantly lower for both the AASHTO and moment-curvature analytical methods. The difference is due to where the initial cracking occurs. In Test 2, Test 3, and Test 4, the initial cracking occurred in the repair section of the girder and these sections of the girder were not compressed by the prestressing strands as compared to the original concrete.

Table 30 compares the nominal moment using the AASHTO equations and design material properties as tested with the nominal moment using the AASHTO equations and design material properties with a full deck of 88 in as shown in the plans. The addition of the deck increased the moment capacity of the girder.

**Table 30. AASHTO Design Nominal Moment Calculations With and Without Deck**

<b>Test</b>	<b>Description</b>	<b>AASHTO without Full Deck (ksi)</b>	<b>AASHTO with Full Deck (ksi)</b>	<b>Ratio of Increased Capacity</b>
<b>1</b>	<b>Control Test</b>	2720	3610	1.33
<b>2</b>	<b>8-Strand Spliced</b>	2380	3670	1.54
<b>3</b>	<b>4-Strands Severed with FRP</b>	2960	4370	1.48
<b>4</b>	<b>4-Strand Spliced</b>	2350	3660	1.56

## CHAPTER V: Conclusions and Recommendations

### 5.1: Conclusions

This report discusses the results from testing two prestressed girder repair methods: strand splicing and surface bonded FRP. The first specimen was a piece from an undamaged girder. The second specimen was a girder with eight severed strands that were re-tensioned with Grabb-it strand splices (Prestress Supply Incorporated, 2010). The third specimen was a girder with four severed strands that was repaired with V-wrap 400 FRP (Structural Group Incorporated, 2015). The fourth specimen was a girder with four severed strands that were re-tensioned with Grabb-it strand splices (Prestress Supply Incorporated, 2010). Material tests were conducted on the girder and repair materials. The material test averages are detailed in Chapter 4 and summarized in Table 31.

**Table 31. Material Test Averages**

<b>Girder Concrete</b>		<b>V-wrap C400 FRP</b>	
Compressive Strength (psi)	6650	1-ply Ultimate Strength (ksi)	188
Tensile Strength (psi)	424	2-ply Ultimate Strength	136
<b>Deck Concrete</b>		1-ply Ultimate Strain (in/in)	0.017
Compressive Strength (psi)	6020	2-ply Ultimate Strain (in/in)	0.011
<b>Tstrata Repair Concrete</b>		1-ply Modulus of Elasticity (ksi)	11000
1-day Compressive Strength (psi)	4060	2-ply Modulus of Elasticity (ksi)	12100
2-day Compressive Strength (psi)	5730	<b>Reinforcing Bar</b>	
7-day Compressive Strength (psi)	6250	Tensile Strength (ksi)	78.5
<b>Prestressing Strand</b>			
Tensile Strength (ksi)	262		
Effective Prestress (ksi)	132.4		

Based on the results of the laboratory tests presented in Chapter 4, strand splices alone were not able to restore the full moment capacity of the original girder. With four severed strands, they were able to restore 105% of the nominal strength of the undamaged girder as calculated using the design material properties and the AASHTO equations. With eight severed

strands, they were only able to restore 88% of the average nominal strength of the undamaged girder as calculated using the design material properties and the AASHTO equations. Therefore, strand splices alone are only a valid repair method when a low percentage of strands are damaged. In the event that more strength is required, FRP is a better primary restoration system. As a passive repair, the FRP did not restore the original prestress to the strands, but when paired with the strand splice, or applying moments during the repair, this could be remedied. In addition, the linear stress-strain relationship of FRP did not significantly change the behavior of the girder as a whole when only four strands were severed. The remaining strands provided enough ductility to allow the girder to deflect at higher loads.

The analytical modeling consisted of AASHTO calculations, strain compatibility calculations, and non-linear finite element modeling. The AASHTO calculations had an average ratio of nominal to applied failure moments of 1.02 with a standard deviation of 0.07. The moment-curvature calculations had an average ratio of nominal to applied failure moments of 1.07 with a standard deviation of 0.08. The non-linear finite element models had an average ratio of nominal to applied failure moments of 1.00 with a standard deviation of 0.07. When predicting the cracking moment, the AASHTO average ratio was 1.20 with a standard deviation of 0.65 and moment-curvature average ratio was 1.26 with a standard deviation of 0.75. Based on these results, the AASHTO and finite element models were the best way to predict failure while neither of the methods accurately predicted cracking.

In this project, the girders were removed from the bridge and tested individually. In reality, a bridge is comprised of more than one girder. In addition to the results from this project, there are many other variables that must be considered when choosing a repair technique. A girder that is damaged in place would have a much larger deck to help provide a larger

compression surface area. This would reduce the possibility of the compression failure observed for the third and fourth specimen. A loss in camber or a change in sweep from the impact that may cause unnecessary shear and torsion stress should be considered. Other considerations include whether or not additional girders were damaged in the impact. In the event that multiple girders are damaged, the ratio of damaged to undamaged strands in an individual girder as well as the ratio of damaged to undamaged strands in the overall bridge should be considered.

## **5.2: Recommendations**

Recommendations for immediate implementation:

- 1) Ensure areas in need of repair are prepared appropriately to allow proper bonding
  - a. Remove loose and damaged concrete
  - b. Clear approximately 0.5 in around strands that are exposed
  - c. Ensure strands are not damaged during concrete removal
  - d. Clean and hydrate surface
- 2) Load bridge during repair to reduce the probability of cracking by inducing positive and negative moments to increase the effective prestress restored and provide precompression in the repair material
- 3) Install FRP along the full length of the girder to reduce the potential for a debonding failure and increase the transfer between the matrix and the substrate

Recommendations for further research into the repair methods of impact damaged prestressed bridge girders include:

- 1) Replicate overloading and traffic patterns with cyclic loads to determine fatigue failure modes and approximate life-span.

- 2) Research into the asymmetrical effects of loading due to loads not directly above the girder would give some insight into how the girder reacts differently when strands are cut and change the centroid of the prestressing strands.
- 3) Research the maximum amount of damage for a girder with an FRP repair to retain ductility from the undamaged strands before failure.
- 4) Compare results from unstressed externally bonded FRP to pretensioned FRP repairs to determine the capacity of FRP to restore the effective prestressing force in the girder.
- 5) Investigate the effects of repair techniques on different girder cross sections.

## References

- ACI Committee 549. (2013). *Guide to Design and Construction of Externally Bonded Fabric-Reinforced Cementitious Matrix (FRCM) Systems for Repair and Strengthening Concrete and Masonry Structures*. Farmington Hills: American Concrete Institute.
- Agrawal, A. K., Xu, X., & Chen, Z. (2013, January 15). *Strikes on Low Clearance Bridges by Over-Height Trucks in New York State*. Retrieved December 05, 2014, from United States Department of Transportation:  
[http://www.rita.dot.gov/utc/publications/spotlight/2013\\_01/html/spotlight\\_0113.html](http://www.rita.dot.gov/utc/publications/spotlight/2013_01/html/spotlight_0113.html)
- Aktan, A. E., Culmo, M. P., Frangopol, D. M., French, C. W., Rabbat, B. G., Sanders, D. H., . . . Woods, S. W. (1994). *Concrete Bridges*. Washington D.C.: Transportation Research Board: Committee on Concrete Bridges. Retrieved December 8, 2014
- American Association of State Highway and Transportation Officials. (2012). *AASHTO LRFD Bridge Design Specifications, Customary US Units* (6th ed.). Washington DC: American Association of State Highway and Transportation Officials (AASHTO).
- ASTM International. (2015). *ASTM Standards and Publications*. Retrieved May 2, 2015, from ASTM International: <http://www.astm.org/Standards.htm>
- Bao, B. (2015). *Grabb-It Cable Splice Chuck Tensile Test*. Virginia Polytechnic Institute and State University, Civil and Environmental Engineering, Blacksburg.
- Brice, R. (2013). *Precast-Prestressed Concrete Girders Damaged by Over-Height Load Impacts*. Olympia: Washington State Department of Transportation. Retrieved December 13, 2014
- Davis, S. L., & Goldberg, D. (2013, June 19). *The Fix We're In For: The State of Our Nation's Bridges 2013*. Retrieved December 4, 2014, from Transportation for America:  
<http://t4america.org/docs/bridgereport2013/2013BridgeReport.pdf>

- ElSaftey, A., Graeff, M. K., & Fallaha, S. (2014, March). Behavior of Laterally Damaged Prestressed Concrete Bridge Girders Repaired with CFRP Laminates Under Static and Fatigue Loading. *International Journal of Concrete Structures and Materials*, VIII(1), 43-59. Retrieved December 7, 2014
- Fu, C. C., Burhouse, J. R., & Chang, G.-L. (2003). *Study of Overheight Vehicle Collisions with Highway Bridges*. University of Maryland, Department of Civil & Environmental Engineering. College Park: Transportation Research Board of the National Academies. Retrieved December 7, 2014
- Gangi, M. (2015). *Nonlinear Beam Modeling of the Repair of Impact-Damaged Prestressed Bridge Girders*. Virginia Polytechnic and State University, Department of Civil and Environmental Engineering. Blacksburg: Virginia Center for Transportation Innovation and Research.
- Harries, K. A., Kasan, J., & Aktas, C. (2009). *Repair Methods for Prestressed Girder Bridges*. University of Pittsburgh, Department of Civil and Environmental Engineering. Harrisburg: Commonwealth of Pennsylvania Department of Transportation.
- Harries, K. A., Kasan, J., Miller, R., & Brinkman, R. (2012). *Updated Research for Collision Damage and Repair of Prestressed Concrete Beams*. NCHRP Project 20-07, Task 307, University of Pittsburgh, Department of Civil Engineering, Pittsburgh. Retrieved December 10, 2014
- Hognestad, E. (1956). *Ultimate Strength of Reinforced Concrete in American Design Practice*. Research and Development Laboratories. London: Portland Cement Association.
- International Code Council Evaluation Service. (2014). *ICC-ES Evaluation Report - V-Wrap Fiber-Reinforced Polymer Composite System*. Hanover: Structural Technologies, LLC.

- Jones, M. (2015). *Repair Techniques of Impact Damaged Prestressed Bridge Girders Using Strand Splice and Fiber Reinforced Cementitious Matrix*. Virginia Polytechnic Institute and State University, Department of Civil and Environmental Engineering. Blacksburg: Virginia Center for Transportation Innovation and Research.
- Kasan, J. L. (2009). *Structural Repair of Prestressed Concrete Bridge Girders*. University of Pittsburgh, Department of Civil and Environmental Engineering . Pittsburgh: Swanson School of Engineering. Retrieved December 7, 2014
- Loflin, B. J. (2008). *Bond and Material Properties of Grade 270 and Grade 300 Prestressing Strands*. Virginia Polytechnic Institute and State University, Department of Civil and Environmental Engineering. Blacksburg: Virginia Transportation Research Council.
- Michael, A. (2010, August 2). *Moment-Curvature: Bonded Tendons*. Retrieved May 5, 2015, from Frederick University, Department of Civil Engineering ACES 480 Class Notes: [http://staff.fit.ac.cy/eng.ma/Aces480notes/Prestressed\\_Moment\\_Curvature.pdf](http://staff.fit.ac.cy/eng.ma/Aces480notes/Prestressed_Moment_Curvature.pdf)
- Nanni, A., Huang, P. C., & Tumialan, J. G. (2001). *Strengthening of Impact Damaged Bridge Girder Using FRP Laminates*. University of Missouri - Rolla, Center for Infrastructure Engineering Studies, Rolla.
- Nilson, A. H. (1987). *Design of Prestressed Concrete* (2nd ed.). New York, New York, United States: John Wiley & Sons.
- Park, R., & Ruitong, D. (1988, March 1). Ductility of Doubly Reinforced Concrete Beam Sections. *American Concrete Institute Structural Journal*, 85(2), 217-225.  
doi:10.14359/2760

- Pino, V., & Nanni, A. (2015). *Repair of Damaged Prestressed Concrete Girder with Fabric Reinforced Cementitious Matrix and Fiber Reinforced Polymer Composites*. University of Miami, College of Engineering, Gables.
- Prestress Supply Incorporated. (2010). *Grabb-It Cable Splice*. Retrieved December 12, 2014, from Prestress Supply:  
<http://www.prestresssupply.com/Products/StrandRepair/GRABBITCableSplice.aspx>
- Rasheed, H. A. (2015). *Strengthening Design of Reinforced Concrete with FRP*. (E. J. Barbero, Ed.) Boca Raton, Florida, United States of America: CRC Press.
- Salomon, A. L. (2014, July 23). Tension Testing. Blacksburg, Virginia, United States of America.
- Structural Group Incorporated. (2015). *Structural Technologies*. Retrieved May 1, 2015, from Structural Technologies, A Structural Group Company:  
<http://www.structuraltechnologies.com>
- Taly, N. (2015). *Highway Bridge Superstructure Engineering: LRFD Approaches to Design and Analysis*. Boca Raton, Florida, United States of America: CRC Press.
- Wipf, T. J., Klaiber, F. W., Rhodes, J. D., & Kempers, B. J. (2004a). *Effective Structural Concrete Repair*. Iowa State University of Science and Technology, Department of Civil, Construction and Environmental Engineering. Ames: Iowa Department of Transportation.
- Wipf, T. J., Klaiber, F. W., Rhodes, J. D., & Kempers, B. J. (2004b). *Effective Structural Concrete Repair: Repair of Impact Damaged Prestressed Concrete Beams with Carbon Fiber Reinforced Polymer (CFRP)*. Iowa State University, Department of Civil, Construction, and Environmental Engineering. Ames: Iowa Department of Transportation. Retrieved December 12, 2014

YRC Worldwide. (2015). *Trailer Dimensions*. (WordPress.com) Retrieved February 8, 2015,  
from YRC Freight: <http://yrc.com/trailer-dimensions/>

Zobel, R. S., Jirsa, J. O., Fowler, D. W., & Carrasquillo, R. L. (1997). *Evaluation and Repair of Impact-Damaged Prestressed Concrete Bridge Girders*. The University of Texas at Austin, Center for Transportatio Research. Austin: Texas Department of Transportation. Retrieved December 12, 2014



<p><b>DIVISION I</b></p> <p><b>SECTION 010 - GENERAL PROVISIONS</b></p> <p><b>SECTION 010.01 - PARTIAL PAYMENTS</b></p> <p>Page 25: Section 010.01 - Partial Payments. Add the following:</p> <p>1. The contractor shall submit a schedule of partial payments to the Engineer at least 14 days before the start of work. The schedule shall be based on the estimated cost of work to be performed during each 14-day period. The schedule shall be subject to the approval of the Engineer. The contractor shall not be entitled to payment until the work has been completed to the satisfaction of the Engineer. The contractor shall be responsible for the cost of the work until it has been completed to the satisfaction of the Engineer.</p>	<p><b>DIVISION II</b></p> <p><b>SECTION 400 - BRIDGES AND STRUCTURES</b></p> <p><b>SECTION 400.01 - CONCRETE REINFORCEMENT</b></p> <p>Page 26: Section 400.01 - Concrete Reinforcement. Add the following:</p> <p>1. The contractor shall use only the materials and methods specified in the specifications. The contractor shall be responsible for the quality of the materials and the workmanship. The contractor shall be responsible for the cost of the materials and the workmanship. The contractor shall be responsible for the cost of the materials and the workmanship.</p>	<p><b>DIVISION III</b></p> <p><b>SECTION 400 - BRIDGES AND STRUCTURES</b></p> <p><b>SECTION 400.02 - CONCRETE</b></p> <p>Page 27: Section 400.02 - Concrete. Add the following:</p> <p>1. The contractor shall use only the materials and methods specified in the specifications. The contractor shall be responsible for the quality of the materials and the workmanship. The contractor shall be responsible for the cost of the materials and the workmanship. The contractor shall be responsible for the cost of the materials and the workmanship.</p>	<p><b>DIVISION IV</b></p> <p><b>SECTION 400 - BRIDGES AND STRUCTURES</b></p> <p><b>SECTION 400.03 - FORMS</b></p> <p>Page 28: Section 400.03 - Forms. Add the following:</p> <p>1. The contractor shall use only the materials and methods specified in the specifications. The contractor shall be responsible for the quality of the materials and the workmanship. The contractor shall be responsible for the cost of the materials and the workmanship. The contractor shall be responsible for the cost of the materials and the workmanship.</p>
<p><b>DIVISION V</b></p> <p><b>SECTION 400 - BRIDGES AND STRUCTURES</b></p> <p><b>SECTION 400.04 - CURING OF CONCRETE</b></p> <p>Page 29: Section 400.04 - Curing of Concrete. Add the following:</p> <p>1. The contractor shall use only the materials and methods specified in the specifications. The contractor shall be responsible for the quality of the materials and the workmanship. The contractor shall be responsible for the cost of the materials and the workmanship. The contractor shall be responsible for the cost of the materials and the workmanship.</p>	<p><b>DIVISION VI</b></p> <p><b>SECTION 400 - BRIDGES AND STRUCTURES</b></p> <p><b>SECTION 400.05 - FINISHES</b></p> <p>Page 30: Section 400.05 - Finishes. Add the following:</p> <p>1. The contractor shall use only the materials and methods specified in the specifications. The contractor shall be responsible for the quality of the materials and the workmanship. The contractor shall be responsible for the cost of the materials and the workmanship. The contractor shall be responsible for the cost of the materials and the workmanship.</p>	<p><b>DIVISION VII</b></p> <p><b>SECTION 400 - BRIDGES AND STRUCTURES</b></p> <p><b>SECTION 400.06 - PAINTS</b></p> <p>Page 31: Section 400.06 - Paints. Add the following:</p> <p>1. The contractor shall use only the materials and methods specified in the specifications. The contractor shall be responsible for the quality of the materials and the workmanship. The contractor shall be responsible for the cost of the materials and the workmanship. The contractor shall be responsible for the cost of the materials and the workmanship.</p>	<p><b>DIVISION VIII</b></p> <p><b>SECTION 400 - BRIDGES AND STRUCTURES</b></p> <p><b>SECTION 400.07 - PROTECTIVE COATINGS</b></p> <p>Page 32: Section 400.07 - Protective Coatings. Add the following:</p> <p>1. The contractor shall use only the materials and methods specified in the specifications. The contractor shall be responsible for the quality of the materials and the workmanship. The contractor shall be responsible for the cost of the materials and the workmanship. The contractor shall be responsible for the cost of the materials and the workmanship.</p>

Office of the Bridge Engineer  
 Richmond, Virginia  
 August, 1967



COMMONWEALTH OF VIRGINIA  
 DEPARTMENT OF HIGHWAYS  
 ROUTE 66, RICHMOND, VIRGINIA  
 PROJECT NO. 67-100

<p>6</p> <p>The strength shall be determined by testing. The test shall be performed in the presence of the Engineer and a representative of the contractor. The test shall be performed on a specimen of concrete which has been cast in the same manner as the concrete to be tested. The test shall be performed on a specimen of concrete which has been cast in the same manner as the concrete to be tested. The test shall be performed on a specimen of concrete which has been cast in the same manner as the concrete to be tested.</p> <p><b>SECTION 410 - BRIDGE OR OVERPASS-REINFORCED CONCRETE PILES</b></p> <p>Page 302: Section 410.03 Reinforced Concrete Piles. The following shall apply to the construction of reinforced concrete piles: (a) The concrete shall be of the same quality as that specified in the contract documents. (b) The piles shall be cast in place and shall be cured in accordance with the specifications. (c) The piles shall be tested in accordance with the specifications. (d) The piles shall be installed in accordance with the specifications.</p>	<p>7</p> <p><b>SECTION 412 - REINFORCEMENT</b></p> <p>Page 303: Section 412.02 Reinforcement is supplemented as follows: (a) All reinforcement shall be in accordance with the specifications. (b) The reinforcement shall be installed in accordance with the specifications. (c) The reinforcement shall be tested in accordance with the specifications. (d) The reinforcement shall be installed in accordance with the specifications.</p> <p><b>SECTION 413 - REINFORCEMENT</b></p> <p>Page 304: Section 413.02 Reinforcement is supplemented as follows: (a) All reinforcement shall be in accordance with the specifications. (b) The reinforcement shall be installed in accordance with the specifications. (c) The reinforcement shall be tested in accordance with the specifications. (d) The reinforcement shall be installed in accordance with the specifications.</p>	<p>8</p> <p>Page 305: Section 414.02 Reinforcement is supplemented as follows: (a) All reinforcement shall be in accordance with the specifications. (b) The reinforcement shall be installed in accordance with the specifications. (c) The reinforcement shall be tested in accordance with the specifications. (d) The reinforcement shall be installed in accordance with the specifications.</p> <p><b>SECTION 415 - REINFORCEMENT</b></p> <p>Page 306: Section 415.02 Reinforcement is supplemented as follows: (a) All reinforcement shall be in accordance with the specifications. (b) The reinforcement shall be installed in accordance with the specifications. (c) The reinforcement shall be tested in accordance with the specifications. (d) The reinforcement shall be installed in accordance with the specifications.</p>	<p>9</p> <p>Page 307: Section 416.02 Reinforcement is supplemented as follows: (a) All reinforcement shall be in accordance with the specifications. (b) The reinforcement shall be installed in accordance with the specifications. (c) The reinforcement shall be tested in accordance with the specifications. (d) The reinforcement shall be installed in accordance with the specifications.</p> <p><b>SECTION 417 - REINFORCEMENT</b></p> <p>Page 308: Section 417.02 Reinforcement is supplemented as follows: (a) All reinforcement shall be in accordance with the specifications. (b) The reinforcement shall be installed in accordance with the specifications. (c) The reinforcement shall be tested in accordance with the specifications. (d) The reinforcement shall be installed in accordance with the specifications.</p>	<p>RT. 614 UNDERPASS SUPPLEMENTAL SPECIFICATIONS</p> <p>Virginia Department of Highways Office of the Bridge Engineer Charlottesville - August 1974</p> <p>Revised October 4, 1977</p> <p>CXXVIV-19 Sheet 3 of 10</p>
--	--	--	--	---

Figure 102. Arcadia Bridge Blueprint Page 3

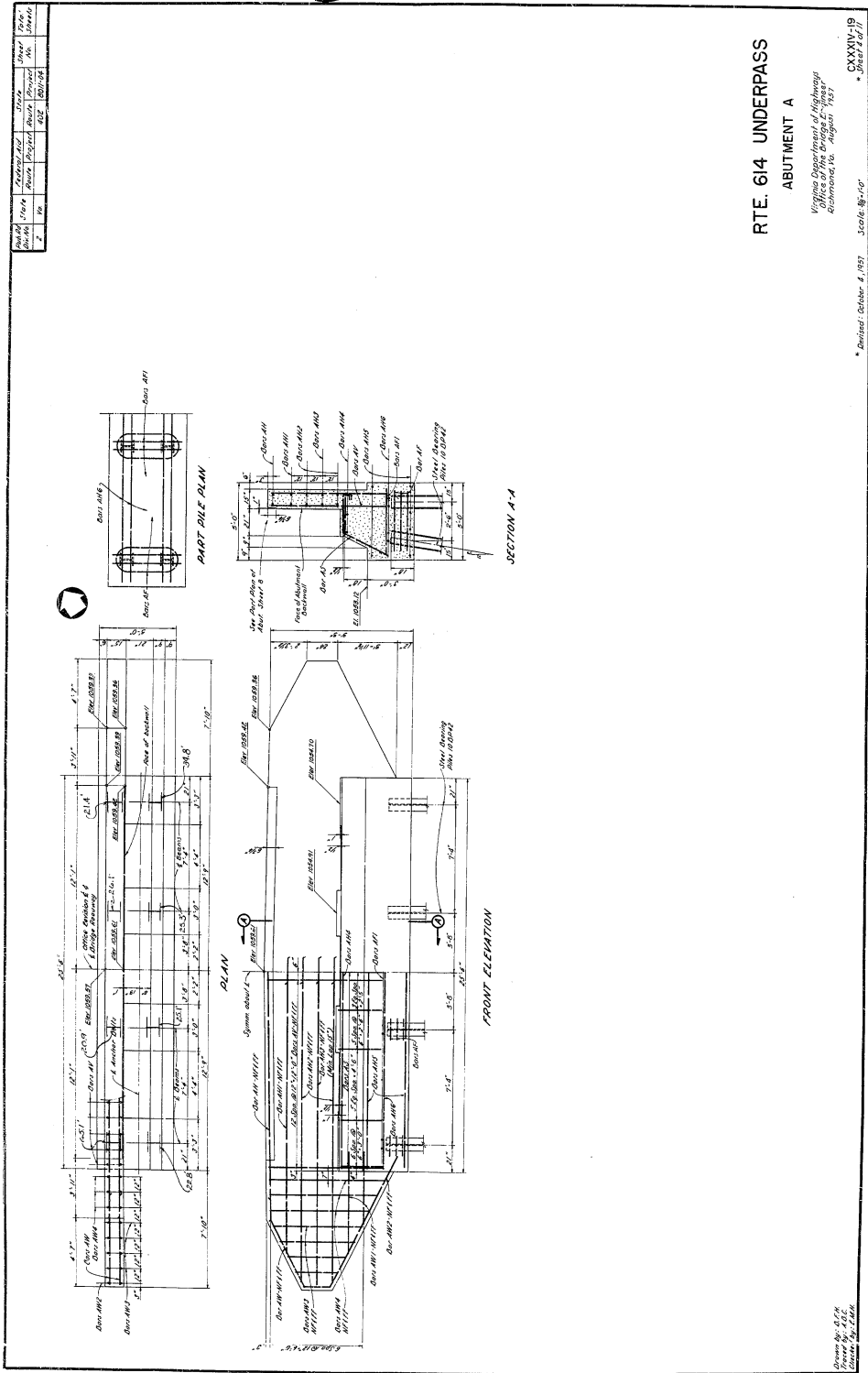


Figure 103. Arcadia Bridge Blueprint Page 4

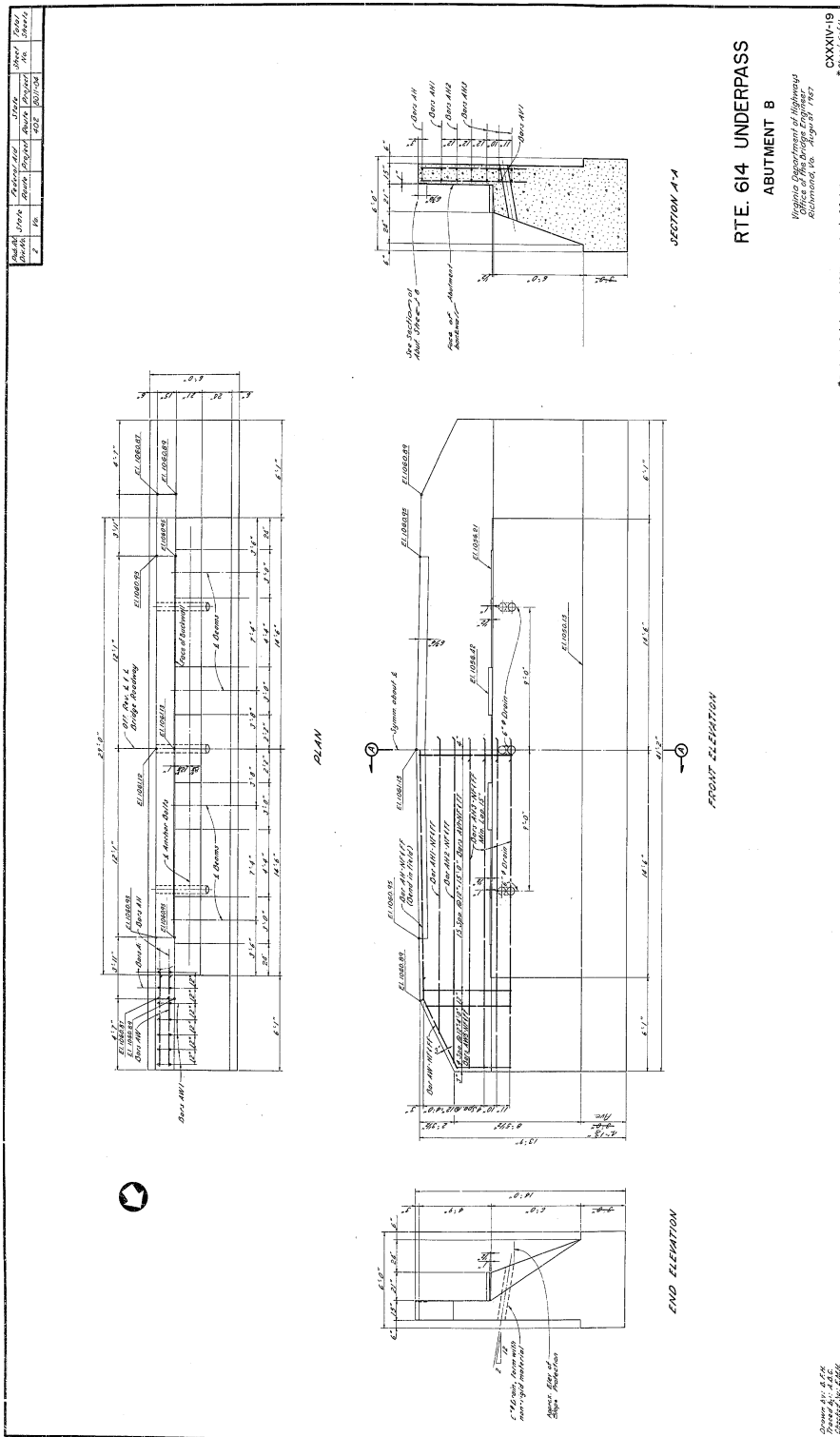


Figure 104. Arcadia Bridge Blueprint Page 5



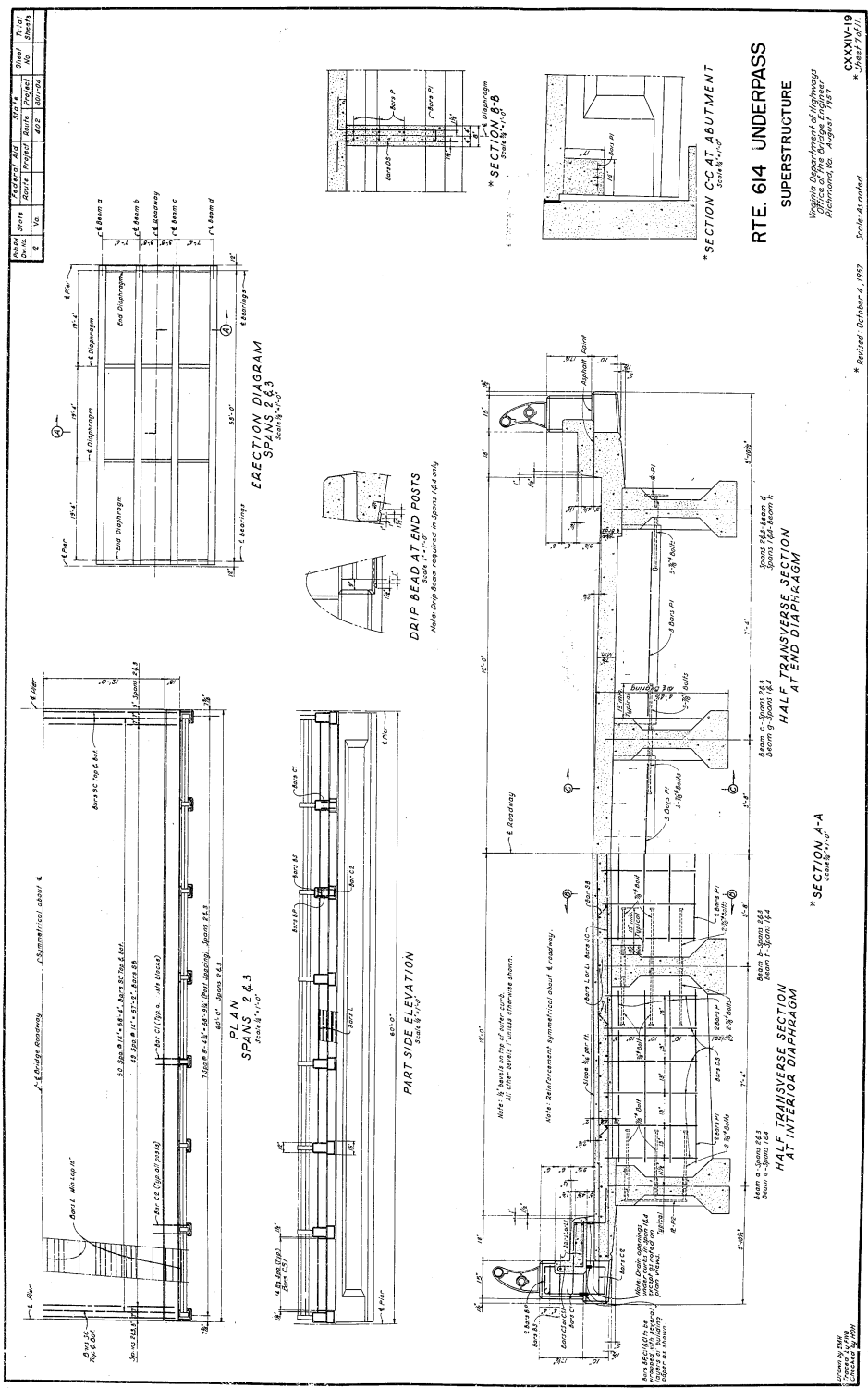


Figure 106. Arcadia Bridge Blueprint Page 7

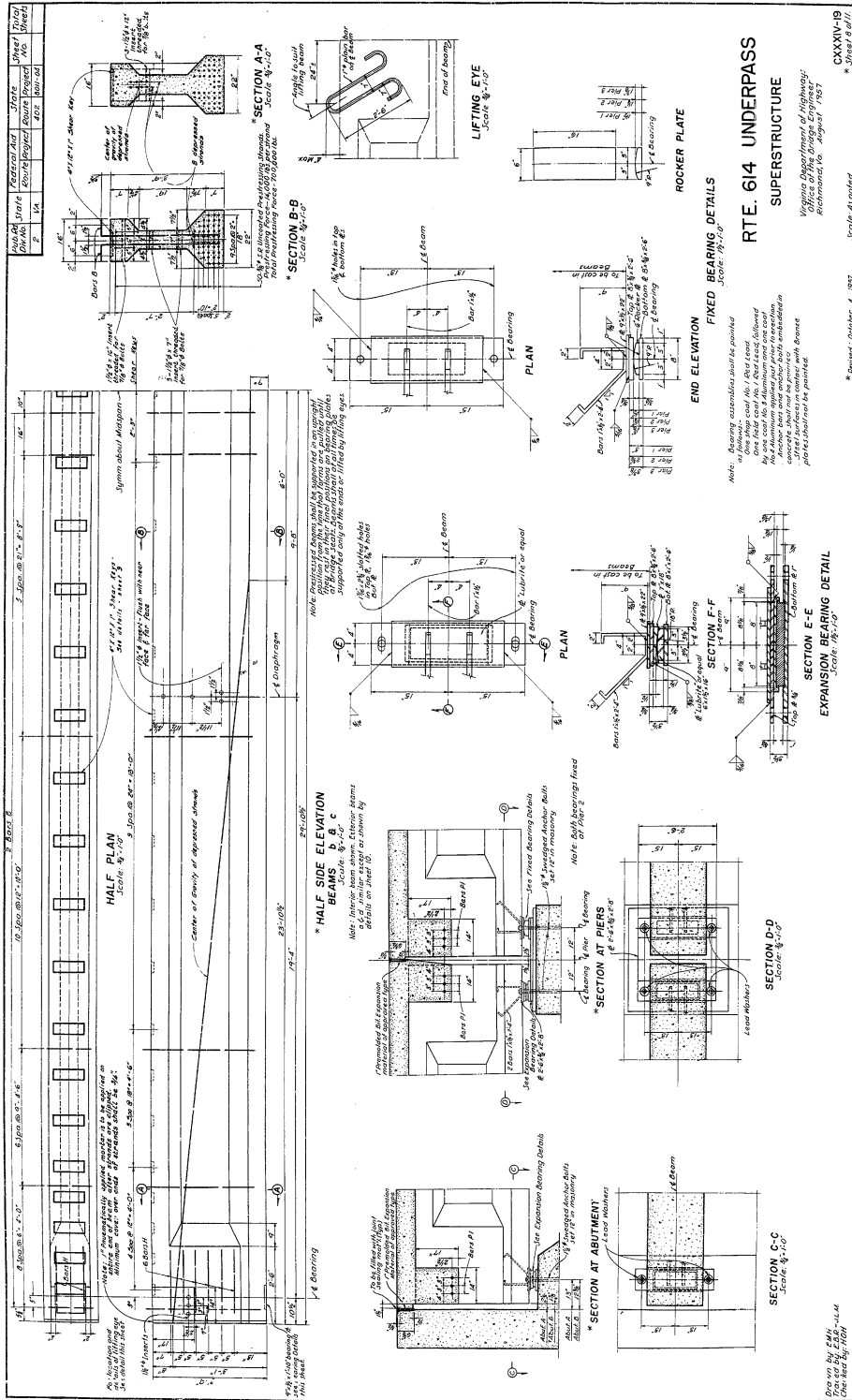
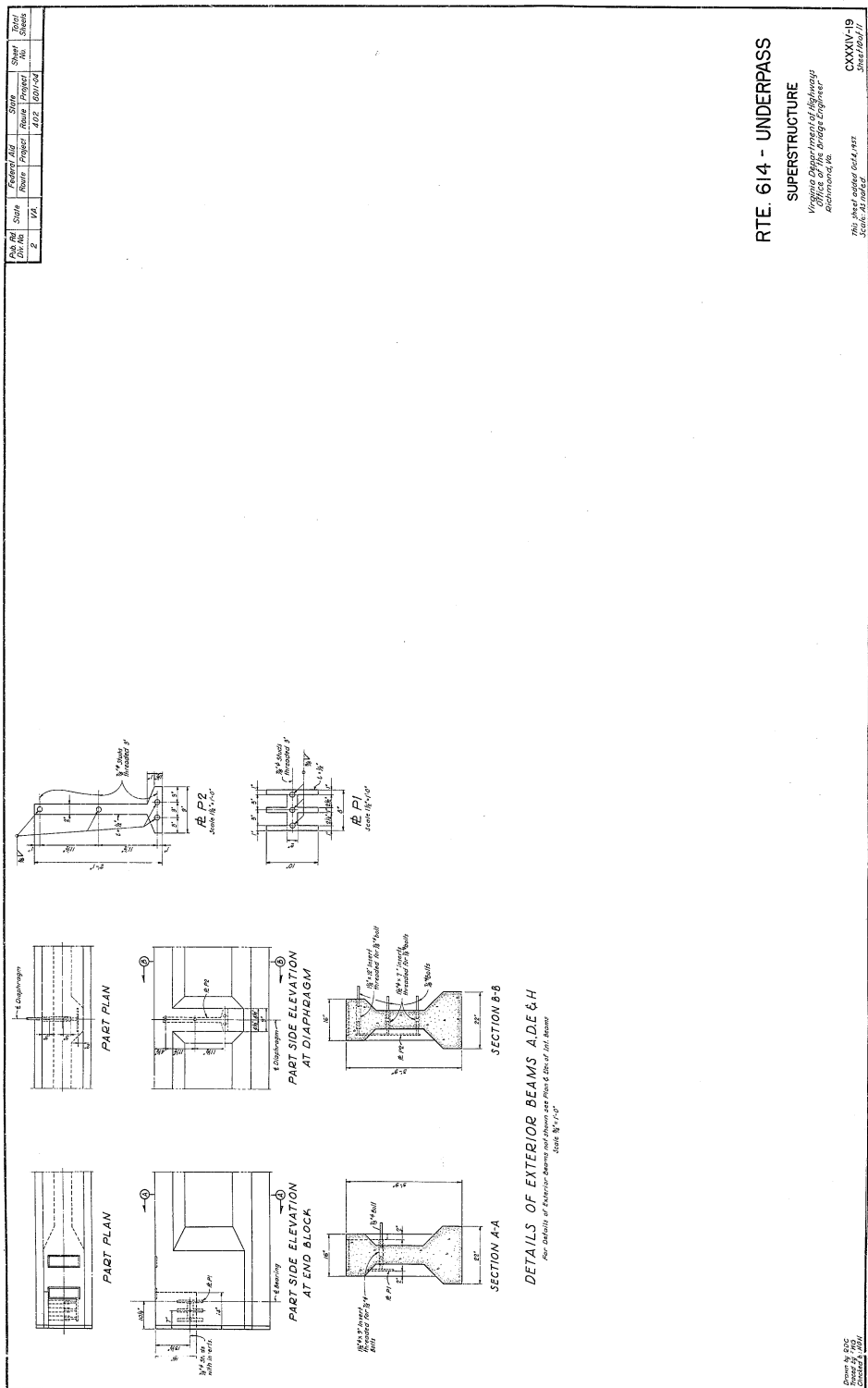


Figure 107. Arcadia Bridge Blueprint Page 8





**RTE. 614 - UNDERPASS**  
**SUPERSTRUCTURE**  
*Virginia Department of Highways*  
 Richmond, Va.  
 This work is not for sale  
 Scale: 3/4" = 1'-0"  
 CXXXIV-19  
 Sheet No. 11

Figure 109. Arcadia Bridge Blueprint Page 10

1 3 4-1 9 1 1 F

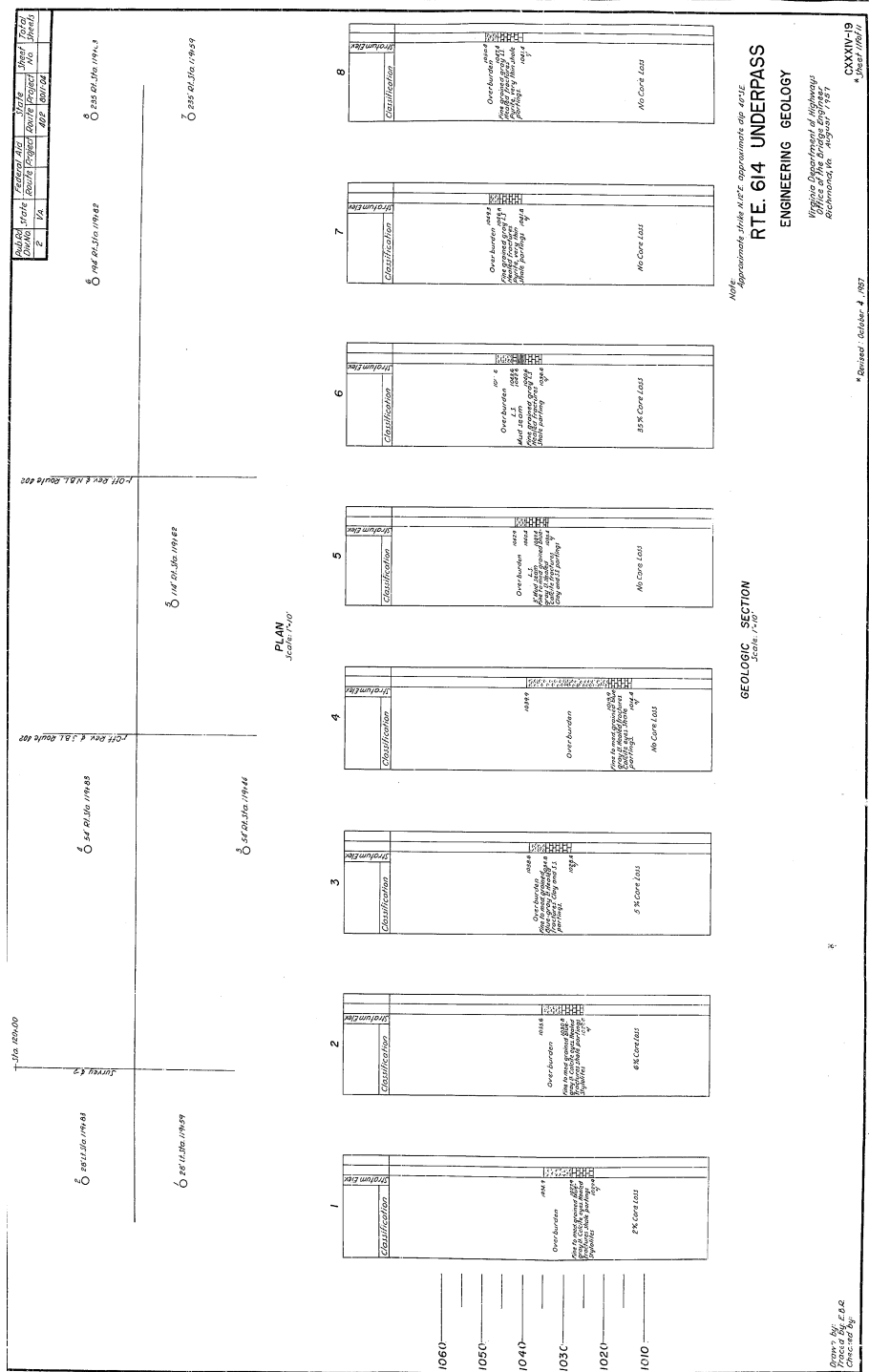


Figure 110. Arcadia Bridge Blueprint Page 11

## APPENDIX B: AASHTO Calculations

AASHTO Equation 5.7.3.2.2-1 for Nominal Moment

$$M_n = A_{ps}f_{ps} \left( d_p - \frac{a}{2} \right) + A_s f_s \left( d_s - \frac{a}{2} \right) - A'_s f'_s \left( d'_s - \frac{a}{2} \right) + 0.85 f'_c (b - b_w) h_f \left( \frac{a}{2} - \frac{h_f}{2} \right)$$

Where:

$M_n$  = Nominal Moment, in-k

$A_{ps}$  = Total Area of Prestressing Strands, in<sup>2</sup>

$$f_{ps} = f_{pu} \left( 1 - k \frac{c}{d_p} \right)$$

$f_{pu}$  = Strand Ultimate Stress, ksi

$$k = 2 \left( 1.04 - \frac{f_{py}}{f_{pu}} \right)$$

$f_{py}$  = Strand Yield Stress, ksi

$$c = \frac{A_{ps}f_{ps} + A_s f_s - A'_s f'_s - 0.85 f'_c (b - b_w) h_f}{0.85 f'_c \beta_1 b_w + k A_{ps} \frac{f_{pu}}{d_p}}$$

$c$  = Neutral Axis, in

$d_p$  = Prestressing Depth, in

$$a = \beta_1 c$$

$f'_c$  = Concrete Compressive Strength, ksi

$b$  = Width of Compression Block, in

$\beta_1$  = Stress Block Factor

$A_s$  = Total Area of Tension Reinforcement, in<sup>2</sup>

$f_s$  = Stress in Tension Reinforcement, ksi

$d_s$  = Tension Reinforcing Depth, in

$A'_s$  = Total Area of Compression Reinforcement, in<sup>2</sup>

- $f'_s$  = Stress in Compression Reinforcement, ksi
- $d'_s$  = Compression Reinforcing Depth, in
- $b_w$  = Web Width, in
- $h_f$  = Compression Flange Depth, in

AASHTO Equation 5.7.3.3.2-1 for Cracking Moment

$$M_{cr} = \gamma_3 \left[ (\gamma_1 f_r + \gamma_2 f_{cpe}) S_c - M_{dnc} \left( \frac{S_c}{S_{nc}} - 1 \right) \right]$$

Where:

- $S_c$  = Composite Tensile Section Modulus, in<sup>3</sup>
- $f_r$  = Concrete Modulus of Rupture, ksi
- $f_{cpe}$  = Compressive Stress from Prestress, ksi
- $M_{dnc}$  = Unfactored Dead Load Moment on Non-Composite Section, in-k
- $S_{nc}$  = Non-Composite Tensile Section Modulus, in<sup>3</sup>
- $\gamma_1$  = Flexural Cracking Variability Factor = 1.6
- $\gamma_2$  = Prestress Variability Factor = 1.1
- $\gamma_3$  = Reinforcement Ratio of Yield to Tensile Strength = 1.0

**Table 32. Test 1 AASHTO Calculations**

<b>Tested Properties</b>			<b>Design Properties</b>		
<b>Concrete Properties</b>			<b>Concrete Properties</b>		
Girder Concrete Strength, f <sub>c</sub>	6650	psi	Girder Concrete Strength, f <sub>c</sub>	5000	psi
Deck Concrete Strength, f <sub>c</sub>	6020	psi	Deck Concrete Strength, f <sub>c</sub>	4000	psi
Deck Height, hd	8.75	in	Deck Height, hd	8.75	in
Top Flange Height, h <sub>tf</sub>	7	in	Top Flange Height, h <sub>tf</sub>	7	in
Deck Width, bd	16	in	Deck Width, bd	16	in
Top Flange Width, b <sub>tf</sub>	16	in	Top Flange Width, b <sub>tf</sub>	16	in
<b>Steel Properties</b>			<b>Steel Properties</b>		
# Strands	50	ea	# Strands	50	ea
Strand Diameter, D <sub>s</sub>	0.375	in	Strand Diameter, D <sub>s</sub>	0.375	in
Area of Strand, A <sub>s</sub> (each)	0.08	in <sup>2</sup>	Area of Strand, A <sub>s</sub> (each)	0.08	in <sup>2</sup>
Total Strand Area, A <sub>ps</sub>	4	in <sup>2</sup>	Total Strand Area, A <sub>ps</sub>	4	in <sup>2</sup>
Ultimate Stress, f <sub>pu</sub> (ε=.06)	262	ksi	Ultimate Stress, f <sub>pu</sub> (ε=.06)	250	ksi
Yield Stress, f <sub>py</sub> (ε=.009)	242	ksi	Yield Stress, f <sub>py</sub> (ε=.009)	210	ksi
<b>AASHTO Calculations</b>			<b>AASHTO Calculations</b>		
k	0.233		k	0.4	
β <sub>1, deck</sub>	0.75		β <sub>1, deck</sub>	0.85	
dp	46.4	in	dp	46.4	in
c	15.7	in	c	18.0	in
a	11.8	in	a	15.3	in
f <sub>ps</sub>	241	ksi	f <sub>ps</sub>	211	ksi
M <sub>n</sub>	39099	in-k	M <sub>n</sub>	32655	in-k
	3258	k-ft		2721	k-ft

**Table 33. Test 2 AASHTO Calculations**

<b>Tested Properties</b>			<b>Design Properties</b>		
<b>Concrete Properties</b>			<b>Concrete Properties</b>		
Girder Concrete Strength, f'c	6650	psi	Girder Concrete Strength, f'c	5000	psi
Deck Concrete Strength, f'c	6020	psi	Deck Concrete Strength, f'c	4000	psi
Deck Height, hd	8.75	in	Deck Height, hd	8.75	in
Top Flange Height, htf	7	in	Top Flange Height, htf	7	in
Deck Width, bd	11	in	Deck Width, bd	11	in
Top Flange Width, btf	16	in	Top Flange Width, btf	16	in
Web Width, bw	7	in	Web Width, bw	7	in

<b>Steel Properties</b>			<b>Steel Properties</b>		
# Strands	42	ea	# Strands	42	ea
Strand Diameter, Ds	0.375	in	Strand Diameter, Ds	0.375	In
Area of Strand, As (each)	0.08	in <sup>2</sup>	Area of Strand, As (each)	0.08	in <sup>2</sup>
Total Strand Area, Aps	3	in <sup>2</sup>	Total Strand Area, Aps	3	in <sup>2</sup>
Ultimate Stress, fpu ( $\epsilon=.06$ )	262	Ksi	Ultimate Stress, fpu ( $\epsilon=.06$ )	250	Ksi
Yield Stress, fpy ( $\epsilon=.009$ )	242	Ksi	Yield Stress, fpy ( $\epsilon=.009$ )	210	Ksi
# Splices	8		# Splices	8	
Total Strand Splice Area	0.64	in <sup>2</sup>	Total Strand Splice Area	0.64	in <sup>2</sup>
Splice Ultimate Stress, fpu	262	ksi	Splice Ultimate Stress, fpu	225	ksi
Splice Yield Stress, fpy	242	ksi	Splice Yield Stress, fpy	210	ksi
Average Ultimate Stress	262	ksi	Average Ultimate Stress	246	ksi
Average Yield Stress	242	ksi	Average Yield Stress	210	ksi

<b>AASHTO Calculations</b>			<b>AASHTO Calculations</b>		
k	0.233		k	0.373	
$\beta_{1, deck}$	0.75		$\beta_{1, deck}$	0.85	
dp	47.7	in	dp	47.7	in
c	22.7	in	c	27.6	in
a	17.0	in	a	23.4	in
fps	233	ksi	fps	193	ksi
Mn	36691	in-k	Mn	28576	in-k
	3058	k-ft		2381	k-ft

**Table 34. Test 3 AASHTO Calculations**

<b>Tested Properties</b>			<b>Design Properties</b>		
<b>Concrete Properties</b>			<b>Concrete Properties</b>		
Girder Concrete Strength, f'c	6650	psi	Girder Concrete Strength, f'c	5000	psi
Deck Concrete Strength, f'c	6020	psi	Deck Concrete Strength, f'c	4000	psi
Deck Height, hd	8.75	in	Deck Height, hd	8.75	in
Top Flange Height, htf	7	in	Top Flange Height, htf	7	in
Deck Width, bd	11	in	Deck Width, bd	11	in
Top Flange Width, btf	16	in	Top Flange Width, btf	16	in
Web Width, bw	7	in	Web Width, bw	7	in
<b>Steel Properties</b>			<b>Steel Properties</b>		
# Strands	46	ea	# Strands	46	ea
Strand Diameter, Ds	0.375	in	Strand Diameter, Ds	0.375	in
Area of Strand, As (each)	0.08	in <sup>2</sup>	Area of Strand, As (each)	0.08	in <sup>2</sup>
Total Strand Area, Aps	4	in <sup>2</sup>	Total Strand Area, Aps	4	in <sup>2</sup>
Ultimate Stress, fpu (ε=.06)	262	Ksi	Ultimate Stress, fpu (ε=.06)	250	ksi
Yield Stress, fpy (ε=.009)	242	Ksi	Yield Stress, fpy (ε=.009)	210	ksi
<b>FRP Properties</b>			<b>FRP Properties</b>		
# Sheets	2		# Sheets	2	
Thickness	0.08	in	Thickness	0.08	in
Width	22	in	Width	22	in
Area	3.52	in <sup>2</sup>	Area	3.52	in <sup>2</sup>
fu	136	ksi	fu	121	ksi
dfrp	53.83	in	dfrp	53.83	in
Strain at Failure	0.00793		Strain at Failure	0.00997	
Modulus of Elasticity	12100	ksi	Modulus of Elasticity	11900	ksi
Stress at Failure	96.0	ksi	Stress at Failure	119	ksi
<b>AASHTO Calculations</b>			<b>AASHTO Calculations</b>		
k	0.233		k	0.4	
β <sub>1, deck</sub>	0.75		β <sub>1, deck</sub>	0.85	
dp	47.3	in	dp	47.3	in
c	35.4	in	c	40.4	in
a	26.6	in	a	34.3	in
fps	216	ksi	fps	165	ksi
Mn	42490	in-k	Mn	35540	in-k
	3541	k-ft		2962	k-ft

**Table 35. Test 4 AASHTO Calculations**

<b>Tested Properties</b>			<b>Design Properties</b>		
<b>Concrete Properties</b>			<b>Concrete Properties</b>		
Girder Concrete Strength, f'c	6650	psi	Girder Concrete Strength, f'c	5000	psi
Deck Concrete Strength, f'c	6020	psi	Deck Concrete Strength, f'c	4000	psi
Deck Height, hd	8.75	in	Deck Height, hd	8.75	in
Top Flange Height, htf	7	in	Top Flange Height, htf	7	in
Deck Width, bd	11	in	Deck Width, bd	11	in
Top Flange Width, btf	16	in	Top Flange Width, btf	16	in
Web Width, bw	7	in	Web Width, bw	7	in

<b>Steel Properties</b>			<b>Steel Properties</b>		
# Strands	46	ea	# Strands	46	ea
Strand Diameter, Ds	0.375	in	Strand Diameter, Ds	0.375	in
Area of Strand, As (each)	0.08	in <sup>2</sup>	Area of Strand, As (each)	0.08	in <sup>2</sup>
Total Strand Area, Aps	4	in <sup>2</sup>	Total Strand Area, Aps	4	in <sup>2</sup>
Ultimate Stress, fpu ( $\epsilon=.06$ )	262	ksi	Ultimate Stress, fpu ( $\epsilon=.06$ )	250	ksi
Yield Stress, fpy ( $\epsilon=.009$ )	242	ksi	Yield Stress, fpy ( $\epsilon=.009$ )	210	ksi
# Splices	4		# Splices	4	
Total Strand Splice Area	0.32	in <sup>2</sup>	Total Strand Splice Area	0.32	in <sup>2</sup>
Splice Ultimate Stress, fpu	262	ksi	Splice Ultimate Stress, fpu	225	ksi
Splice Yield Stress, fpy	242	ksi	Splice Yield Stress, fpy	210	ksi
Average Ultimate Stress	262	ksi	Average Ultimate Stress	248	ksi
Average Yield Stress	242	ksi	Average Yield Stress	210	ksi

<b>AASHTO Calculations</b>			<b>AASHTO Calculations</b>		
k	0.233		k	0.386	
$\beta_{1, deck}$	0.75		$\beta_{1, deck}$	0.85	
dp	47.3	in	dp	47.3	in
c	22.6	in	c	27.4	in
a	17.0	in	a	23.3	in
fps	233	ksi	fps	192	ksi
Mn	36304	in-k	Mn	28217	in-k
	3025	k-ft		2351	k-ft

## APPENDIX C: Strain-Compatibility Moment-Curvature Calculations

The following tables show the properties used to determine the moment-curvature relationships using strain-compatibility for each test.

**Table 36. Test 1 Moment-Curvature Calculations**

Concrete Properties			Steel Properties		
Girder Concrete Strength, $f_c$	6650	psi	Web Area, $A_w$	133	$\text{in}^2$
Deck Concrete Strength, $f_c$	6020	psi	Bottom Haunch Area, $A_{bh}$	109	$\text{in}^2$
Modular Ratio, $n$	0.905		Bottom Flange Area, $A_{bf}$	154	$\text{in}^2$
Deck Height, $h_d$	8.75	in	Total Girder Area, $A_g$	396	$\text{in}^2$
Top Flange Height, $h_{tf}$	7	in	Deck Transformed Area, $A_{dt}$	127	$\text{in}^2$
Top Haunch Height, $h_{th}$	4.5	in	Composite Area Transformed, $A_{ct}$	522	$\text{in}^2$
Web Height, $h_w$	19	in	Deck Moment of Inertia, $I_d$	893	$\text{in}^4$
Bottom Haunch Height, $h_{bh}$	7.5	in	Deck Transformed Moment of Inertia, $I_{dt}$	809	$\text{in}^4$
Bottom Flange Height, $h_{bf}$	7	in	Girder Moment of Inertia, $I_g$	125165	$\text{in}^4$
Girder Height, $h_g$	45	in	Total Moment of Inertia, $I$	207157	$\text{in}^4$
Total Height, $h$	53.8	in	Deck Center of Gravity, $y_g$	49.4	in
Deck Width, $b_d$	16	in	Girder Center of Gravity, $y_g$	20.3	in
Transformed Deck Width, $b_{td}$	14.5	in	Composite Center of Gravity, $y_c$	27.3	in
Top Flange Width, $b_{tf}$	16	in	Transformed Top to COG, $c_{tt}$	26.4	in
Top Haunch Width, $b_{th}$	4.5	in	Transformed Bottom to COG, $c_{tb}$	27.3	in
Web Width, $b_w$	7	in	Girder Modulus of Elasticity, $E_{cg}$	4648	ksi
Bottom Haunch Width, $b_{bh}$	7.5	in	Ultimate Strain, $\epsilon_{cu}$	0.003	
Bottom Flange Width, $b_{bf}$	22	in	$0.5f_c$	3325	psi
Deck Area, $A_d$	140	$\text{in}^2$	Strain, $\epsilon$ (3.3 ksi)	0.000715	
Top Flange Area, $A_{tf}$	112	$\text{in}^2$	$0.5f_c$	3325	psi
Top Haunch Area, $A_{th}$	51.8	$\text{in}^2$	$\Delta$	0	psi
			$\epsilon_0$	0.00244	
			# Strands	50	ea
			Strand Diameter, $D_s$	0.375	in
			Area of Strand, $A_s$	0.08	$\text{in}^2$
			Total Strand Area, $A_{ps}$	4	$\text{in}^2$
			Strand COG, $c_{gps}$	7.15	in
			Depth of Strands, $d_{ps}$	46.6	in
			Ultimate Stress, $f_{pu}$	250	ksi
			Ultimate Strain, $\epsilon$	0.06	
			Modulus of Elasticity, $E_{ps}$	27000	ksi
			Effective Prestress, $f_{pe}$	132	ksi
			Yield Stress, $f_{py}$	242	ksi
			Yield Strain, $\epsilon$	0.009	
			$f_p$ ( $\epsilon=0.015$ )	246	ksi
			$\epsilon$ ( $f_p=246.18$ )	0.015	
			$f_p$ ( $\epsilon=0.009$ )	242	ksi
			$\epsilon$ ( $f_p=241.91$ )	0.009	
			Effective Prestress Force, $P_e$	528	k
			Eccentricity, $e$	20.2	in

<b>No applied Moment</b>		
<b>Top Fiber Stress</b>		
Pe/A	-1.01	ksi
Peectop/I	1.36	ksi
ft	0.349	ksi
<b>Bottom Fiber Stress</b>		
Pe/A	-1.01	ksi
Peecbott/I	-1.41	ksi
fb	-2.42	ksi
<b>Curvature</b>		
Top Fiber Strain, $\epsilon_t$	0.000075	
	75	$\mu\epsilon$
Bottom Fiber Strain, $\epsilon_b$	-0.000520	
	-520	$\mu\epsilon$
Neutral Axis Depth, c	6.77	in
Curvature, $\Phi$	-0.0000111	$\epsilon/\text{in}$
	-11.1	$\mu\epsilon/\text{in}$
Steel Strain Increase, $\epsilon_2$	0.000441	
	441	$\mu\epsilon$
Prestress Steel Strain, $\epsilon_1$	0.00489	
	4889	$\mu\epsilon$
Total Steel Strain, $\epsilon_1+\epsilon_2$	0.00533	
	5330	$\mu\epsilon$
Moment, M	0	in-lbs
	0	k-ft

<b>Prestress Decompression</b>		
Decompression Stress in Straind, fps	144	ksi
Decompression Force, Pdecomp	576	k
<b>Top Fiber Stress</b>		
Pe/A	-1.10	ksi
Peectop/I	1.48	ksi
ft	0.38	ksi
<b>Bottom Fiber Stress</b>		
Pe/A	-1.10	ksi
Peecbott/I	-1.53	ksi
fb	-2.64	ksi
<b>Curvature</b>		
Neutral Axis Depth, c	6.77	in
Required Steel Stress, fps	2.24	ksi
Additional Top Stress, ft2	3.05	ksi
Additional Bottom Stress, fb2	3.05	ksi
Second Neutral Axis Depth, c2	26.9	in
Top Fiber Stress, ft	2.67	ksi
Bottom Fiber Stress, fb	0.409	ksi
Top Fiber Strain, $\epsilon_t$	0.000573	
Curvature, $\Phi$	0.0000123	$\epsilon/\text{in}$
	12.3	$\mu\epsilon/\text{in}$
Moment, M	22926457	in-lbs
	1911	k-ft

<b>Cracking Stress</b>		
Cracking Stress, fr	0.424	ksi
Bottom Fiber Stress at Decompression, fb	0.409	ksi
Additional Stress to Crack, fbadd	0.0150	ksi
Additional Moment to Crack, Madd	113750	in-k
<b>Curvature</b>		
Top Fiber Stress, ft	2.68	ksi
Bottom Fiber Stress, fb	0.424	ksi
Top Fiber Strain, $\epsilon_t$	0.000577	
Bottom Fiber Strain, $\epsilon_b$	0.0000912	
Curvature, $\Phi$	0.0000124	$\epsilon/\text{in}$
	12.4	$\mu\epsilon/\text{in}$
Moment, M	23040206	in-lbs
	1920	k-ft

Strand Strain is 0.009		
Strand Strain, $\epsilon_s$	0.009	
Stress in Strand, fps	242	ksi
Tensile Force, T	968	k
Neutral Axis Depth, c	16.3	in
Top Fiber Strain, $\epsilon_t$	0.00197	
Curvature, $\Phi$	0.000121	$\epsilon/\text{in}$
	121	$\mu\epsilon/\text{in}$
Compression Force, Cc1	927570	lbs
Compression Force, Cc2	24963	lbs
Compression Force, Cc3	55.4	lbs
Compression Force, Cc	952478	lbs
	952	k
Equilibrium	15.2	lbs
xbar 1	10.4	in
xbar 2	4.95	in
xbar 3	0.369	in
Moment, M1	37718847	in-lbs
Moment, M2	879761	in-lbs
Moment, M3	1699	in-lbs
Moment, M	38596909	in-lbs
	3216	k-ft

Top Fiber Strain is 0.0015		
Top Fiber Strain, $\epsilon_t$	0.0015	
Neutral Axis Depth, c	17.8	in
Curvature, $\Phi$	0.0000843	$\epsilon/\text{in}$
	84.3	$\mu\epsilon/\text{in}$
Compression Force, Cc1	836982	lbs
Compression Force, Cc2	25483	lbs
Compression Force, Cc3	1905	lbs
Compression Force, Cc	860560	lbs
	861	k
Compatible Steel Strain, $\epsilon_{\text{comp}}$	0.00243	
Incompatible Steel Strain, $\epsilon_{\text{ic}}$	0.00533	
Steel Strain, $\epsilon_{\text{ps}}$	0.00776	
fps	215	
Tensile Force, T	861	kips
Equilibrium	0	lbs
xbar 1	11.5	in
xbar 2	5.94	in
xbar 3	1.36	
Moment, M1	33720486	in-lbs
Moment, M2	885495	in-lbs
Moment, M3	57456	
Moment, M	34548525	in-lbs
	2879	k-ft

Top Fiber Strain is 0.003		
Top Fiber Strain, $\epsilon_t$	0.003	
Neutral Axis Depth, c	13.7	in
Curvature, $\Phi$	0.000219	$\epsilon/\text{in}$
	219	$\mu\epsilon/\text{in}$
Compression Force, Cc1	959280	lbs
Compression Force, Cc2	19040	lbs
Compression Force, Cc3	0	lbs
Compression Force, Cc	978320	lbs
	978	k
Compatible Steel Strain, $\epsilon_{\text{comp}}$	0.00718	
Incompatible Steel Strain, $\epsilon_{\text{ic}}$	0.00533	
Steel Strain, $\epsilon_{\text{ps}}$	0.0125	
fps	245	
Tensile Force, T	978	kips
Equilibrium	0	lbs
xbar 1	8.36	in
xbar 2	3.25	in
xbar 3	-1.36	
Moment, M1	39551404	in-lbs
Moment, M2	687678	in-lbs
Moment, M3	0	
Moment, M	40239081	in-lbs
	3353	k-ft

**Table 37. Test 2 Moment-Curvature Calculations**

Concrete Properties			Steel Properties					
Girder Concrete Strength, $f_c$	6650	psi	Deck Area, $A_d$	96.3	$\text{in}^2$	# Strands	42	ea
Deck Concrete Strength, $f_c$	6020	psi	Top Flange Area, $A_{tf}$	112	$\text{in}^2$	# Repaired Strands	8	ea
Modular Ratio, $n$	0.905		Top Haunch Area, $A_{th}$	51.8	$\text{in}^2$	Strand Diameter, $D_s$	0.375	in
Deck Height, $h_d$	8.75	in	Web Area, $A_w$	133	$\text{in}^2$	Area of Strand, $A_s$ (each)	0.08	$\text{in}^2$
Top Flange Height, $h_{tf}$	7	in	Bottom Haunch Area, $A_{bh}$	109	$\text{in}^2$	Undamaged Strand Area	3.36	
Top Haunch Height, $h_{th}$	4.5	in	Bottom Flange Area, $A_{bf}$	154	$\text{in}^2$	Repaired Strand Area	0.64	
Web Height, $h_w$	19	in	Total Girder Area, $A_g$	0	$\text{in}^2$	Total Strand Area, $A_{ps}$ (total)	4	$\text{in}^2$
Bottom Haunch Height, $h_{bh}$	7.5	in	Deck Transformed Area, $A_{dt}$	87.1	$\text{in}^2$	Strand Center of Gravity, $c_{gps}$	6.08	In
Bottom Flange Height, $h_{bf}$	7	in	Composite Transformed Area, $A_{ct}$	87	$\text{in}^2$	Depth of Strands, $d_{ps}$	47.7	In
Girder Height, $h_g$	45	in	Deck Moment of Inertia, $I_d$	614	$\text{in}^4$	Ultimate Stress, $f_{pu}$	250	Ksi
Total Height, $h$	53.8	in	Deck Transformed Moment of Inertia, $I_{dt}$	556	$\text{in}^4$	Ultimate Strain, $\epsilon$	0.06	
Deck Width, $b_d$	11	in	Girder Moment of Inertia, $I_g$	125165	$\text{in}^4$	Modulus of Elasticity, $E_{ps}$	27000	ksi
Transformed Deck Width, $b_{td}$	9.96	in	Total Moment of Inertia, $I$	125721	$\text{in}^4$	Effective Prestress, $f_{pe}$	132	ksi
Top Flange Width, $b_{tf}$	16	in	Deck Center of Gravity, $y_g$	49.4	in	Yield Stress, $f_{py}$	242	ksi
Top Haunch Width, $b_{th}$	4.5	in	Girder Center of Gravity, $y_g$	20.3	in	Yield Strain, $\epsilon$	0.009	
Web Width, $b_w$	7	in	Composite Center of Gravity, $y_c$	49.4	in	$f_p$ ( $\epsilon=0.015$ )	246	ksi
Bottom Haunch Width, $b_{bh}$	7.5	in	Transformed Top to COG, $c_{tt}$	4.4	in	$\epsilon$ ( $f_p=246.18$ )	0.015	
Bottom Flange Width, $b_{bf}$	22	in	Transformed Bottom to COG, $c_{tb}$	49.4	in	$f_p$ ( $\epsilon=0.009$ )	242	ksi
			Girder Modulus of Elasticity, $E_{cg}$	4648	ksi	$\epsilon$ ( $f_p=241.91$ )	0.009	
			Ultimate Strain, $\epsilon_{cu}$	0.003		Undamaged Prestress Force	444	k
			$0.5f_c$	3325	psi	Repaired Prestress Force	67.6	k
			Strain, $\epsilon$ (3.3 ksi)	0.000715		Effective Prestress Force, $P_e$	511	k
			$0.5f_c$	3325	psi	Eccentricity, $e$	43.3	in
			$\Delta$	0	psi			
			$\epsilon_0$	0.00244				

<b>No applied Moment</b>		
<b>Top Fiber Stress</b>		
Pe/A	-5.87	ksi
Peectop/I	0.77	ksi
ft	-5.10	ksi
<b>Bottom Fiber Stress</b>		
Pe/A	-5.87	ksi
Peecbott/I	-8.69	ksi
fb	-14.6	ksi
<b>Curvature</b>		
Top Fiber Strain, $\epsilon_t$	-0.00110	
	-1096	$\mu\epsilon$
Bottom Fiber Strain, $\epsilon_b$	-0.00313	
	-3132	$\mu\epsilon$
Neutral Axis Depth, c	-29.0	in
Curvature, $\Phi$	-0.0000379	$\epsilon/\text{in}$
	-37.9	$\mu\epsilon/\text{in}$
Steel Strain Increase, $\epsilon_2$	0.00290	
	2901	$\mu\epsilon$
Prestress Steel Strain, $\epsilon_1$	0.00489	
	4889	$\mu\epsilon$
Total Steel Strain, $\epsilon_1+\epsilon_2$	0.00779	
	7790	$\mu\epsilon$
Moment, M	0	in-lbs
	0	k-ft

<b>Prestress Decompression</b>		
Decompression Stress in Straind, fps	210	ksi
Decompression Force, Pdecomp	841	k
<b>Top Fiber Stress</b>		
Pe/A	-9.66	ksi
Peectop/I	1.27	ksi
ft	-8.39	ksi
<b>Bottom Fiber Stress</b>		
Pe/A	-9.66	ksi
Peecbott/I	-14.3	ksi
fb	-24.0	ksi
<b>Curvature</b>		
Neutral Axis Depth, c	-29.0	in
Required Steel Stress, fps	22.2	ksi
Additional Top Stress, ft2	28.7	ksi
Additional Bottom Stress, fb2	28.7	ksi
Second Neutral Axis Depth, c2	26.9	in
Top Fiber Stress, ft	37.1	ksi
Bottom Fiber Stress, fb	4.73	ksi
Top Fiber Strain, $\epsilon_t$	0.00798	
Curvature, $\Phi$	0.000167	$\epsilon/\text{in}$
	167	$\mu\epsilon/\text{in}$
Moment, M	64465816	in-lbs
	5372	k-ft

<b>Cracking Stress</b>		
Cracking Stress, fr	0.424	ksi
Bottom Fiber Stress at Decompression, fb	4.73	ksi
Additional Stress to Crack, fbadd	-4.31	ksi
Additional Moment to Crack, Madd	-10962298	in-k
<b>Curvature</b>		
Top Fiber Stress, ft	32.8	ksi
Bottom Fiber Stress, fb	0.424	ksi
Top Fiber Strain, $\epsilon_t$	0.00705	
Bottom Fiber Strain, $\epsilon_b$	0.0000912	
Curvature, $\Phi$	0.000133	$\epsilon/\text{in}$
	133	$\mu\epsilon/\text{in}$
Moment, M	53503518	in-lbs
	4459	k-ft

<b>Strand Strain is 0.009</b>		
Strand Strain, $\epsilon_s$	0.009	
Stress in Strand, fps	242	ksi
Tensile Force, T	968	k
Neutral Axis Depth, c	18.5	in
Top Fiber Strain, $\epsilon_t$	0.000769	
Curvature, $\Phi$	0.0000415	$\epsilon/\text{in}$
	41.5	$\mu\epsilon/\text{in}$
Compression Force, Cc1	345445	lbs
Compression Force, Cc2	61560	lbs
Compression Force, Cc3	2363	lbs
Compression Force, Cc	404642	lbs
	405	k
Equilibrium	563	lbs
xbar 1	12.2	in
xbar 2	6.47	in
xbar 3	1.84	in
Moment, M1	14272373	in-lbs
Moment, M2	2192516	in-lbs
Moment, M3	73247	in-lbs
Moment, M	16391642	in-lbs
	1366	k-ft

<b>Top Fiber Strain is 0.0015</b>		
Top Fiber Strain, $\epsilon_t$	0.0015	
Neutral Axis Depth, c	19.6	in
Curvature, $\Phi$	0.0000766	$\epsilon/\text{in}$
	76.6	$\mu\epsilon/\text{in}$
Compression Force, Cc1	633478	lbs
Compression Force, Cc2	131176	lbs
Compression Force, Cc3	11293	lbs
Compression Force, Cc	753360	lbs
	753	k
Compatible Steel Strain, $\epsilon_{\text{comp}}$	0.00215	
Incompatible Steel Strain, $\epsilon_{\text{ic}}$	0.00779	
Steel Strain, $\epsilon_{\text{ps}}$	0.00994	
fps	188	
Tensile Force, T	753	kips
Equilibrium	0	kips
xbar 1	12.6	in
xbar 2	7.11	in
xbar 3	2.54	
Moment, M1	25796103	in-lbs
Moment, M2	4616450	in-lbs
Moment, M3	345896	
Moment, M	30066658	in-lbs
	2506	k-ft

<b>Top Fiber Strain is 0.003</b>		
Top Fiber Strain, $\epsilon_t$	0.003	
Neutral Axis Depth, c	17.0	in
Curvature, $\Phi$	0.000176	$\epsilon/\text{in}$
	176	$\mu\epsilon/\text{in}$
Compression Force, Cc1	817328	lbs
Compression Force, Cc2	158733	lbs
Compression Force, Cc3	942	lbs
Compression Force, Cc	975120	lbs
	975	k
Compatible Steel Strain, $\epsilon_{\text{comp}}$	0.00541	
Incompatible Steel Strain, $\epsilon_{\text{ic}}$	0.00779	
Steel Strain, $\epsilon_{\text{ps}}$	0.0132	
fps	244	
Tensile Force, T	975	kips
Equilibrium	0	lbs
xbar 1	10.4	in
xbar 2	5.34	in
xbar 3	0.84	
Moment, M1	33522965	in-lbs
Moment, M2	5713462	in-lbs
Moment, M3	29665	
Moment, M	39206762	in-lbs
	3267	k-ft



<b>No applied Moment</b>		
<b>Top Fiber Stress</b>		
Pe/A	-0.751	ksi
Peectop/I	1.33	ksi
ft	0.578	ksi
<b>Bottom Fiber Stress</b>		
Pe/A	-0.751	ksi
Peecbott/I	-1.09	ksi
fb	-1.84	ksi
<b>Curvature</b>		
Top Fiber Strain, $\epsilon_t$	0.000124	
	124	$\mu\epsilon$
Bottom Fiber Strain, $\epsilon_b$	-0.000396	
	-396	$\mu\epsilon$
Neutral Axis Depth, c	12.8	in
Curvature, $\Phi$	-0.00000968	$\epsilon/\text{in}$
	-9.68	$\mu\epsilon/\text{in}$
Steel Strain Increase, $\epsilon_2$	0.000331	
	331	$\mu\epsilon$
Prestress Steel Strain, $\epsilon_1$	0.00489	
	4889	$\mu\epsilon$
Total Steel Strain, $\epsilon_1+\epsilon_2$	0.00522	
	5220	$\mu\epsilon$
Moment, M	0	in-lbs
	0	k-ft

<b>Prestress Decompression</b>		
Decompression Stress in Straind, fps	141	ksi
Decompression Force, Pdecomp	519	k
<b>Top Fiber Stress</b>		
Pe/A	-0.802	ksi
Peectop/I	1.42	ksi
ft	0.617	ksi
<b>Bottom Fiber Stress</b>		
Pe/A	-0.802	ksi
Peecbott/I	-1.16	ksi
fb	-1.97	ksi
<b>Curvature</b>		
Neutral Axis Depth, c	12.8	in
Required Steel Stress, fps	1.65	ksi
Additional Top Stress, ft2	2.19	ksi
Additional Bottom Stress, fb2	2.19	ksi
Second Neutral Axis Depth, c2	26.9	in
Top Fiber Stress, ft	1.57	ksi
Bottom Fiber Stress, fb	0.222	ksi
Top Fiber Strain, $\epsilon_t$	0.000338	
Curvature, $\Phi$	0.00000718	$\epsilon/\text{in}$
	7.18	$\mu\epsilon/\text{in}$
Moment, M	17763464	in-lbs
	1480	k-ft

<b>Cracking Stress</b>		
Cracking Stress, fr	0.424	ksi
Bottom Fiber Stress at Decompression, fb	0.222	ksi
Additional Stress to Crack, fbadd	0.202	ksi
Additional Moment to Crack, Madd	1578325	in-k
<b>Curvature</b>		
Top Fiber Stress, ft	1.77	ksi
Bottom Fiber Stress, fb	0.424	ksi
Top Fiber Strain, $\epsilon_t$	0.000381	
Bottom Fiber Strain, $\epsilon_b$	0.0000912	
Curvature, $\Phi$	0.00000879	$\epsilon/\text{in}$
	8.79	$\mu\epsilon/\text{in}$
Moment, M	19341789	in-lbs
	1612	k-ft

Strand Strain is 0.009		
Strand Strain, $\epsilon_s$	0.009	
Stress in Strand, fps	242	ksi
FRP Strain	0.0047	
FRP Stress	50.4	ksi
Strand Tensile Force	890	k
FRP Tensile Force	177	k
Tensile Force, T	1067	k
Neutral Axis Depth, c	19.3	in
Top Fiber Strain, $\epsilon_t$	0.00263	
Curvature, $\Phi$	0.000136	$\epsilon/\text{in}$
	136	$\mu\epsilon/\text{in}$
Compression Force, Cc1	882398	lbs
Compression Force, Cc2	200700	lbs
Compression Force, Cc3	15617	lbs
Compression Force, Cc	1067481	lbs
	1067	k
Equilibrium	0	lbs
xbar 1	12.0	in
xbar 2	6.83	in
xbar 3	2.35	in
Moment, M1	35074727	in-lbs
Moment, M2	6944464	in-lbs
Moment, M3	470521	in-lbs
Moment, M	41548669	in-lbs
	3462	k-ft

Top Fiber Strain is 0.0015		
Top Fiber Strain, $\epsilon_t$	0.0015	
Neutral Axis Depth, c	20.4	in
Curvature, $\Phi$	0.0000735	$\epsilon/\text{in}$
	73.5	$\mu\epsilon/\text{in}$
Compression Force, Cc1	659986	lbs
Compression Force, Cc2	145070	lbs
Compression Force, Cc3	19246	lbs
Compression Force, Cc	785810	lbs
	786	k
Compatible Steel Strain, $\epsilon_{\text{comp}}$	0.00196	
Incompatible Steel Strain, $\epsilon_{\text{ic}}$	0.00522	
Steel Strain, $\epsilon_{\text{ps}}$	0.00718	
fps	188	
FRP Strain	0.00246	
FRP Stress	26.3	ksi
Strand Tensile Force	693	
FRP Tensile Force	92.7	k
Tensile Force, T	786	k
Equilibrium	0	k
xbar 1	13.2	in
xbar 2	7.64	in
xbar 3	3.08	in
xbar 4	6.74	in
Moment, M1	26298208	in-lbs
Moment, M2	4979162	in-lbs
Moment, M3	572857	in-lbs
Moment, M4	3863344	in-lbs
Moment, M	34567857	in-lbs
	2881	k-ft

Top Fiber Strain is 0.003		
Top Fiber Strain, $\epsilon_t$	0.003	
Neutral Axis Depth, c	18.9	in
Curvature, $\Phi$	0.000159	$\epsilon/\text{in}$
	159	$\mu\epsilon/\text{in}$
Compression Force, Cc1	909151	lbs
Compression Force, Cc2	210601	lbs
Compression Force, Cc3	12881	lbs
Compression Force, Cc	1106871	lbs
	1107	k
Compatible Steel Strain, $\epsilon_{\text{comp}}$	0.00446	
Incompatible Steel Strain, $\epsilon_{\text{ic}}$	0.00522	
Steel Strain, $\epsilon_{\text{ps}}$	0.00968	
fps	244	ksi
FRP Strain	0.00553	
FRP Stress	59.3	ksi
Strand Tensile Force	898	k
FRP Tensile Force	209	k
Tensile Force, T	1107	k
Equilibrium	0	k
xbar 1	11.5	in
xbar 2	6.54	in
xbar 3	2.10	
xbar 4	6.74	
Moment, M1	36078447	in-lbs
Moment, M2	7308806	in-lbs
Moment, M3	389752	in-lbs
Moment, M4	1408	in-lbs
Moment, M	42998910	in-lbs
	3583	k-ft

**Table 39. Test 4 Moment-Curvature Calculations**

Concrete Properties			Steel Properties		
Girder Concrete Strength, $f_c$	6650	psi	Deck Area, $A_d$	96.3	in <sup>2</sup>
Deck Concrete Strength, $f_c$	6020	psi	Top Flange Area, $A_{tf}$	112	in <sup>2</sup>
Modular Ratio, $n$	0.905		Top Haunch Area, $A_{th}$	51.8	in <sup>2</sup>
Deck Height, $h_d$	8.75	in	Web Area, $A_w$	133	in <sup>2</sup>
Top Flange Height, $h_{tf}$	7	in	Bottom Haunch Area, $A_{bh}$	109	in <sup>2</sup>
Top Haunch Height, $h_{th}$	4.5	in	Bottom Flange Area, $A_{bf}$	154	in <sup>2</sup>
Web Height, $h_w$	19	in	Total Girder Area, $A_g$	560	in <sup>2</sup>
Bottom Haunch Height, $h_{bh}$	7.5	in	Deck Transformed Area, $A_{dt}$	87.1	in <sup>2</sup>
Bottom Flange Height, $h_{bf}$	7	in	Total Composite Transformed Area, $A_{ct}$	647	in <sup>2</sup>
Girder Height, $h_g$	45	in	Deck Moment of Inertia, $I_d$	614	in <sup>4</sup>
Total Height, $h$	53.8	in	Deck Transformed Moment of Inertia, $I_{dt}$	556	in <sup>4</sup>
Deck Width, $b_d$	11	in	Girder Moment of Inertia, $I_g$	125165	in <sup>4</sup>
Transformed Deck Width, $b_{td}$	9.96	in	Total Moment of Inertia, $I$	189479	in <sup>4</sup>
Top Flange Width, $b_{tf}$	16	in	Deck Center of Gravity, $y_g$	49.4	in
Top Haunch Width, $b_{th}$	4.5	in	Girder Center of Gravity, $y_g$	20.3	in
Web Width, $b_w$	7	in	Composite Center of Gravity, $y_c$	24.2	in
Bottom Haunch Width, $b_{bh}$	7.5	in	Transformed Top to COG, $c_{tt}$	29.5	in
Bottom Flange Width, $b_{bf}$	22	in	Transformed Bottom to COG, $c_{tb}$	24.2	in
			Girder Modulus of Elasticity, $E_{cg}$	4648	ksi
			Ultimate Strain, $\epsilon_{cu}$	0.003	
			$0.5f_c$	3325	psi
			Strain, $\epsilon$ (3.3 ksi)	0.000715	
			$0.5f_c$	3325	psi
			$\Delta$	0	psi
			$\epsilon_0$	0.00244	
			# Strands	46	ea
			# Repaired Strands	4	ea
			Strand Diameter, $D_s$	0.375	in
			Area of Strand, $A_s$	0.08	in <sup>2</sup>
			Undamaged Strand Area	3.68	
			Repaired Strand Area	0.32	
			Total Strand Area, $A_{ps}$	4	in <sup>2</sup>
			Strand Center of Gravity, $c_{gps}$	6.66	in
			Depth of Strands, $d_{ps}$	47.1	in
			Ultimate Stress, $f_{pu}$	250	ksi
			Ultimate Strain, $\epsilon$	0.06	
			Modulus of Elasticity, $E_{ps}$	27000	ksi
			Effective Prestress, $f_{pe}$	132	ksi
			Yield Stress, $f_{py}$	242	ksi
			Yield Strain, $\epsilon$	0.009	
			$f_p$ ( $\epsilon=0.015$ )	246	ksi
			$\epsilon$ ( $f_p=246.18$ )	0.015	
			$f_p$ ( $\epsilon=0.009$ )	242	ksi
			$\epsilon$ ( $f_p=241.91$ )	0.009	
			Undamaged Prestress Force	486	k
			Repaired Prestress Force	33.8	k
			Effective Prestress Force, $P_e$	520	k
			Eccentricity, $e$	17.5	in

<b>No applied Moment</b>		
<b>Top Fiber Stress</b>		
Pe/A	-0.803	ksi
Peectop/I	1.42	ksi
ft	0.618	ksi
<b>Bottom Fiber Stress</b>		
Pe/A	-0.803	ksi
Peecbott/I	-1.17	ksi
fb	-1.97	ksi
<b>Curvature</b>		
Top Fiber Strain, $\epsilon_t$	0.000133	
	133	$\mu\epsilon$
Bottom Fiber Strain, $\epsilon_b$	-0.000424	
	-424	$\mu\epsilon$
Neutral Axis Depth, c	12.8	in
Curvature, $\Phi$	-0.0000104	$\epsilon/\text{in}$
	-10.4	$\mu\epsilon/\text{in}$
Steel Strain Increase, $\epsilon_2$	0.000355	
	355	$\mu\epsilon$
Prestress Steel Strain, $\epsilon_1$	0.00489	
	4889	$\mu\epsilon$
Total Steel Strain, $\epsilon_1+\epsilon_2$	0.00524	
	5243	$\mu\epsilon$
Moment, M	0	in-lbs
	0	k-ft

<b>Prestress Decompression</b>		
Decompression Stress in Straind, fps	142	ksi
Decompression Force, Pdecomp	566	k
<b>Top Fiber Stress</b>		
Pe/A	-0.876	ksi
Peectop/I	1.55	ksi
ft	0.673	ksi
<b>Bottom Fiber Stress</b>		
Pe/A	-0.876	ksi
Peecbott/I	-1.27	ksi
fb	-2.15	ksi
<b>Curvature</b>		
Neutral Axis Depth, c	12.8	in
Required Steel Stress, fps	1.80	ksi
Additional Top Stress, ft2	2.39	ksi
Additional Bottom Stress, fb2	2.39	ksi
Second Neutral Axis Depth, c2	26.9	in
Top Fiber Stress, ft	1.71	ksi
Bottom Fiber Stress, fb	0.243	ksi
Top Fiber Strain, $\epsilon_t$	0.000369	
Curvature, $\Phi$	0.00000784	$\epsilon/\text{in}$
	7.84	$\mu\epsilon/\text{in}$
Moment, M	19393397	in-lbs
	1616	k-ft

<b>Cracking Stress</b>		
Cracking Stress, fr	0.424	ksi
Bottom Fiber Stress at Decompression, fb	0.243	ksi
Additional Stress to Crack, fbadd	0.181	ksi
Additional Moment to Crack, Madd	1418690	in-k
<b>Curvature</b>		
Top Fiber Stress, ft	1.90	ksi
Bottom Fiber Stress, fb	0.424	ksi
Top Fiber Strain, $\epsilon_t$	0.000408	
Bottom Fiber Strain, $\epsilon_b$	0.0000912	
Curvature, $\Phi$	0.00000929	$\epsilon/\text{in}$
	9.29	$\mu\epsilon/\text{in}$
Moment, M	20812086	in-lbs
	1734	k-ft

Strand Strain is 0.009		
Strand Strain, $\epsilon_s$	0.009	
Stress in Strand, fps	242	ksi
Tensile Force, T	968	k
Neutral Axis Depth, c	18.4	in
Top Fiber Strain, $\epsilon_t$	0.00241	
Curvature, $\Phi$	0.000131	$\epsilon/\text{in}$
	131	$\mu\epsilon/\text{in}$
Compression Force, Cc1	807639	lbs
Compression Force, Cc2	166399	lbs
Compression Force, Cc3	6398	lbs
Compression Force, Cc	967640	lbs
	968	k
Equilibrium	0	lbs
xbar 1	11.5	in
xbar 2	6.27	in
xbar 3	1.76	in
Moment, M1	3246409	in-lbs
Moment, M2	5815265	in-lbs
Moment, M3	194754	in-lbs
Moment, M	3808461	in-lbs
	3174	k-ft

Top Fiber Strain is 0.0015		
Top Fiber Strain, $\epsilon_t$	0.0015	
Neutral Axis Depth, c	19.6	in
Curvature, $\Phi$	0.000076	$\epsilon/\text{in}$
	6	$\mu\epsilon/\text{in}$
Compression Force, Cc1	633478	lbs
Compression Force, Cc2	131176	lbs
Compression Force, Cc3	11293	lbs
Compression Force, Cc	753360	lbs
	753	k
Compatible Steel Strain, $\epsilon_{\text{comp}}$	0.00211	
Incompatible Steel Strain, $\epsilon_{\text{ic}}$	0.00524	
Steel Strain, $\epsilon_{\text{ps}}$	0.00735	
fps	188	
Tensile Force, T	753	k
Equilibrium	0	k
xbar 1	12.6	in
xbar 2	7.11	in
xbar 3	2.54	
Moment, M1	25426152	in-lbs
Moment, M2	4539843	in-lbs
Moment, M3	339300	
Moment, M	29626695	in-lbs
	2469	k-ft

Top Fiber Strain is 0.003		
Top Fiber Strain, $\epsilon_t$	0.003	
Neutral Axis Depth, c	17.0	in
Curvature, $\Phi$	0.000176	$\epsilon/\text{in}$
	176	$\mu\epsilon/\text{in}$
Compression Force, Cc1	817328	lbs
Compression Force, Cc2	158733	lbs
Compression Force, Cc3	942	lbs
Compression Force, Cc	975120	lbs
	975	k
Compatible Steel Strain, $\epsilon_{\text{comp}}$	0.0053	
Incompatible Steel Strain, $\epsilon_{\text{ic}}$	0.00524	
Steel Strain, $\epsilon_{\text{ps}}$	0.0105	
fps	244	
Tensile Force, T	975	k
Equilibrium	0	lbs
xbar 1	10.4	in
xbar 2	5.34	in
xbar 3	0.84	
Moment, M1	3304564	in-lbs
Moment, M2	5620762	in-lbs
Moment, M3	29115	
Moment, M	3863729	in-lbs
	2	in-lbs
	3220	k-ft

## APPENDIX D: FRP Repair Calculations

The following calculations were used as the design calculations for the FRP installation (Pino & Nanni, 2015).

### Repair of Damaged Prestressed Concrete Girder using Fiber Reinforced Polymer (FRP) Composites

Bridges in the Commonwealth of Virginia and other states are often damaged by impact from over-height vehicles where the impact damage may be quite extensive. For precast, prestressed concrete (PC) beams, extensive damage may be repaired using composite materials such as Fiber Reinforced Polymers (FRP). This program is designed to analyze the strength of two AASHTO Type III girders using AASHTO LRFD Bridge Design Specifications (2010) and ACI 440.2R-08 Guide for the Design and Construction of Externally Bonded FRP Systems for Strengthening of Concrete Structures (2008). The design calculations are organized as follows:

- Section 1 - Material and Geometric Properties of Virgin and Damaged Girder
- Section 2 - Strength of Virgin Girder
- Section 3 - Initial Conditions of Damaged Girder (4 strands lost)
- Section 4 - Strength of Damaged Girder
- Section 5 - Strength of Damaged Girder with Externally Bonded FRP

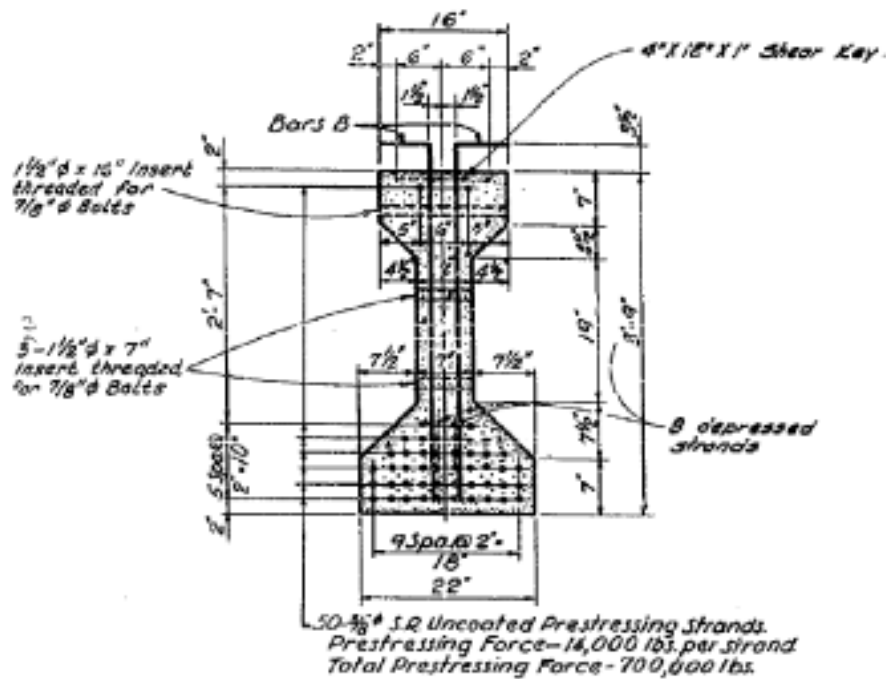


Figure 1 - AASHTO Type III Girder

Note:

1. All highlighted variables indicate a user input value
2. All values of ultimate strength are calculated at a specified location "x" along the span of the girder. For the estimation of prestressing losses, the girder properties at midspan were used.

## Section 1

### Material Properties

Deck concrete strength	$f_{c,slab} = 4\text{ksi}$
	$\beta_{1,deck} = 0.85$
	$E_{c,deck} = 3834\text{ksi}$
Girder concrete strength	$f_{c,girder} = 4.2\text{ksi}$
	$f_{c,girder} = 5\text{ksi}$
	$\beta_{1,girder} = 0.8$
Modulus of elasticity of Girder	$E_{c,girder} = 4286.8257487\text{ksi}$
	$E_{c,girder} = 3928.9406969\text{ksi}$
Modular Ratio between deck and girder	$n = 0.8944272$
Maximum Compressive Strain	$\epsilon_{cu} = .003$
Ultimate prestressing stress	$f_{pu} = 250\text{ksi}$
Yield stress in prestressing steel	$f_{py} = 206.5\text{ksi}$
Modulus of elasticity of prestressing steel	$E_s = 27000\text{ksi}$
Minimum modulus of elasticity	$E_{s,min} = 25500\text{ksi}$

## Girder Geometric Properties

Girder Span Length	$\text{Span} := 60\text{ft}$
At what point along the span do you want to evaluate the properties	$x := \frac{\text{Span}}{3} = 20\text{ft}$
Girder Depth	$h_{nc} := 45\text{in}$
Top flange width	$b_{tf} := 16\text{in}$
Top flange depth	$h_{tf} := 7\text{in}$
Top flange sloped section thickness	$h_{tsf} := 4.5\text{in}$
Bottom flange width	$b_{bf} := 22\text{in}$
Bottom flange depth	$h_{bf} := 7\text{in}$
Bottom flange sloped section thickness	$h_{bsf} := 7.5\text{in}$
Width of web	$b_{web} := 7\text{in}$
Section Area	$A_c := 560\text{in}^2$
Neutral Axis to bottom of beam	$y_b := 20.27\text{in}$
Neutral Axis to top of beam	$y_t := 24.73\text{in}$
Moment of Inertia	$I_g := 125390\text{in}^4$
Section Modulus Top	$S_t = 5070.36\text{in}^3$
Section Modulus Bottom	$S_b = 6185.99\text{in}^3$

### Slab Geometric Properties

Slab thickness

$$t_{\text{slab}} := 8.75 \text{ in}$$

Slab width (same as flange width)

$$b_{\text{slab}} := 11.5 \text{ in}$$

Effective slab width

$$b_{\text{slab.tr}} = 10.29 \text{ in}$$

Slab area transformed

$$A_{\text{slab.tr}} = 90 \text{ in}^2$$

### Reinforcing Steel Properties

Area of non-prestressed tension steel reinforcement

$$A_s := 0 \text{ in}^2$$

yield stress of steel

$$f_y := 60 \text{ ksi}$$

### Prestressing Steel Properties

#### Steel Strands

Strand Type

$$\text{strand}_{\text{type}} := 2$$

Enter: 1 – Low Lax  
2 – Stress Relieved

Tendons

$$\text{Bond} := 1$$

Enter: 1 – Bonded Tendons  
2 – Unbonded Tendons

Nominal Diameter

$$\phi_s := \frac{3}{8} \text{ in}$$

Area of strand

$$A_{\text{strand}} := .0799 \text{ in}^2$$

Harped Strands Slope

$$\text{strand}_{\text{slope}} := \frac{3 \text{ ft} + 9 \text{ in} - 17 \text{ in}}{23 \text{ ft} + 10.5 \text{ in}} = 0.0977312$$

### Virgin Girder

Number of strands total	$n_{ps, total} = 50$
Area of strands Total	$A_{ps, total} = 3.995 \text{ in}^2$
Straight strands	$n_{ps, straight} = 40$
Area of straight strands	$A_{ps, straight} = 3.196 \text{ in}^2$
Number of straight strands in top flange	$n_{ps, straight, top} = 2$
Area of straight strands in the top flange	$A_{ps, straight, top} = 0.1598 \text{ in}^2$
Harped Strands	$n_{ps, harped} = 8$
Area of harped strands	$A_{ps, harped} = 0.6392 \text{ in}^2$

### Damaged Girder

Number of strands total	$n_{ps, total, d} = 46$
Area of strands Total	$A_{ps, total, d} = 3.6754 \text{ in}^2$
Straight strands	$n_{ps, straight, d} = 36$
Area of straight strands	$A_{ps, straight, d} = 2.8764 \text{ in}^2$
Number of straight strands in top flange	$n_{ps, straight, top, d} = 2$
Area of straight strands in the top flange	$A_{ps, straight, top, d} = 0.1598 \text{ in}^2$
Harped Strands	$n_{ps, harped, d} = 8$
Area of harped strands	$A_{ps, harped, d} = 0.6392 \text{ in}^2$
Modular ratio between the prestressing strand and beam	$n_p = 6.2983666$

## Composite Section Properties

Composite Area	$A_{\text{composite}} = 650.0017361 \cdot \text{in}^2$
Height of the composite section	$h_{\text{composite}} = 33.75 \cdot \text{in}$
Distance from centroid of beam to extreme fiber in tension (composite)	$y_{\text{b,composite}} = 24.2999901 \cdot \text{in}$
Distance from centroid of beam to extreme fiber in compression	$y_{\text{t,composite}} = 29.4500099 \cdot \text{in}$
Moment of Inertia of slab	$I_{\text{slab}} = 57163.37 \cdot \text{in}^4$
Moment of Inertia of Beam	$I_{\text{girder}} = 134484.8390903 \cdot \text{in}^4$
Moment of Inertia of composite section	$I_{\text{composite}} = 191648.23 \cdot \text{in}^4$
Section modulus top	$S_{\text{t,composite}} = 6507.5778236 \cdot \text{in}^3$
Section modulus bottom	$S_{\text{b,composite}} = 7886.7617337 \cdot \text{in}^3$

### Virgin Girder - Composite Section Transformed Properties

Center of gravity of harped strands at "x"	$y_{cg,harped} = 13.54 \text{ in}$	from bottom of girder
Center of gravity of harped strands at midspan	$y_{cg,harped,midspan} = 9 \text{ in}$	from bottom of girder
Centroid of prestressing strands at "x"	$y_p = 8.01 \text{ in}$	from bottom of girder
Centroid of prestressing strands at midspan	$y_{p,midspan} = 7.28 \text{ in}$	from bottom of girder
Composite area transformed	$A_{c,tr} = 671.1687106 \text{ in}^2$	
Composite neutral axis transformed	$y_{b,tr} = 23.7861539 \text{ in}$	
Composite inertia transformed	$I_{tr} = 196918.340446 \text{ in}^4$	
Composite section modulus, top of slab	$S_{slab,tr} = 6571.8646298 \text{ in}^3$	
Composite section modulus, top of beam	$S_{top,tr} = 9282.5383664 \text{ in}^3$	
Composite section modulus, bottom of beam	$S_{bot,tr} = 8278.6961434 \text{ in}^3$	
Eccentricity of strands for composite section	$e_{cg,tr} = 15.7790335 \text{ in}$	
Section modulus at level of prestressing steel	$S_{ps,tr} = 12479.7466745 \text{ in}^3$	
Depth to centroid of prestressing strands	$d_{p,c} = 45.7428796 \text{ in}$	
Eccentricity of prestressed strands	$e_c = 16.2928696 \text{ in}$	

Distance from neutral axis of composite section to level of prestressing steel

$$y_{p,c} = 16.2928696 \text{ in}$$

Section modulus at level of prestressing steel

$$S_{b,ps,composite} = 11762.7057721 \text{ in}^3$$

### Virgin Girder - Non-Composite Section Transformed Properties

Modular ratio between the prestressing strand and beam

$$n_p = 6.2983666$$

Non - composite area transformed

$$A_{nc,tr} = 581.1669745 \text{ in}^2$$

Non - composite area transformed at midspan

$$A_{nc,tr, \text{midspan}} = 581.1669745 \text{ in}^2$$

non composite neutral axis transformed

$$y_{b,nc,tr} = 19.8233675 \text{ in}$$

from bottom of girder

non composite neutral axis transformed at midspan

$$y_{b,nc,tr, \text{midspan}} = 19.7968847 \text{ in}$$

from bottom of girder

Non composite inertia transformed

$$I_{nc,tr} = 128345.4111876 \text{ in}^4$$

$$I_{nc,tr, \text{midspan}} = 128706.2807343 \text{ in}^4$$

Radius of gyration of Non composite transformed section

$$r_{nc,tr} = 14.8607151 \text{ in}$$

Non composite transformed section modulus top at "x"

$$S_{top,nc,tr} = 5097.7989684 \text{ in}^3$$

Non composite transformed section modulus top at midspan

$$S_{top,nc,tr, \text{midspan}} = 5106.7607757 \text{ in}^3$$

Non composite transformed section modulus bottom at "x"

$$S_{bot,nc,tr} = 6474.4504782 \text{ in}^3$$

Non composite transformed section modulus bottom at midspan

$$S_{bot,nc,tr, \text{midspan}} = 6501.3401252 \text{ in}^3$$

Non composite transformed section modulus at level of prestressing

$$S_{p,nc,tr} = 10861.7744965 \text{ in}^3$$

Non composite transformed section  
modulus at level of prestressing at midspan

$$S_{ps,nc,tr, midspan} = 10282.6129672 \text{ in}^3$$

eccentricity of prestressed strands in  
non-composite transformed section

$$e_{cg,nc,tr} = 11.8162471 \text{ in}$$

$$e_{cg,nc,tr, midspan} = 12.5168847 \text{ in}$$

Depth to prestressing steel in  
non-composite section

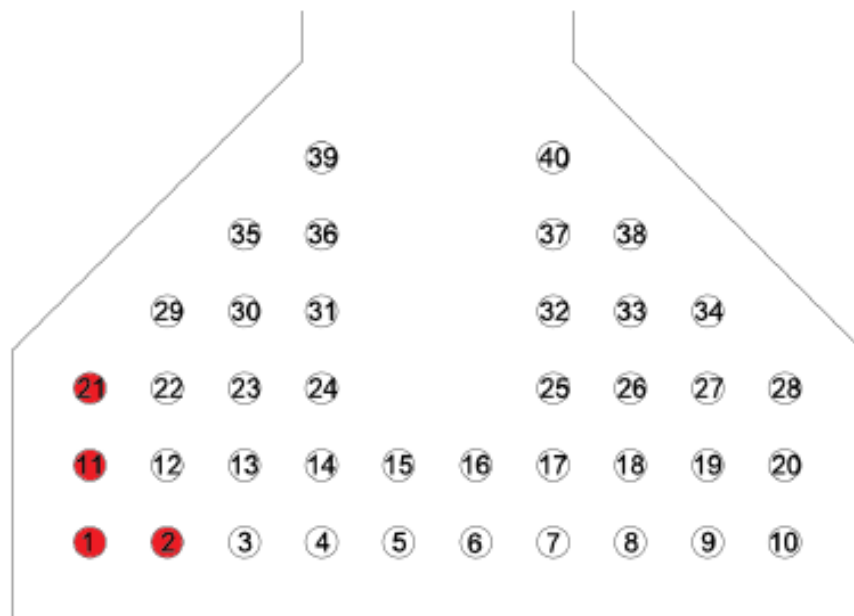
$$d_{p,nc} = 36.9928796 \text{ in}$$

Eccentricity in prestressing  
steel in non-composite section

$$e_{nc} = 12.2628796 \text{ in}$$

### Strand Damage

Four strands were damaged as shown in the following figure at location L/3



## Damaged Girder - Composite Section Transformed Properties

### Prestressing Geometric Properties

Total area of prestress	$A_{ps,d} = 3.6754 \text{ in}^2$	
Center of gravity of harped strands at "x"	$y_{cg,harped,d} = 13.54 \text{ in}$	from bottom of girder
Centroid of prestressing strands at "x"	$y_{p,d} = 8.7 \text{ in}$	from bottom of girder
Composite area transformed	$A_{c,tr,d} = 669.4753526 \text{ in}^2$	
Composite neutral axis transformed	$y_{b,tr,d} = 23.8463181 \text{ in}$	from bottom of girder
Composite Inertia transformed	$I_{tr,d} = 196113.6919699 \text{ in}^4$	
Composite section modulus, top of slab at "x"	$S_{slab,tr,d} = 6558.1787812 \text{ in}^3$	
Composite section modulus, top of beam at "x"	$S_{top,tr,d} = 9270.9010707 \text{ in}^3$	
Composite section modulus, bottom of beam at "x"	$S_{bot,tr,d} = 8224.0659109 \text{ in}^3$	
Eccentricity of strands for composite section	$e_{cg,tr,d} = 15.1429264 \text{ in}$	
Section modulus at level of prestressing steel	$S_{ps,tr,d} = 12950.8449868 \text{ in}^3$	
Depth to prestressed of composite_section	$d_{p,c,d} = 45.0466082 \text{ in}$	
Eccentricity of prestressed strands in composite section	$e_{c,d} = 15.5965983 \text{ in}$	
Distance from neutral axis of composite section to level of prestressing steel	$y_{p,c,d} = 15.5965983 \text{ in}$	
Section modulus at level of prestressing steel in composite section	$S_{b,ps,composite,d} = 12287.8225165 \text{ in}^3$	

## Damaged Girder - Non-Composite Section Transformed Properties

Depth to prestressing strands from top of girder	$d_{p,nc,d} = 36.3\text{-in}$	
Eccentricity of prestressed strands in girder	$e_{nc,d} = 11.5666082\text{-in}$	
Modular ratio between the prestressing strand and beam	$n_p = 6.2983666$	
Non - composite area transformed	$A_{nc,tr,d} = 579.4736165\text{-in}^2$	
Non - composite neutral axis transformed	$y_{b,nc,tr,d} = 19.881296\text{-in}$	from bottom of girder
Non - composite inertia transformed	$I_{nc,tr,d} = 127823.1416068\text{-in}^4$	
Radius of gyration of non - composite transformed section	$r_{nc,tr,d} = 14.8521016\text{-in}$	
Non - composite transformed section modulus top	$S_{top,nc,tr,d} = 5088.7634083\text{-in}^3$	
Non - composite transformed section modulus bottom	$S_{bot,nc,tr,d} = 6429.3163479\text{-in}^3$	
Section modulus at level of prestressing steel in composite transformed section	$S_{ps,nc,tr,d} = 11435.340514\text{-in}^3$	
Eccentricity of prestressed strands in non-composite transformed section	$e_{cg,nc,tr,d} = y_{b,nc,tr,d} - y_{p,d} = 11.1779043\text{-in}$	

## Loads

Self weight of girder

$$w_g := 583\text{plf}$$

Moment Due to self weight of girder

$$M_{dl}(x) := \frac{w_g \cdot x}{2} \cdot (\text{Span} - x)$$

Moment due to self weight at "x"

$$M_{dlx} = 233.2\text{-kip}\cdot\text{ft}$$

Moment due to self weight at midspan

$$M_{dl\text{ midspan}} = 262.35\text{-kip}\cdot\text{ft}$$

Weight of Deck

$$w_{deck} := t_{slab} \cdot b_{slab} \cdot 150\text{pcf} = 104.8177083\text{-plf}$$

Moment due to weight of deck

$$M_{deck}(x) := \frac{w_{deck} \cdot x}{2} \cdot (\text{Span} - x)$$

Moment due to weight of deck at "x"

$$M_{deckx} = 41.9270833\text{-kip}\cdot\text{ft}$$

Virgin Girder Prestressing Force

$$F_{ps} := 14\text{kip}\cdot\text{strands}_{total} = 700\text{-kip}$$

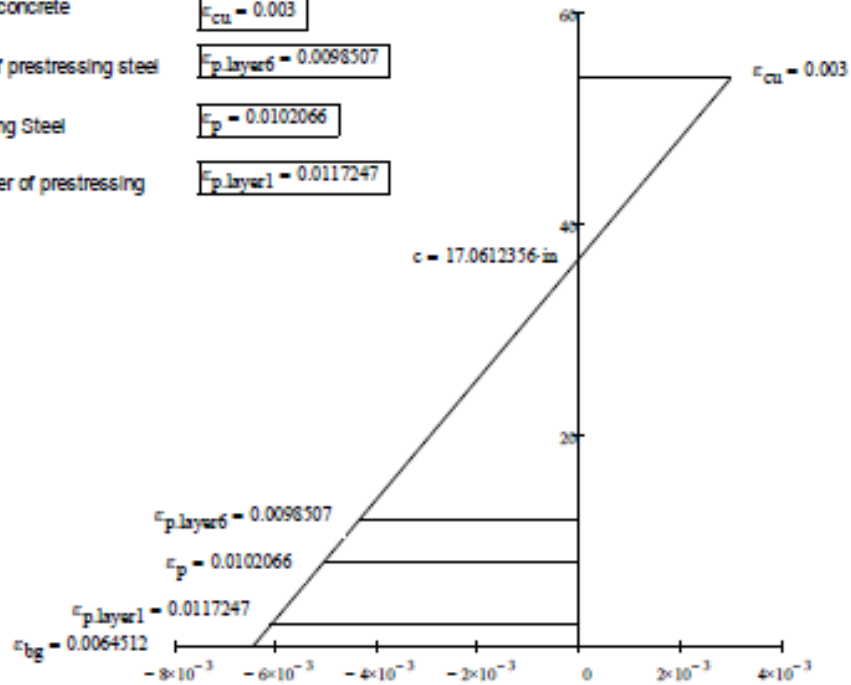
Damaged Girder Prestressing Force

$$F_{ps,d} := 14\text{kip}\cdot\text{strands}_{total,d} = 644\text{-kip}$$

## Section 2

### Ultimate Strength of Virgin Girder

Height of Composite Section	$b_{\text{composite}} = 53.75 \text{ in}$
Center of Compression	$y = 7.55 \text{ in}$
Moment Capacity of Damaged Girder	$M_{n,\text{virgin}} = F_p(c)(d_{p,c} - y) = 2.728 \times 10^3 \text{ kip}\cdot\text{ft}$
Depth to Neutral Axis	$c = 17.0612356 \text{ in}$
Maximum Strain in the concrete	$\epsilon_{cu} = 0.003$
Strain in the top layer of prestressing steel	$\epsilon_{p,\text{layer6}} = 0.0098507$
Strain in the Prestressing Steel	$\epsilon_p = 0.0102066$
Strain in the bottom layer of prestressing steel	$\epsilon_{p,\text{layer1}} = 0.0117247$



### Section 3

#### Initial Conditions of Damaged Girder

Effective prestressing force after losses  $f_{ps} = 129.88 \text{ ksi}$

Final prestressing force  $P_{ps, \text{final}} = 518.88 \text{ kip}$

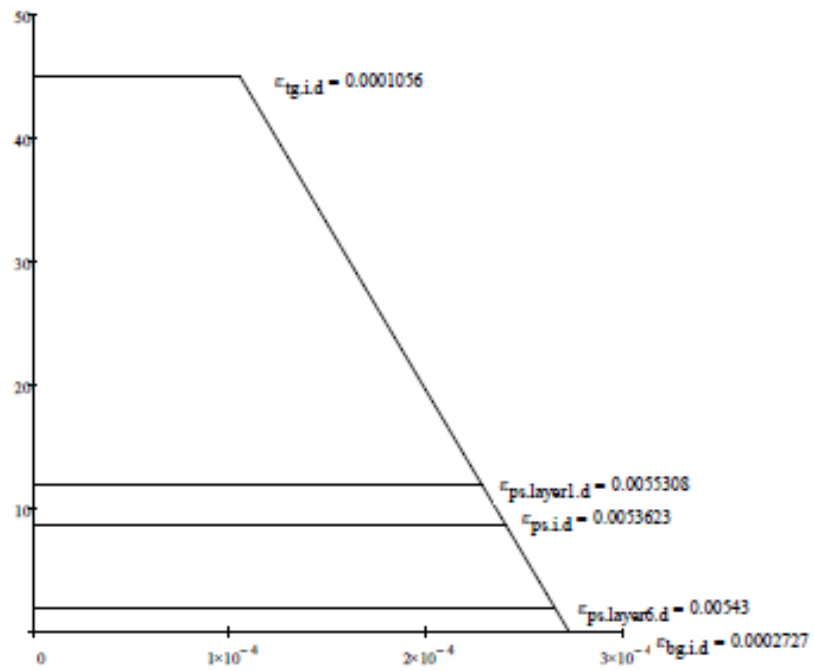
Strain at top of girder  $\epsilon_{tg, id} = 0.0001056$

Strain in the top layer of prestressing steel  $\epsilon_{ps, \text{layer1}, d} = 0.0055308$

Strain at level of prestressing centroid  $\epsilon_{ps, id} = 0.0053623$

Strain in the bottom layer of prestressing steel  $\epsilon_{ps, \text{layer6}, d} = 0.00543$

Strain at bottom of girder  $\epsilon_{bg, id} = 0.0002727$



## Section 4

### Ultimate Strength of Damaged Girder

Center of Compression  $y = 7.14 \text{ in}$

Strength of Damaged Girder  $M_{n,damaged} := F_p(c) \cdot (d_{p,c,d} - y) = 2.506 \times 10^3 \text{ kip-ft}$

Strength of Undamaged Virgin Girder  $M_{n,virgin} = 2.728 \times 10^3 \text{ kip-ft}$

Difference in strength between un-damaged and damaged girder  $M_{n,FRP} := M_{n,virgin} - M_{n,damaged} = 221.9390203 \text{ kip-ft}$

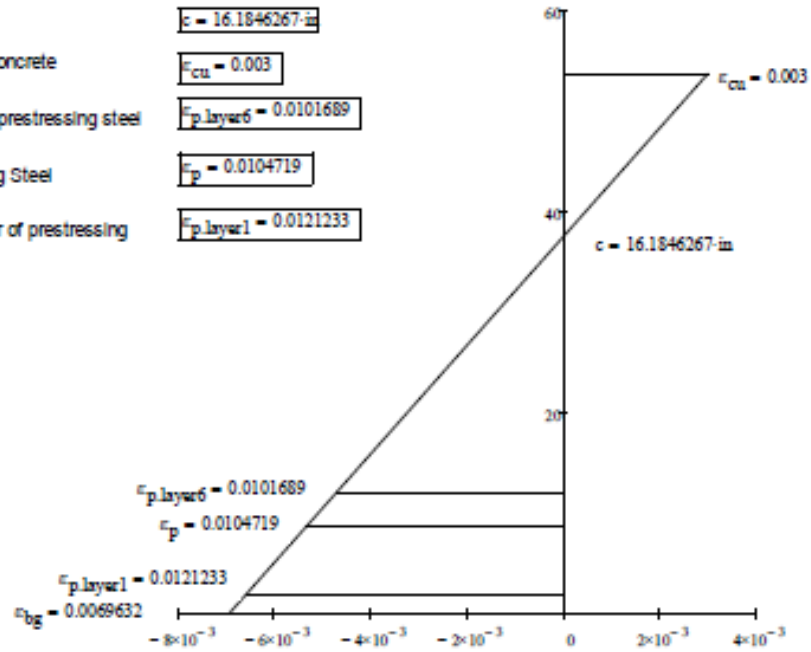
Depth to Neutral Axis  $c = 16.1846267 \text{ in}$

Maximum Strain in the concrete  $\epsilon_{cu} = 0.003$

Strain in the top layer of prestressing steel  $\epsilon_{p,layer6} = 0.0101689$

Strain in the Prestressing Steel  $\epsilon_p = 0.0104719$

Strain in the bottom layer of prestressing steel  $\epsilon_{p,layer1} = 0.0121233$



Yield Stress of Prestressing  $f_{py} = 212.5 \text{ ksi}$

Ultimate Prestressing Stress  $f_{pu} = 250 \text{ ksi}$

Stress in Prestressing Steel at Failure  $F_p(c) = 215.87 \text{ ksi}$  at level of prestressing centroid  
Steel = "YIELDING BUT NO RUPTURE"

## Section 5

### Ultimate Strength of Damaged Girder with Externally Bonded FRP

#### FRP Material Properties:

Design coefficients	$C_E := 1$ $\psi_f := 1$
Modulus of Elasticity from characterization	$E_f := 10.72 \cdot 10^6 \text{ psi}$
Ultimate Strain from characterization	$\epsilon_{fu} := .017$
Width of soffit	$w := b_{bf} = 22 \text{ in}$
Number of plies	$n := 2$
Thickness of FRP	$t_f := .08 \text{ in}$ for C400
Area of FRP	$A_f := w \cdot n \cdot t_f = 3.52 \text{ in}^2$
Ultimate Stress from characterization tests	$F_{tu} := 182.81 \text{ ksi}$
Standard deviation of ultimate stress from characterization tests	$\sigma_{fu} := 9.56 \text{ ksi}$
	$f_{fu, design} := F_{tu} = 182.81 \text{ ksi}$
Design ultimate stress	$f_{fu} := f_{fu, design} = 182.81 \text{ ksi}$
Depth to FRP	$d_f := h_{composite} = 53.75 \text{ in}$

FRP Design Using Procedure from ACI 440.2R-08

Estimate  $c_{trial}$  and iterate until  $c_{trial}$  matches  $c$

$c_{trial} = 19.9464106in$

Result:

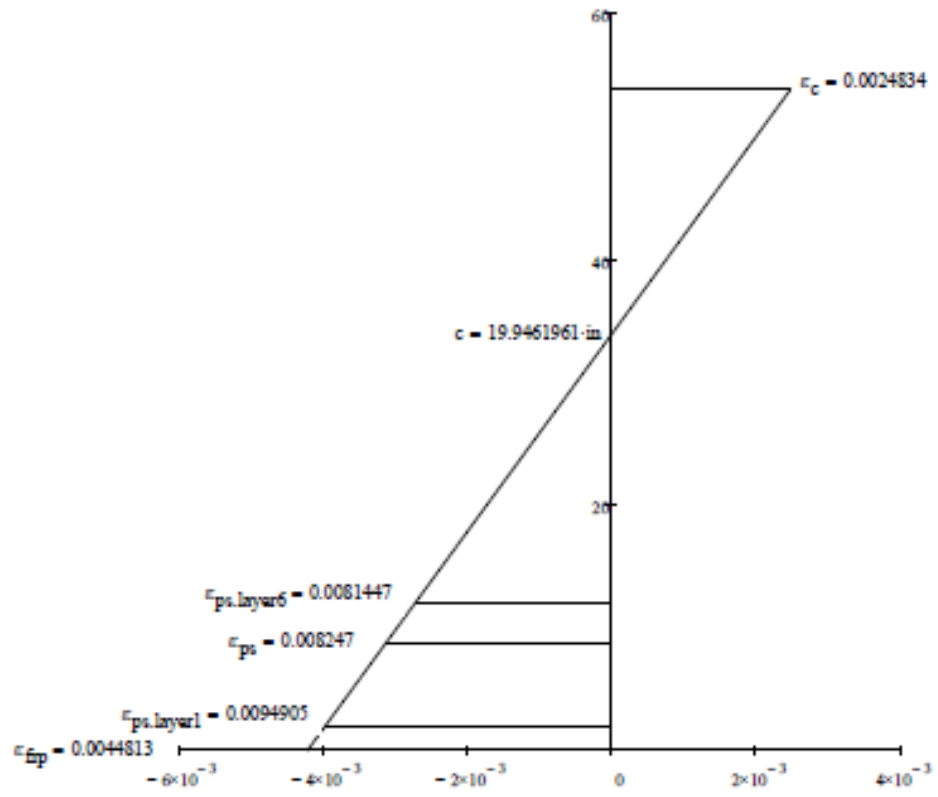
$c = 19.9461961in$

Check<sub>c</sub> = "OK"

**Results:**

Height of Composite Section	$b_{composite} = 53.75 in$	
Depth to Neutral Axis	$c = 19.9461961 in$	
Strain in Concrete at Failure	$\epsilon_c = 0.0024834$	
Strain in Soffit at Failure	$\epsilon_{bg} = 0.0042088$	
Strain in Prestressing Steel at Failure	$\epsilon_{ps} = 0.008247$	
Strain in FRP at Failure	$\epsilon_{fp} = 0.0044813$	← This strain is greater than the strain in the soffit because there is an initial compressive strain due to prestressing force
Stress in Prestressing Steel at Failure	$f_{ps} = 228.3436158 ksi$	
Stress in FRP at Failure	$f_{fp} = 48.0397231 ksi$	
Yield stress of Prestressing Steel	$f_{py} = 212.5 ksi$	
Ultimate Stress of Prestressing Steel	$f_{pu} = 250 ksi$	
Failure Mode	FailureMode = "FRP Failure"	
Flexural Capacity of Virgin Girder	$M_{n,virgin} = 2728.0968338 kip-ft$	
Flexural Capacity of Virgin Girder	$M_{n,damaged} = 2506.1578135 kip-ft$	
Flexural Capacity of Strengthened Girder	$M_{n,fp} = 3.177 \times 10^3 kip-ft$	
	Check <sub>FRP Strength</sub> = "OK"	

Depth to Neutral Axis	$c = 19.9461961\text{-in}$
Strain In Concrete at Failure	$\epsilon_c = 0.0024834$
Strain In Top Layer of Prestressing Steel at Failure	$\epsilon_{ps,layer6} = 0.0081447$
Strain In Prestressing Steel at Failure	$\epsilon_{ps} = 0.008247$
Strain In Top Layer of Prestressing Steel at Failure	$\epsilon_{ps,layer1} = 0.0094905$
Strain In FRP at Failure	$\epsilon_{fp} = 0.0044813$
Strain In Soffit at Failure	$\epsilon_{bz} = 0.0042086$



## APPENDIX E: Applied Moment Calculations

$$M_{a,max} = \left( \frac{P_{a,max}}{l} (l - a + b) \right) a + \frac{w_0 * a}{2} (l - a)$$

With:

- $M_{a,max}$  = Failure Moment, k-ft
- $P_{a,max}$  = Applied Load at Each Point (1/2 Failure Load), kips
- $l$  = Span Length, ft
- $a$  = Longer Distance from Bearing to Load Point, ft
- $b$  = Shorter Distance from Bearing to Load Point, ft
- $w_0$  = Self-Weight, k/ft

## APPENDIX F: Shear Calculations

$$V_n = V_s + V_c$$

With

$V_s$  = Shear Capacity of the Steel, kip

$$V_s = \frac{A_v f_y d_v \cot \theta}{s}$$

$A_v$  = Area of Stirrups, in<sup>2</sup>

$f_y$  = Steel Yield Strength, ksi

$d_v$  = Effective Shear Depth, in

$s$  = Stirrup Spacing, in

$\cot \theta = 1.0$  if  $V_{ci} < V_{cw}$

$$\cot \theta = 1.0 + 3 \left( \frac{f_{pc}}{\sqrt{f'_c}} \right) \leq 1.8 \text{ if } V_{ci} > V_{cw}$$

$f_{pc}$  = Concrete Compressive Stress at Centroid, ksi

$V_c$  = Shear Capacity of the Concrete, kip

$V_c = \min V_{ci} \text{ and } V_{cw}$

$$V_{ci} = 0.02 \sqrt{f'_c} b_v d_v + V_d + \frac{V_i M_{cre}}{M_{max}} \geq 0.06 \sqrt{f'_c} b_v d_v$$

$b_v$  = Web Width, in

$V_d$  = Shear Force from Unfactored Dead Load, kip

$V_i$  = Shear Force from Applied Load, kip

$M_{max}$  = Maximum Factored Moment from Applied Load, in-k

$$V_{cw} = (0.06 \sqrt{f'_c} + 0.3 f_{pc}) b_v d_v + V_p$$

$V_p$  = Shear Force from Prestress, kip

## APPENDIX G: Curvature-Ductility Calculations

$$\mu = \frac{\varphi_u}{\varphi_{cr}}$$

With:

- $\mu$  = Curvature-Ductility
- $\varphi_u$  = Curvature at Ultimate
- $\varphi_{cr}$  = Curvature at Cracking

$$\varphi = \frac{\varepsilon_{41} - \varepsilon_2}{41 - 2}$$

With:

- $\varepsilon_n$  = Recorded Strain at n location

## **APPENDIX H: Specimen Preparation for Strand Splice and FRP Repairs**

The procedures in the following section were adapted from observations during the repair process conducted by Structural Technologies (Structural Group Incorporated, 2015). Specifics may vary based on manufacturer specific requirements.

Areas requiring concrete removal were identified by visual inspection and a hammer tap test.

The hammer tap test produced a hollow sound for areas that were cracked or delaminated. Any area that was determined to be affected by the damaged was marked for removal. In addition, a perimeter of approximately 1 in around damaged areas was marked for removal (Rasheed, 2015).

In order to remove the damaged section, the area was marked to eliminate any sharp or inside corners. Inside corners are corners that cause increased stress concentrations by coming to a point in the direction of the repair.

A grinder with a diamond concrete blade was used to make a 0.5 in saw cut around the perimeter of the damaged area.

An electric chipping gun was used to remove an additional 0.5 in depth of concrete for a minimum of 1 in depth of concrete removed from the damaged area.

The damaged area surrounding the strands was cleared and the concrete was removed to a diameter of 0.5 in from around any exposed strand to allow sufficient room for aggregate to consolidate around the strands and bond with the original concrete. Special care was taken when operating the electric chipping gun around prestressing strands to ensure the strands were not damaged further during the excavation process.

In addition to clearing 0.5 in diameter around exposed strands, concrete around any severed strands was be cleared 24 in from the cut in both directions along the length of the strand. This

was done to provide sufficient room for the splice chucks and to provide room for the new concrete to bond with the strand.

In corners and along the outside edges of the damaged section, reinforcement bars or prestressing strands were exposed and a 0.5 in diameter was cleared around them to provide sufficient materials to create a bond with the new concrete.

After all the damaged concrete was removed, any excess debris was cleaned with an air hose.

Then, the repair section was sand blasted to remove any corrosion on the strands and to open the concrete. Next, a pressure washer was used to remove any more debris and to hydrate the original concrete in preparation for the repair concrete to be placed.

For Tests 2 and 4, the Grabb-in Cable Splice was installed. The procedures followed for their installation are described in APPENDIX I: Strand Splice Repair Procedures.

After the site was prepared and strand splices installed, the formwork was built and erected in preparation for the concrete placement.

The Tstrata IRC was a self-consolidating proportioned concrete mix that was used as the concrete in the patch. It is an early high strength mix used to minimize the time between placement and further repairs or use (Structural Group Incorporated, 2015).

The concrete was allowed to cure for 24 hr before the formwork was removed and the finishing work completed. For Test 3, detailed finishing work is discussed in APPENDIX J: Fiber Reinforced Polymer Repair Procedures.

## **APPENDIX I: Installation of Strand Splices**

After the area was prepared, the Grabb-It cable splices were laid out to determine the proper spacing. Splice chucks were positioned to ensure that there was no overlap of the turnbuckles where the cross section of the splice chuck was not as robust. In order to ensure that there was no overlap and to remove any nicked or damaged portions of the strands, additional prestressing cable was cut to length and used to connect the original prestressing strands where they were not as significantly damaged.

Once the layout was determined, the strand splices were installed by tightening the turnbuckle with a calibrated torque wrench to the manufacturer suggested torque of 150 ft-lbs which translated to a force of 200 kips.

In order to tighten the splice chuck, three personnel were required to hold wrenches and prevent the splice from turning the strand and unraveling some of the wires.

After the splices were installed and tightened to the proper torque, the section was ready for the erection of the formwork and the placement of the concrete.

## **APPENDIX J: Fiber Reinforced Polymer Repair Procedures**

While the concrete is curing, the sheets of fabric were cut to the appropriate length and the equipment required for installation were set-up

After the concrete was placed and allowed to cure for 24 hr, the formwork was removed and a hammer tap test was conducted to make sure that there was sufficient bond between the Tstrata and the original girder concrete.

Next, the surface was prepared for the FRP. This included making sure there were not any raised sections or inconsistencies from the formwork. In addition, corners where the fabric was going to be applied were rounded to a minimum of a 0.5 in radius (Rasheed, 2015). This is to ensure that there are not any locations that can cause voids, damage, or increased stress in the fabric.

Because the FRP system is a “contact critical” system, a grinder is then used to roughen the surface of the concrete “to the aggregate level” (Rasheed, 2015). The surface preparation is done to ensure that the epoxy has sufficient materials with which to bond

After the surface was prepared, the resin was mixed and applied to the substrate surface as a primer (Nanni, Huang, & Tumialan, 2001). After the primer was applied to the girder, a resin putty mixture is applied to fill in any voids on the surface of the girder and create as smooth of a surface as possible for the fabric to bond with (Rasheed, 2015).

The fabric sheets were pulled through the epoxy and rolled through a press to ensure that the epoxy sufficiently penetrated the fibers. The saturated fabric was then stretched along the length of the repair section and a ribbed roller was pressed against it to help it to bond with the putty (Nanni, Huang, & Tumialan, 2001).

After the first layer of fabric was installed, an additional layer of putty was spread across the sheet and the second layer of fabric was saturated, pressed, and rolled onto the bottom of the girder.

A third layer of putty was applied and FRP sheets were saturated and installed in the transverse direction to provide confinement and help resist out of plane stresses that the longitudinal sheets would not resist.

After the transverse sheets were applied, a final layer of putty was spread across them and leveled to provide a clean and smooth outer surface that was free of abnormalities.

The resin was then allowed to cure for 24 hr. The cure time for the resin is temperature dependent and after the 24 hr period was over, it was tested using a hammer tap test (Rasheed, 2015).